REGULATION OF VACUOLAR TRAFFICKING BY Vps45p IN THE PATHOGENIC FUNGUS *CRYPTOCOCCUS NEOFORMANS*

by

Erik David Nielson

BSc, The University of Guelph, 2010

A THESIS SUBMITTED IN PARTIAL FULFILLMENT OF
THE REQUIREMENTS FOR THE DEGREE OF

MASTER OF SCIENCE

in

THE FACULTY OF GRADUATE AND POSTDOCTORAL STUDIES

(Microbiology & Immunology)

THE UNIVERSITY OF BRITISH COLUMBIA
(Vancouver)

April 2014

Abstract

Virulence factor elaboration of the human pathogenic fungus *Cryptococcus neoformans* is strongly regulated by extracellular iron content and type. In addition, acquisition of iron from the host has been shown to be essential for pathogenic growth. Previously, the endosomal sorting complex required for transport was identified as an essential component of iron acquisition from the ferrophore heme. In this study, we further show that iron acquisition from hemin requires the translocation of this molecule to the vacuole by specific deletion of the gene encoding the vacuolar trafficking regulatory protein Vps45p. In addition to decreased ability to utilize extracellular hemin, this mutant is also retarded for growth in the presence of $FeCl_3$, and is defective for cell wall integrity pathway responses when challenged by NaCl, sodium dodecyl sulphate, calcofluor white, or caffeine. These mutants have dramatically increased sensitivities to the vacuolar-accumulating drugs chloroquine and quinacrine. No associated defects in virulence factor elaboration such as loss of melanin deposition or extracellular capsule are observed. However, upon *in vitro* challenge by mouse J774a.1 and human THP-1 derived macrophage cell lines, mutants in the *VPS45* gene were markedly unable to survive when compared to wild-type cells under identical conditions. These data underscore a growing theme in fungal genetics that the importance of vacuolar protein trafficking extends beyond nutrient storage. Vacuolar function in *C. neoformans* appears to strongly correlate with iron acquisition, extracellular signalling response with respect to cell wall integrity, and survival within the phagolysosomal compartment of macrophage-like cells.

Preface

I, Erik David Nielson, oversaw the experimental design and execution of this research under the guidance of Dr. James W. Kronstad. The experiments carried out under the subsection detailing "*in vitro* macrophage clearance of a *vps45*Δ mutant of *C. neoformans* is increased" were performed by Dr. Mélissa Caza and the subsequent data analysis and conclusions were a collaboration between her and I. All other conclusions drawn in the discussion were solely formed by myself and in personal correspondence with Dr. James W. Kronstad. The work herein does not appear in any published journal articles, or manuscripts in progress.

Table of Contents

List of Tables

List of Figures

List of Acronyms

3HAA	3-hydroxyanthranilic acid
AIDS	acquired immunodeficiency syndrome
ARG1	inositol polyphosphate kinase
BBB	blood brain barrier
BC	British Columbia
BLASTp	basic local alignment search tool protein
BMEC	brain microvessel endothelial cells
BPS	bathophenanthroline disulfonate
C3	complement component 3
CAP	capsule associated gene
CccA	vacuolar iron importer
CD	cluster of differentiation
CDC	Center for Disease Control and Prevention
CFO1	*Cryptococcus neoformans* ferroxidase one
CFT	*Cryptococcus neoformans* ferric transporter
CFU	colony forming units
CFW	calcofluor white
CIG1	cytokine inducing glycoprotein 1
CIR1	*Cryptococcus* iron regulator 1
coA	coenzyme A
COPI	coat protein 1
COPII	coat protein 2
CPY1	carboxypeptidase y
CTAB	cetrimonium bromide
CWI	cell wall integrity
Da	Dalton
ddH_2O	double distilled water
DHN	1,8-dihydroxynapthalene
DIC	differential interference contrast
DMEM	Dulbecco's modified Eagle's medium
DNA	deoxyribonucleic acid
dNTP	deoxyribonucleotide triphosphate
EDTA	ethylenediaminetetraacetic acid
ER	endoplasmic reticulum
ESCRT	endosomal sorting complex required for transport
FASL	fas ligand
FASR	fas receptor
FcγRIIB	low affinity IgG receptor
FRE	ferric iron reductase
GFP	green fluorescent protein
GRASP	Golgi reassembly and stack protein
GXM	glucuronoxylomannan
GXMGal	glucuronoxylomannogalactan
HAART	highly active antiretroviral therapy

Habc	helices A, B and C forming a singular domain
HIV	human immunodeficiency virus
HOG	high-osmolarity glycerol
HSP90	heat shock protein 90
IL-10	interleukin10
IL-1β	interleukin 1 beta
IL-6	interleukin 6
IREA	iron responsive element A
LAC1	laccase 1
LAC2	laccase 2
LIM	low iron medium
Mab	monoclonal antibody
MAN1	phosphomannose isomerase
MAPK	mitogen-activated protein kinase
MAPKK	MAPK kinase
MAPKKK	MAPKK kinase
MHC	major histocompatability complex
MLT1	MRP-like transporter
MP	mannoprotein
NADH	nicotinamide adenine dinucleotide
NRG1	negative regulator of glucose-controlled genes 1
N-terminal	amino terminal
PCR	polymerase chain reaction
PEP12	carboxypeptidase y deficient mutant 12
PHO80	phosphate metabolism
PHO8	alkaline phosphatase
PHOB	phosphate metabolism
Pka1	protein kinase A1
PLB1	phospholipase B1
PLC1	phospholipase C 1
PMC1	plasma membrane calcium
PVC	prevacuolar compartment
q-SNARE	glutamine containing SNARE
RIM101	regulator of Ime2
RNA	ribonucleic acid
RNase	ribonuclease
RPMI	Roswell Park Memorial Institute medium
r-SNARE	arginine containing SNARE
SAGE	serial analysis of gene expression
SDS	sodium dodecyl sulphate
SEC	secretory mutant
SM	Sec1p/Munc18p family proteins
SNAP	soluble N-ethylmaleimide-sensitive factor attachment protein
SNARE	SNAP receptor
SOD1	superoxide dismutase
SSC	saline-sodium citrate

TAE	tris-acetate EDTA
TLG	transport late Golgi
TLR4	Toll-like receptor 4
TNF	tumor necrosis factor
t-SNARE	target associated SNARE
TUP1	dTMP-uptake
UDP	uracil diphosphate
UGD1	UDP-glucose dehydrogenase
UGE1	UDP-glucose epimerase
URA5	uracil requiring
UXS1	UDP-xylose synthase
V-ATPase	vacuolar H+-ATPase
VCX1	vacuolar H+/Ca2+ exchanger
VMA	vacuolar membrane ATPase
VPH1	vacuolar pH
VPS	vacuolar protein sorting
v-SNARE	vesicle localized SNARE
WU-BLAST2p	Washington University BLASTp version 2
YNB	yeast nitrogen base
YPD	yeast extract peptone dextrose
YPT52	yeast protein

Acknowledgments

I would like to thank first and foremost my supervisor Dr. James W. Kronstad for his support, guidance, and input into this project and my development. I would also like to thank my supervisory committee for their invaluable assistance: Dr. Phillip Hieter, Dr. Rachel Fernandez, and Dr. Vivien Measday. I would also like to thank NSERC for providing scholarship funding of my Masters work. Additionally, I would like to thank the funding agencies of CIHR, and NIH for providing funding to the Kronstad Laboratory during my tenure.

In particular, I would like to thank Mélissa Caza for her invaluable work in providing me with mammalian tissue culture experiments. I would like to thank the members of the Kronstad Laboratory, past and present, for scientific advice and moral support, especially Scott Lambie, Emma Griffiths, and Rodgoun Attarian.

I would like to thank my mother and father for providing endless support and motivation throughout my life and career.

Finally, I would like to give a very special thank you to Courtney Choutka for her tireless effort, boundless motivation and tremendous support in the last years of my Masters degree.

To my mother, father, and sister.

To my partner, friends, and colleagues.

Introduction

Cryptococcus neoformans

Cryptococcus neoformans is a unicellular basidiomycete fungus which has been frequently isolated from soil and trees, and that has a global distribution. *C. neoformans* and a related species *Cryptococcus gattii* are the primary causative agents of a fungal infection referred to as cryptococcosis. Typically initial infection follows inhalation of fungal spores or desiccated yeast cells although the fungus can also be ingested with contaminated food or water. *C. neoformans* is an opportunistic human pathogen as it requires an immunocompromised host but there are also many non-pathogenic *Cryptococcus* spp. [3]. This suggests that pathogenic *Cryptococcus* spp. have specifically evolved the ability to grow and survive in vertebrates such as humans, birds and small mammals. Commonly environmental reservoirs are largely attributed to bird populations with many cryptococcal isolates observed in bird excreta and nests. The mechanisms of environmental resilience, which are hypothesized to include the ability of *C. neoformans* to inhabit amoeba as a large microbial niche, may have allowed adaptation of the fungus to the mammalian host. In this case, the selective pressures encountered by predatory amoebae have been explored as a source of anti-phagocytic survival strategies [4, 5]. Strikingly, the similarities between amoeba engulfment and innate immune responses by phagocytic cells are numerous [5]. Thus, the molecular mechanisms required for cryptococcal invasion, evasion, and proliferation within host environments have garnered high levels of research interest.

As previously stated, host colonization occurs first by inhalation of spores or desiccated yeast cells from the environment; laboratory infection experiments have demonstrated that both cell types can be infective in animal models [6, 7]. The fungal cells can reach the alveolar space unless the action of mucosal movements and host cilia can effectively achieve clearance [6]. Cryptococcal cells preferentially adhere to lung epithelial cells through an action mediated by alveolar surfactant [8]. Within surfactant are proteins which maintain surface tension of the fluid, and those which recognize invasive organisms and allergens [9]. Surfactant protein D, a member of the latter group of proteins, binds to cryptococcal cells [8]. This promotes uptake by macrophages and the fungal cells can proliferate within the phagolysosome [10]. Once the

alveoli is reached, *C. neoformans* can survive either externally or transit deeper into tissues within the phagolysosomes of infected alveolar macrophages [11]. It is at this point that host-immune status will determine the prognosis of infection. The fungal cells can be cleared by alveolar macrophages, or sequestered in granulomas in a Th1-dependent response that results in a latent lung infection [12]. Alternatively, the alveolar compartment can serve as an entry point for host invasion as *C. neoformans* proceeds to disseminate into the blood [13, 14]. Exit from the alveolar space can occur through two different mechanisms: transcytotic movement through epithelial cells, which is dependent on epithelial cell phagocytosis and has been linked to the development of "Titan cells" [15-19], or by the "Trojan horse" model of colonization [12]. Briefly, "Titan cells," or "giant cells" are a morphologically distinct form of *C. neoformans* with diameters up to 30 μm (a ten-fold increase in size from the yeast form); these cells are polyploid, and are capable of producing daughter yeast cells [16, 17]. "Trojan horse" invasion requires that the fungal cells survive, and replicate within the phagolysosome of resident alveolar macrophages [15, 20, 21]. These cryptococcal-loaded macrophages move into the bloodstream where passenger yeast can either burst the macrophage by outgrowth [22], pass from macrophage to macrophage without exposure to the extracellular milieu [23], or non-lytically escape [22, 24]. The initial outcome of alveolar macrophage interaction with *C. neoformans* plays a pivotal role in pathogenesis because granuloma formation or clearance occur in healthy patients, while dissemination can occur in those that are iummunocompromised [10, 13, 14, 25].

Upon hematogenic dissemination of *C. neoformans,* colonization and disease presentation can occur in tissues such as the skin [26, 27], heart [28], and liver [29]. However, the predominant preference is migration to the central nervous system with specific affinity for colonization of the brain [30, 31]. Typically, the blood brain barrier (BBB) is largely impermeable to microbial pathogens, pharmaceuticals, and other circulating bodies. Regardless, *C. neoformans* is readily able to enter the brain where it causes lethal meningoencephalitis if untreated [31, 32]. The BBB is composed of brain microvessel endothelial cells (BMECs) which are connected by many narrow tight junctions that inhibit paracellular diffusion, a feature not present in vasculature elsewhere. Pericytes incompletely surround the BMECs which regulate vascular development, and together form an extracellular basal lamina membrane [33]. End foot projections from local astrocytes imbed within the basal lamina and form a secondary lamina

[33, 34]. These structures compose the majority of the BBB and are the primary mechanisms for regulating the selectively impermeable barrier. *C. neoformans, however,* possesses three penetration strategies. The first is by "Trojan Horse" dissemination by macrophages that carry engulfed fungal cells through the intracellular BMEC tight junctions that line the vessels [35]. The second method is by transcytosis of the BBB through BMECs mediated by CD44 host-fungal interactions [36]. This interaction is dependent on cryptococcal phospholipase B1 (Plb1p) activity which promotes BMEC endocytosis of the fungal cells [37]. Finally, cryptococcal secreted mannoproteins and urease increase local concentrations of plasmin and urea that erode BMEC tight junctions, allowing intracellular penetration and dissemination into the parenchyma [38-41]. It is important to note that HIV/AIDS positive status is correlated with a weakened BBB status that may partially account for an increase of morbidity and mortality associated with co-infection [42]. The primary symptoms of brain infection are sensitivity to light, headaches, fever, and change in mental status. If the infection is mild to moderate, primary treatment is provided with the triazole drug, fluconazole, while in severe infections treatment is initiated with the polyene drug, amphotericin B, and then generally followed by fluconazole. Highly active antiretroviral therapy (HAART) is required if the patient is human immunodeficiency virus (HIV) or acquired immunodeficiency syndrome (AIDS) positive.

Epidemiology of Cryptococcosis

Cryptococcosis, the disease associated with *Cryptococcus* spp. infection, is rare among the developed world with rates as low as 0.4-1.3 cases per 100,000 people [43, 44]. However, the largest affected populations are those suffering from HIV/AIDS. A recent study by the Center for Disease Control and Prevention (CDC) found that rates in this highly affected group exceeded 2-7 per thousand persons in the United States, and mortality rates are approximately 12% [44]. Cryptococcosis is associated with immunocompromised status, and has been documented in organ transplant recipients, patients on immune suppressants, or in cases involving immune disorders. Given that infection rates are quite low and access to affordable HIV therapeutics is increasing, there is a positive outlook for treating the disease in the developed world. Nevertheless, the largest determinant of successful disease prognosis is access to appropriate healthcare. Developing nations, especially those in Sub-Saharan Africa, Southeast Asia, and India, where the HIV/AIDS pandemic is ongoing or on the rise, represent the world's largest

cohort susceptible to or affected by co-infection. Globally it is estimated that approximately one million people are suffering from cryptococcosis and a further ~625,000 succumb to fatal meningoencephalitis; a mortality rate of 62.5 %. The largest determinant of a positive prognosis is accessibility of care and in the United States fatal resolution occurs in 1/8 of all cases in comparison to the global figure which is estimated to be 5/8. It is therefore a global health imperative to study *C. neoformans* and the associated illness, cryptococcosis, as it represents a significant health concern with the potential to grow as the HIV/AIDS epidemic spreads.

A related species, *C. gattii*, is also capable of causing cryptococcosis, including fatal infections in humans [45]. Importantly, *C. gattii* is able to infect immunocompetent hosts, and elicits a pro-inflammatory host response [46]. This fungus had been typically isolated in tropical and sub-tropical regions [47, 48]; however, an outbreak of *C. gattii* on Vancouver Island that began in 1997 has since spread inland and isolates have been discovered in the lower mainland of British Columbia, and in the states of Washington, Oregon, California, and Utah [45]. It appears that this fungus has a broad permissible environmental range, and is not restricted to warmer climates as once thought. The disease outbreak and incidence has been best reported in British Columbia (BC), with a total of 303 cases since 1997 and 19 deaths in BC have been attributed to *C. gattii* as of 2007 [49]. In the United States fewer reports have been uncovered, and to date only 60 cases have been identified, with 20 confirmed deaths [49]. Although, these numbers are much lower than the global burdens of *C. neoformans*, the trends suggest an expanding environmental niche for *C. gattii* in the Pacific Northwest.

Virulence Factors

Pathogenesis is dependent on three essential virulence factors of *C. neoformans*: 1) the ability to produce a polysaccharide capsule; 2) the biosynthesis of melanin from host-derived precursors, and; 3) the ability to proliferate at 37°C [25, 31]. The polysaccharide capsule promotes infection by shielding fungal cells from damage by a variety of immune cells and antifungal drugs [14, 50, 51], through modulation of host immune function [52-54], and possibly by regulating the movement of *C. neoformans* across the blood brain barrier (supported by *in vitro* evidence) [36, 41]. Melanization is able to shield the cells from oxidative stress caused by the macrophage oxidative burst, and to protect the cells against nitrosative stress, and antifungal drugs [55-57]. The biosynthesis of melanin is dependent on the extracellular secretion of cell

wall-associated laccases (encoded by the *LAC1*, and *LAC2* genes) [58]. Finally, the ability for *Cryptococcus spp.* to survive at 37°C is a requisite adaptation to proliferate within the mammalian host. Temperature stress appears to act as a potent signal for pathogenic growth exacerbating many factors triggered by other environmental signals such as cell cycle arrest, hyphal growth, formation of fruiting polykaryotic giant cells, capsule biogenesis, melanization, gene expression, protein content, and endosomal membrane system restructuring [59-61]. Many other genetic elements are required for cryptococcal virulence and pathogenesis, however, capsule, melanin and growth at host temperature are considered the canonical virulence factors of the fungus. These factors are discussed in the following sections along with the uptake of iron from exogenous sources by *C. neoformans*. The latter topic is included because iron homeostasis is strongly correlated with survival, virulence factor expression, and pathogenesis [62-64].

Capsule

Encapsulation is a common strategy of invasive respiratory microorganisms, and many examples exist in bacterial species such as *Neisseria meningitidis, Salmonella typhii,* and S*treptococcus pneumonia* [65]. The primary function of an extracellular polysaccharide capsule appears to be evasion of phagocytosis which allows the organism an extended growth period before B-cell derived clearing occurs. Similarly, capsular components are utilized by *C. neoformans* to modulate host immunity and promote survival, replication, and dissemination throughout the host [66]. The defensive properties of capsule affect both innate and adaptive immunity by allowing escape of initial phagocytosis, and suppression of host adaptive immunity [67]. In addition to cell-associated capsule, secretion and sloughing of free polymers occurs. These components are recognized by monocyte surface receptors and actively engulfed [68]. Capsule at concentrations of up to 1-3 μg/mL can be detected in blood serum; and may exceed 20 μg/mL, and 10μg/mL in the spleen and liver, respectively [69, 70]. Although capsule provides an effective shield against the innate immune response, it is highly antigenic and anti-capsular antibodies are used to diagnose cryptococcosis in a clinical setting [71].

Encapsulated cells are less readily engulfed by macrophages in the lung because the major capsule polysaccharide glucuronoxylomannan (GXM) is largely protective against the innate immune response [50]. Antigenicity of capsule is varied throughout the infection cycle allowing prolonged escape from detection in an undefined process that may be an example of

phenotype switching [72]. Once engulfed, encapsulated strains are capable of intracellular replication [73] and are protected from oxidative and nitrosative stress [74], host defensins [50], and the antifungal drug, amphotericin B [50]. The immunomodulatory properties of capsule have a broad range of targets and effects. An anti-inflammatory cytokine response is elicited from macrophage and monocytes by recognition of GXM and subsequent release of interleukin (IL)-10 [54, 75]. Capsular-dependent down regulation of the major histocompatability complex (MHC) class I and II proteins in antigen-presenting and dendritic cells inhibits the display of cryptococcal antigens [76]. Endothelial adhesion, and chemokinesis of neutrophils and leukocytes to *C. neoformans* infected tissues is impaired by the presence of capsule, thereby slowing the immune response in areas of high GXM abundance [53, 77]. Apoptosis of host immune cells can also be triggered by binding of capsule to macrophages, monocytes, and T cells by surface expression of the FasR and FasL gene products [78, 79]. Many of these effects appear to be due to the ability of GXM to bind to the surface receptors FcγRIIB, TLR-4, CD14, and CD18 [78, 80]. The immunosuppressive properties of GXM have been applied to the study of rheumatoid arthritis, where evidence suggests that an increased IL-10 production was able to cause beneficial, anti-inflammatory effects [81]. These mechanisms of action have determined that the *C. neoformans* capsule is a potent modulator of host immunity and underlined capsular participation in infiltration, escape, and survival within the host.

Historically, classification of *C. neoformans* varieties was defined by serotype analysis of the capsule. *C. gattii* and *C. neoformans* are the only two pathogenic cryptococcal species, and as such are the most widely studied and characterized. Four serotypes belonging to three varieties exist. Serotype A was designated *C. neoformans var. grubii*, and this variety is the most common clinically observed type of isolate emerging in about 95% of all HIV/AIDS positive patients diagnosed with cryptococcosis. Serotypes B and C were determined to be a separate species, *C. gattii*, by analysis of chromosomal composition, and randomly amplified polymorphic DNA analysis [82, 83]. Serotype D was previously annotated as *C. neoformans* var. *neoformans*, which is classified based on capsule immunologic reactivity, DNA fingerprinting and *URA5* sequence analysis [82, 84]. Capsule synthesis occurs rapidly and initially exists as an elastic network that becomes increasingly rigid over time [85]. During this aging process the capsule becomes more dense and less permeable to solutes, and binding of capsule-specific antibodies is altered [72,

86]. Especially given the antigenic properties of the capsule, much work has been done on characterizing this unique feature of *Cryptococcus spp*.

Almost all acapsular mutant strains of *C. neoformans* are avirulent or have reduced virulence phenotypes when assayed in murine models of cryptococcosis [67]. Many genes required for capsule growth have been identified, including *CAP10*, *CAP59*, *CAP60*, and *CAP67;* these have yet to be functionally characterized as the mechanisms of capsule synthesis have proven to be enigmatic [51, 87-90]. Structural studies have shown that the capsule has three primary constituents: glucuronoxylomannan (GXM, as mentioned above), glucuronoxylomannogalactan (GXMGal), and mannoproteins (MP), which occupy distinct spatial environments [91]. MPs appear to be cell-wall associated, along with the closely associated GXMGal core. The majority of medial and distal capsular elements appear to be networks of GXM in decreasing densities. The repeating subunits of GXM are predominantly a motif comprised of mannose trisaccharides, but the branching structures are undefined [92]. This implied flexibility of synthesis appears to provide a vast potential for structural confirmations.

The biosynthetic reactions required to build capsule monomers and polymers have begun to be described and investigated by the Doering and Janbon groups (reviewed in [67]). Briefly, initial capsule monomers are collected in the cytosol by conversion of carbon metabolism derivatives, an example being the conversion of UDP-glucose to UDP-glucuronic acid via UDP-glucose dehydrogenase (Ugd1p) [93]. Through similar enzymatic steps, a pool of capsule monomers including UDP-glucuronic acid is collected [94]. Uge1p epimerase isomerises UDP-galactose from free UDP-glucose [95]. Uxs1p decarboxylates UDP-glucuronic acid producing UDP-xylose [96]. The predicted enzymatic steps to synthesize GDP-mannose require a phosphomannomutase, a GDP-mannose pyrophosphorylase, and a recently identified phosphomannose isomerase, Man1p [94]. These subunits are then polymerized in an uncharacterized manner, during which the polysaccharide can be modified via addition of xylose, mannose and acetate [97-100]). Precursor capsular polymers are then secreted in a manner requiring, in part, exocytic vesicles termed exosomes which are Sec6p dependent [101]. In addition, the exocyst complex has been implicated in capsule export by analysis of Sec4p [102], as well as the Golgi reassembly and stack protein (GRASP), a mutant of which had decreased capsule size in a knockout study [103].

Growth at 37°C

Given that many successful organisms do not invest heavily in temperature homeostasis, it is unclear why or how endothermic animals are the current dominant form of life. One hypothesis is that a "thermal exclusionary zone" is generated by regulated body temperature, which provides resistance to infections [104]. A unique phenomenon exists wherein there appears to be a paucity of successful fungal mammalian pathogens relative to the large number of fungal species. Fungi have adapted mechanisms of pathogenesis on plants, insects, reptiles, and amphibians yet their presence is greatly reduced in mammalian hosts. The thermal exclusionary zone might constitute the means by which mammals are capable of reducing the ability of fungal species to survive during infection. A collection of over 4800 unique fungal species were analyzed for temperature-dependent growth and only approximately 50% were viable at 37°C [105]. Of these 50%, the most frequently observed species were originally isolated from endothermic animals, however, many of the fungal groups that could tolerate growth at 37°C were isolated from plants, environmental sources, and exothermic animals. These experiments were conducted utilizing the optimal media *in vitro* to assay for growth, an environment much different than the hostile conditions of a host. It appears as though temperature stress represents a significant barrier for fungal growth, and that survival at 37°C is not a frequently observed trait.

During the initial temperature stress response by *C. neoformans* a global transcription change occurs [106], as well as the induction of several protein-mediated temperature stress responses [60, 107, 108]. After the initial phase of host incubation, many temperature stress response genes have returned to low levels of expression, with some responses peaking at one hour and returning to basal levels by three hours [109]. Temperature stress caused cell cycle arrest of *C. neoformans* within the range of 35-40 °C, during which cryptococcal cells increased in diameter and were capable of growing monokaryotic hyphae while fruiting viable haploid daughter cells [61]. This indicates that thermotolerance is indeed a stressor for *C. neoformans*, but is quickly recognized and acclimation occurs through a complex process of transcriptional regulation, posttranscriptional regulation, chaperone protein function to derepress calcineurin dependent pathways, and indirect modulation of the cell cycle via cyclins and cyclin dependent kinases.

In *Candida albicans,* Hsp90p, an ATP-dependent molecular chaperone, has been described as a major regulator of temperature stress response, by repressing filamentation [110], inhibiting signal transduction[111, 112] and interfering with cell cycle progression [113, 114]. Hsp90p is essential in *A. fumigatus* where low copy regulated strains have shown defective filamentation, conidiation, spore viability, virulence in murine inhalation models, increased drug sensitivity, and cell wall defects [115, 116]. In a murine infection model of *C. neoformans* the *HSP90* transcript was upregulated 5-fold during initial colonization, 13-fold when incubated in rabbit cerebrospinal fluid, and 15-fold in a defined low iron medium [106]. Protein interaction studies of *C. albicans* Hsp90p have identified calcineurin, a phosphatase which is a global regulator of cell wall integrity and drug tolerance, as a potential effector of signalling [117, 118]. Likewise, in *C. neoformans* a physical interaction between calcineurin and Hsp90p was observed and calcineurin is required for virulence [107, 108]. Disruption of the catalytic subunit causes dramatic loss of survival within a murine infection model and in host-like *in vitro* conditions [108]. Further studies of calcineurin have indicated an association between the Golgi and endoplasmic reticulum (ER) trafficking proteins Sec28p and Sec13p during 37°C temperature stress [107]. Unlike *C. albicans* and *C. neoformans*, there appears to be no link between Hsp90p and calcineurin activity in *A. fumigatus* [119], although temperature stress in this fungus activates the high-osmolarity glycerol (HOG) mitogen-activated protein kinase (MAPK) [120], and the unfolded protein response via *IREA* [121]. Together these studies suggest that the unfolded protein response and alternate ER stressors are necessary for the thermotolerance signalling that triggers virulence expression in fungi [122-126], including *C. neoformans* [60].

Melanization

The ability of C. *neoformans* to form melanin is not unique among the pathogenic fungi. In fact melanization has been observed in *Aspergillus nidulans, Aspergillus niger, Aspergillus fumigatus, Alternaria alternata, Cladosporium carrionii, C. gattii, Exophiala (Wangiella) dermatitidis, Exophiala jeanselmei, Fonsecae compacta, Fonsecae pedrososi, Hendersonulla toruloidii, Phaeoannellomyces werneckii, Phialophora richardsiae, Phialophora verrucosa, Xylohypha bantiana and Sporothrix schenckii* [127-131]. Many fungal species utilize acetyl coenzyme A (coA) or malonyl coA as substrates for melanin biosynthesis via a polyketide synthase followed by a series of reduction and dehydration reactions to create 1,8-

dihydroxynapthalene (DHN) [132]. Spontaneously, DHN polymerizes to form eumelanin, a dark brown to black pigment, composed of carbon, oxygen and hydrogen [133]. An alternate pathway to polyketide synthesis can produce melanin in a one-step oxidization reaction utilizing exogenous substrates via the enzyme laccase to yield quinone intermediates which auto-oxidize to form melanins [131]. Laccase-dependent melanin biosynthesis can include additional atoms such as nitrogen or sulphur [134]. *C. neoformans* is able to generate the characteristic black pigment in the cell wall by a laccase-dependent reaction. Structural characterization of melanins is quite difficult since the molecule is insoluble in standard solutions used for biochemical analysis, and because of the spontaneous reactions involved in the polymerization, as well as a wide variety of viable substrates; a singular organism can generate many distinct melanin polymers.

C. neoformans melanization requires a functional laccase encoded by *LAC1* and *LAC2* [135, 136]. Lac1p accounts for the majority of melanization activity observed, but the transcriptional response and subcellular localization of the two cryptococcal laccases differs. The substrates L-dopa, D-dopa, methyldopa, epinephrine, norepinepherine, plant-derived flavonoids, caffeic acid, and bacterially-derived homogentisic acid have been shown to be suitable for cryptococcal laccases [58, 137-139]. Interestingly, due to the inability to generate precursors for melanin synthesis, melanin composition and structure produced by *C. neoformans* laccases can be quite varied. The melanins produced from the wide variety of substrates have several differences: colour (reddish-yellow to black), net charge, yield, and thickness of melanised cell wall components are observed. It is also important to note that *C. neoformans* laccase requires the presence of copper as several albino mutants were identified to have mutated copper uptake systems [140], and copper sulfate supplementation can increase the efficiency of the cryptococcal melanising laccases [141]. Additionally, treatment of cryptococcal cells with microplusan, an antimicrobial peptide capable of chelating copper, was fungistatic and cells were non-melanized and had reduced capsule size [142]. These physical and chemical properties are of specific implication because melanization of *C. neoformans* has been strongly linked to virulence [57].

Cryptococcal melanin deposition occurs on the proximal leaf of the cell wall where it is covalently cross-linked with mannose containing components of the cell wall [143]. Several

studies involving *LAC1* and *LAC2* mutants [135, 136], albino strains [57], melanin inhibiting therapeutics [144], a direct inhibitor of laccase (glyphosate) [145], and melanin-binding monoclonal antibodies (Mabs) [146] associate melanization with virulence. Melanization is critical for avoidance of phagocytosis [55], as well as reducing sensitivity to oxidants [147], reductive stress [148], and hydrolytic enzymes [149]. In lipopolysaccharide-stimulated phagocytic cells, chemically synthesized melanin was able to arrest mRNA translation of host cytokines including tumor necrosis factor (TNF), IL-1β, IL-6, and IL-10 [150]. In a more sinister role, functional laccase is also a primary constituent of extracellular vesicles and may be present to generate reactive intermediates with potentially toxic effects in host cells [151, 152]. Melanin polymers are able to bind the antifungal drugs amphotericin B and caspofungin and may well contribute to fungal survival during therapeutic treatment [153]. When treated with trifluparazine, an inhibitor of melanization, the drug resistance of the melanized cryptococcal cells was lost [154]. Paradoxically, cryptococcal melanin is antigenic and promotes a T-cell independent alternative complement response, as deposition of C3 fragments can occur on capsule-free cryptococcal cells [155]. This may represent a conserved evolutionary response against melanin, as utilization of Mabs capable of recognizing cryptococcal melanins were utilized to detect unknown melanization states of other fungal pathogens [156, 157].

Additional analyses of cryptococcal melanization depict an amazing array of potential functions for this enigmatic molecule. Firstly, melanization can be utilized to survive basic environmental challenges such as ultraviolet (UV) radiation [158], temperature extremes [159], free radical damage [160], and amoebae killing [161]. Most interestingly, *C. neoformans* is able to utilize ionizing radiation to generate metabolic energy via reduction of NADH [162]. In a controlled experiment, wild type and *lac1*Δ *C. neoformans* cells were analyzed for colony forming unit (CFU) production (30 hr irradiation), C^{14} labelled acetate assimilation (30 hr irradiation), and biomass accumulation (20 hr irradiation). In all experiments the melanised cryptococcal cells exhibited marked enhancement in growth when compared to the albino mutant. Further experiments utilizing a melanized electrode showed that a detectable electrical current was generated upon gamma ray bombardment [163]. These experiments indicated that melanin polymers are able to provide free electrons that may be used in the reduction of NADH. Additionally, the protective effects of laccase were able to permit survival of *C. neoformans*

when challenged with ionizing radiation in a laboratory setting [162]. Another surprising property of melanin polymers is their ability to bind to a broad range of molecules including lipids [151], heavy metals [164, 165], and synthetic small molecules [56]. Further materials research of melanin polymers may yield advancements in radiation therapeutics, energy transduction, bioremediation, and small molecule development.

Iron Acquisition

In addition to capsule production, proliferation at 37°C, and production of melanina, nutritional requirements limit the pathogenicity of *C. neoformans,* in particular, iron availability. Passive immunity can be generated by maintaining iron in host fluids at extremely low levels (10^{-18} M) by the action of the iron-sequestering proteins ferritin, transferrin, lactoferrin, and by binding in heme molecules [166]. Pathogenic microbes must acquire iron from these sources because they require 10^{-6} to 10^{-7} M iron for growth. Pathogens have developed multiple strategies for iron uptake such as small molecules with high affinity for iron, called siderophores, as well as unique pathways to metabolize heme [63, 166]. In *C. neoformans* iron availability has been shown to influence capsule size [167], transcription of laccase [168], and to have a crucial role in the calcineurin-dependent response to temperature stress [59, 108, 169, 170]. In general, iron sensing has a potent influence on virulence factor regulation in *C. neoformans,* and many methods of uptake have been determined (Figure 1).

Intracellular iron concentrations influence a suite of responsive transcription factors which regulate expression of iron acquisition genes as well as virulence factors. Serial analysis of gene expression (SAGE) studies originally identified 69 and 212 genes up-regulated in either iron-limited or in iron-replete conditions, respectively [171]. A major global iron response regulator, Cir1p, was identified and confirmed to differentially regulate 2311 genes under iron limitation and 1623 upon iron repletion [63]. In addition to Cir1p, the transcription regulators Tup1p, Nrg1p, Rim101p, and HapXp regulate iron homeostasis or are downstream regulators of the response to intracellular iron concentration [172-175].

Iron uptake in *C. neoformans* has been best characterized with regard to extracellular ferric iron scavenging. Ferric iron at the plasma membrane is first reduced through interaction

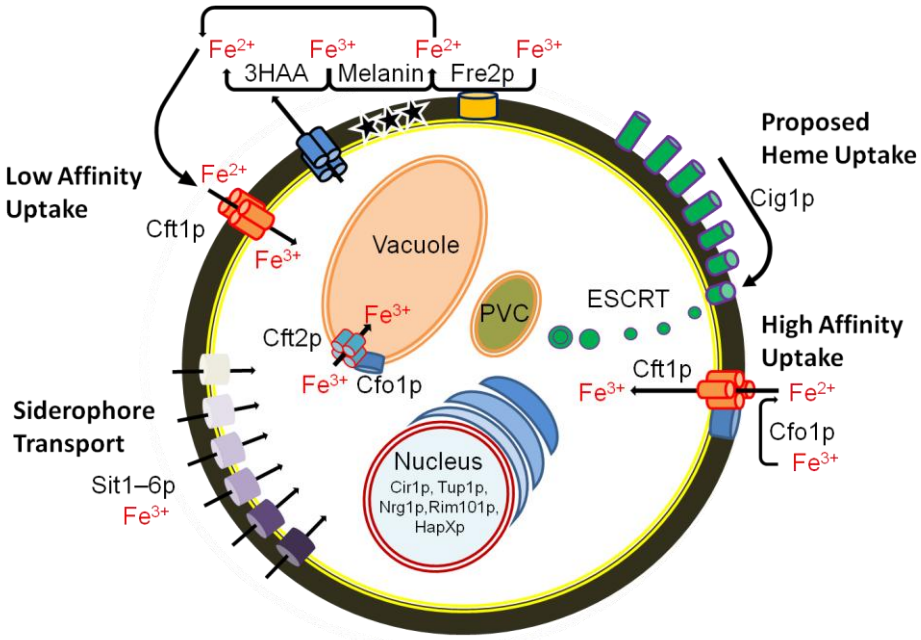

Figure 1. Iron uptake pathways in *C. neoformans*. The proposed mechanisms utilize low affinity uptake, heme acquisition coupled to endocytosis, high affinity uptake, and siderophore transport. Low affinity uptake requires reduction of ferric iron to ferrous via the extracellular reductants including 3HAA, melanin (black stars) and Fre2p (yellow and blue cylinder) followed by uptake by Cft1p (orange and red cylinder cluster) [176, 177]. Heme uptake is hypothesized to require binding of the extracellular protein Cig1p (green and purple cylinder), subsequent cellular uptake via the ESCRT pathway (green and purple circles), the prevacuolar complex (PVC), and metabolism in the vacuole [178, 179]. High affinity uptake of extracellular iron involves the formation of a hypothesized reduction and transport complex Cfo1p (blue and blue cylinder) and Cft1p [63, 64, 180]. Siderophore scavenging and transport into the cytosol is mediated by the Sit1-6p protein family (purple to white cylinders) [181]. Vacuolar trafficking is hypothesized to be mediated by function of the permease Cft2p (blue and red cylinder cluster) [64] and Cfo1p (this study). Finally, cytosolic and extracellular iron concentration is responsive to the regulatory factors Cir1p, Tup1p, Nrg1p, Rim101p, and HapXp [172-175].

with either 3-hydroxyanthranilic acid (3HAA), melanin, or by cell surface reductases [176, 177]. Ferrous iron is then transported through the plasma membrane via the permease, Cft1p, that is coupled to a ferroxidase, Cfo1p, for high affinity uptake [63]. Deletion of *CFT1* reduced growth when either ferric chloride or transferrin were used as the sole iron source, and the mutant was attenuated for virulence in a mouse model of infection [64]. A reduction in the brain fungal burden of mice infected with the *cft1*Δ mutant was also observed, thus suggesting a requirement for reductive iron acquisition during colonization of the central nervous system by *C. neoformans*. In this study the low affinity iron permease, Cft2p, played no apparent role in iron acquisition but did influence virulence.

Further exploration of iron reductases in *C. neoformans* led to the annotation of eight genes (*FRE1-8*) encoding candidate iron reductase proteins as determined by predicted amino acid similarity [177]. These genes were then mutated by disruption or deletion and the resulting mutants were assayed for differential growth in response to different iron sources. Interestingly, only disruption of the gene encoding Fre2p reduces iron acquisition in the presence of extracellular heme, and this mutation is reduced for virulence in a murine disease model. The *fre2*Δ phenotype was exacerbated in a double mutant lacking *CFO1* indicating that iron reduction, oxidation, and uptake may be coupled in high affinity iron uptake. A secondary gene, *FRE4*, encoding a putative reductase was required for melanization and had increased sensitivity to azole drugs. Azole drugs are typically more effective against iron starved cells because they inhibit an essential iron-dependent cytochrome P450, lanosterol 14 α-demethylase [182]. These observations prove that iron acquisition is facilitated by proteinaceous iron reductants.

Iron scavenging from host proteins or molecules is utilized by *C. neoformans* as well. *C. neoformans* can take up siderophores in the environment [181], although it is unknown if the fungus can synthesize or secrete siderophores independently [183]. Endocytosis can be utilized for uptake of plasma membrane bound moieties, as deletion mutants of the endosomal sorting complex required for transport (ESCRT) uptake system are required for heme uptake [179]. A null mutant lacking the ESCRT-1 complex protein Vps23p was hypocapsular, and avirulent in a murine model of cryptococcosis. Additional mutations in the ESCRT-0, ESCRT-II, and ESCRT-III complexes have heme-related growth phenotypes (G. Hu, unpublished data). The extracellular mannoprotein, Cig1p, contributes to heme binding and deletion mutants also lacking *CFO1* were attenuated for virulence during a murine infection model [178]. Cig1p has been isolated from

extracellular vesicles, the plasma membrane, and appears to be distributed in capsule-associated puncta [178]. Currently, *CIG1* is the only described hemophore in *C. neoformans*. The pathogenic importance of high affinity iron uptake, the presence of unique iron acquisition adaptations, like the modified ESCRT function, and novel genes like *CIG1*, provide a strong argument to leverage these pathways as potential options for drug development.

The Fungal Vacuole

The fungal vacuole is a dynamic organelle originating from multiple vesicular fusion events. It lays at the heart of endocytosis as protein degradation occurs within these structures [184], and it plays a central role in the regulation of autophagy in fungal cells [185]. It is also utilized as a storage site for many small organic compounds like amino acids and sugars, as well as inorganic molecules like metals and polyphosphates [184]. Thus, the fungal vacuole is also responsible for maintaining cellular homeostasis through regulating cytosolic pH, ion concentrations, osmotic pressure, and turgor pressure of the cell. The vacuole is a site of tremendous activity receiving cargo originating from the cytosol directly, from the plasma membrane via the ESCRT pathway, from post-Golgi targeting, and via fusion with autophagic membranes [186]. Not only is the vacuole a terminal hub of intracellular trafficking, many of the membrane proteins required for vacuolar targeting are recycled and are returned to their resident compartments. Upon vacuolar localization, resident proteins can undergo functional activation by resident protease activity, post-translational modifications, or auto-activation induced by specific vacuolar conditions [187]. A suite of chemicals have been utilized to visualize fungal vacuoles under the microscope, such as the lipophillic dye FM4-64 that is internalized through endocytosis, or weak bases that can easily penetrate membranes and fluoresce in acidic environments where they accumulate. The best described model for vacuolar trafficking and function is the budding yeast *Saccharomyces cerevisiae*, although much progress has also been made studying the fission yeast *Schizosaccharomyces pombe* [186, 188, 189].

Vacuolar Mutants in *Saccharomyces cerevisiae*

Vacuole trafficking was originally described by analyzing the transport of one gene product in *S. cerevisiae*, carboxypeptidase y (Cpy1p). Groups of mutants were demarcated into three classes (A-C) [190]. Class A mutants retain wild-type-like vacuolar structure while still mislocalizing Cpy1p. Class B contained numerous small vacuolar-like structures, and

mislocalized Cpy1p. Finally, class C had an abolished vacuole and mislocalized Cpy1p. Introduction of more sophisticated microscopy techniques and subcellular localization studies of vacuolar proteins allowed broader classification of the original groupings into classes A-F. Microscopic analysis allowed accurate tracking of segregation and inheritance of vacuolar compartments during budding in the mutant libraries. Greater understanding of protein trafficking pathways was developed by monitoring the maturation and compartmentalization of two vacuolar resident proteins, alkaline phosphatase (Pho8p) and Vma2p [191]. Pho8p is an integral membrane protein that localizes to the inner vacuolar membrane layer in wild-type vacuoles [192]. Vma2p is 60 kDa subunit of the multimeric membrane protein complex known as the vacuolar H^+-ATPase (V-ATPase) which is required for vacuolar acidification[193]. Specifically, this subunit is a peripheral membrane protein that localizes to the cytosolic face of the vacuolar membrane. These studies found that these two proteins arrive at the vacuole independently of each other and thus provided a broader profile of vacuolar protein sorting classes than solely analyzing Cpy1p trafficking. Thus the current definitions of vacuolar protein sorting mutants are based on the following properties: Cpy1p localization and maturation, vacuolar morphology, vacuolar segregation structures, vacuolar inheritance, Pho8p localization, and V-ATPase localization.

The original classes A-C remain unchanged in their definitions but have been expanded to include additional criteria [190, 191]. Thus, class A describes mutants that are lacking in any detectable measure of vacuolar deficiency other than Cpy1p secretion. Class B mutants have a large number of segmented vacuole-like structures that have positive Pho8p localization, vacuolar acidification, and properly segment and inherit vacuoles into developing buds. Class C mutants lack all apparent vacuole-like structures, have diffuse fluorescent staining of V-ATPase, and punctuate Pho8p labelling with no plasma membrane association of either marker. Class D mutants retain a large morphologically distinct vacuole, and secrete abundant amounts of newly synthesized Cpy1p. They are, however, unable to generate a vacuolar pH gradient, and lack vacuolar localization of the V-ATPase. Additionally, these mutants have vacuole inheritance defects- they do not form segregation structures during budding, and the vacuoles of mother cells seem to spontaneously generate *de novo* from precursors. Of particular note, the gene *VPS45*

encodes a protein which is a member of this class and null mutants are typified by mislocalization of the 60 kDa subunit of the V-ATPase.

Class E mutants were observed to have a novel organelle, originally referred to as the class E compartment, and later described as the multi-vesicular body. Many of these class E mutants have been further described as components of the highly studied ESCRT pathway, at all stages from ESCRT-0 to ESCRT-III [194]. Finally, the class F mutants retain a hybrid phenotype somewhere between class A and class B. This group of mutants has a large central vacuole that is surrounded by smaller vacuole-like structures that both test positive for Pho8p and V-ATPase localization, and retain proper vacuolar acidification [191]. Study of the prevacuolar compartment (PVC) morphology in known vacuolar protein sorting (VPS) mutants has shown alignment with protein-interaction data and this has been suggested as a new level of classification [195].

Vacuolar Functions in Fungal Pathogens

Many fungal species have adapted the vacuole to enable a wide array of functions [196]. Due to the nutrient limitations encountered during host invasion, it is no surprise that modifications to the vacuole structure, function, and content are required for successful colonization. Not only does the vacuole serve as a reservoir of nutrients, but vacuolar segregation is requisite for hyphal growth in some filamentous fungi [197]. Herein the current understandings of vacuolar import in host invasion, adaptation, and pathogenesis for *C. albicans*, *Aspergillus* spp., and *C. neoformans* will be synthesized to provide a broader view of vacuolar contributions.

As previously mentioned, hyphal and pseudohyphal growth is mandatory for *C. albicans* invasion. These morphological switches are tightly regulated by signalling cascades that alter gene expression and cell cycle progression. The vacuole is involved in adaptation to host stress conditions and hyphal growth [198]. Mechanistic studies have shown that vacuolar acidification via Vph1p, a subunit of the V-ATPase, is required for resistance to metal toxicity, hyphal growth and virulence in a murine model [199]. Suppression of the gene encoding Vma3p, another subunit of the V-ATPase, yields decreased vacuolar acidification, aberrant vacuole morphology, impaired secretion of protease and lipases, and loss of hyphal growth [200]. Acidification is

requisite because many of the transport channels from the cytosol to the vacuole require proton antiport [196]. Without these transporters, vacuolar storage and detoxification is severely inhibited, allowing toxic materials to accumulate in the cytosol. Morphogenesis of hyphae requires vacuolar recruitment to sub-apical compartments, allowing the apical compartment to be predominantly occupied by cytosol [198]. If vacuolar acidification is inhibited, recruitment of vacuoles to the sub-apical compartments is impeded and hyphae cannot develop. Mutation of predicted *C. albicans* Rab GTPases that are believed to co-ordinate vacuolar morphogenesis via vesicular fusion events at the PVC caused reduced hyphal growth [201]. Specifically, in synthetic null mutants of *VPS21* and *YPT52* there were misshapen and fragmented vacuoles. Furthermore, these mutants had reduced ability to accumulate vacuolar FM4-64, indicating non-functional endocytosis and abrogated vacuolar localization of the virulence associated protein Mlt1p. These findings indicate that vacuolar-dependent processes can impact the emergent virulence of *C. albicans*.

Aspergillus spp. are ubiquitous environmental filamentous ascomycetous fungi that have a broad host range; several species are highly capable plant pathogens, while some colonize mammalian hosts, and still others are non-pathogenic. *A. nidulans* was the first filamentous fungal species to have a fully sequenced genome by 2003, and has been widely used as a genetic model in eukaryotic organisms. In general the study of *A. nidulans* has illuminated much of our understanding of the physiology of these pathogens. Of specific importance are two common human pathogens, *A. fumigatus*, and *A. clavatus*. Cellular morphogenesis from conidia to hyphal growth is required by *A. fumigatus* to evade innate immunity and to penetrate host lung tissues. Observations in *A. nidulans* have indicated that endosome recycling at the hyphal tip is strongly correlated with hyphal growth rates; these endosomes traverse the cell on microtubules in a dynein and kinesin-dependent manner [202]. These internalized endosomes recruit Rab5p, a rab GTPase, that in turn recruits Vps45p, a modulator of PVC targeting [203]. Vacuolar size was reduced in a *rabBΔ* mutant that lacks a subunit of Rab5p, indicating that these proteins target bound endosomes for vacuolar degradation. Endosomes have also been implicated in the pH stress response by manipulating components of the ESCRT 0-III complexes [204]. Thus, not only are endosomes responsible for returning protein from the hyphal tip for degradation, but they may also be a uniquely adapted environmental sensor for pH [204].

In the pathogen *A. fumigatus*, vacuolar perturbation affects morphology, hyphal growth, and nutrient acquisition. The major phosphate sensitive transcription factor in *A. fumigatus*, PhoBp, (which is homologous to Pho80p in *S. cerevisiae*) was determined to be an upstream regulator of 1422 genes. Cells lacking PhoBp exhibited decreased hyphal emergence, constitutive uptake of phosphate to the vacuole, increased sensitivity to cyclosporine A and calcium, and a general inability to appropriately respond to cellular phosphate signalling [205]. The vacuolar iron transporter CccAp is required for uptake of cytosolic iron from ferricrocin, an intercellular siderophore, internalized extracellular siderophores, and soluble iron [206]. When *CCCA* is deleted, toxic accumulation of iron occurs regardless of ferricrocin abundance or the presence of siderophore degradation products which functionally chelate cytoplasmic iron and accumulate in the cytosol of *cccaΔ* mutants [206]. Thus, the flow of cytosolic iron and phosphate into the vacuole can have a dramatic effect on hyphal growth which is indirectly related to pathogenicity.

Vacuolar Functions in *Cryptococcus* spp.

Vacuolar function is of great significance during the adaptation to the host environment. In *C. albicans*, exploration of the linkage between vacuolar pH and pathogenesis was first characterized by gene deletion strains of the cryptococcal V-ATPase gene, *VPH1*. Deletion strains exhibit avirulence in murine infection models, decreased intracellular survival in macrophage interaction assays, decreased melanization, reduced viability upon growth at 37°C, and reduced capsule size [207]. Mutations in the vacuolar homotypic fusion gene *VPS41* resulted in avirulence in mice and inability to survive in macrophages which has been linked to exit from the G2 phase during the starvation response [208]. In *C. gattii*, vacuolar superoxide dismutase, *SOD1*, is necessary for survival when challenged by oxidative stress in a neutrophil cell line [209]. Deletion mutants were attenuated for virulence in a murine model, and also had severe vacuolar fragmentation. Like in *A. fumigatus*, disruption of the ion transport process into the vacuole of *C. neoformans* has also been associated with defects in virulence factor elaboration and pathogenesis. Two vacuolar calcium ion transporters Vcx1p and Pmc1p, are responsible for maintaining cytosolic calcium homeostasis and subsequently have deleterious effects on calcineurin-dependent signalling [210, 211]. *VCX1* deletion mutants are inefficiently phagocytosed by macrophages, have increased susceptibility to cyclosporine A, have a decreased

abundance of extracellular free GXM, and were hypovirulent in a murine infection model [210]. *PMC1* when deleted in the background of a *vcx1*Δ mutant causes increased levels of cytosolic calcium, and hypovirulence in a murine model with a decrease in pulmonary and brain colonization[211]. These trends do seem to implicate the importance of the vacuole as a bifurcated reservoir, primarily as storage, but also in the recruitment of cytosolic ions that can block extracellular signalling cues.

Vacuolar morphology is influenced by signalling functions including protein kinase A (Pka1), a major regulator of virulence [212]. In a constitutively active Pka1p mutant of *C. neoformans*, vacuole diameter is six-fold greater than wild-type cells [213]. Induction of melanization, capsule, and hypervirulence are also associated with this mutation. In *S. cerevisiae*, *v*acuolar morphology changes have been associated with an accumulation of discrete inositol phosphates. These signalling molecules impact a variety of cellular processes including apoptosis, autophagy, cell motility, endocytosis, differentiation, and growth [214]. Mutational analysis of this signalling pathway in *C. neoformans* identified a link between Pka1p and virulence [215]. Inositol signalling requires the polyphosphorylation of a phosphatidylinositol and the cleavage of this moiety to release a free inositol triphosphate. The enzymes responsible for these steps have been determined in *C. neoformans*: Arg1p is the primary inositol polyphosphate kinase and Plc1p is the primary phospholipase [216]. *ARG1* deletion mutants have a single large vacuole, are hypovirulent in a murine model, and have decreased cell wall integrity when exposed to Congo red stress. *PLC1* deletion mutants also accumulate a single large vacuole, exhibit defective endocytosis, and are similarly hypovirulent in a murine model. Treatment of *C. neoformans* with the anti-malarial drugs, quinacrine and chloroquine, results in high titre vacuolar accumulation of the drug that correlates with decreased thermotolerance, capsule elaboration, and melanization [217]. Additionally, these drugs increase macrophage killing of *C. neoformans*, and are protective against fungal infection in murine models of cryptococcosis [217, 218]. When taken together, a strong correlation which integrates multiple signalling pathways between vacuolar function and virulence can be observed in *C. neoformans*.

Vacuolar Trafficking in S*accharomyces cerevisiae*

Eukaryotic trafficking involves the movement of cargo, which can be composed of proteins, lipids, sterols, sugars or waste products, between compartments in the cell that are

separated from the cytosol by lipid membranes. To facilitate this process, eukaryotes utilize small membrane structures called vesicles. To generate these vesicles large protein scaffolds bind to existing membranes, cause deformation, lipid extrusion, and eventually encapsulation resulting in a final separation from the mother membrane. There are three well-described mechanisms for generating these vesicles and they are defined by the coat protein from which the vesicle is derived. Clathrin-coated vesicles function to facilitate vesicle budding between the trans-Golgi network and the plasma membrane, the trans-Golgi network and endosomes, and the plasma membrane and endosomes [219]. COPII-coated vesicles originate at the endoplasmic reticulum and traffic proteins towards the *cis*-Golgi network through to the *trans*-Golgi network [220]. COPI vesicles function in retrograde transport from the *trans*-Golgi network to the endoplasmic reticulum [221]. Once these vesicles are generated, a complex process that manages the transport, targeting, and fusion begins.

Vesicular fusion with the intended membrane is generated via a complex system of cytosolic proteins (soluble N-ethylmaleimide-sensitive factor attachment proteins (SNAP's)), integral membrane proteins (SNAP receptors (SNARE's)), chaperone-like proteins (Sec1/Munc18 family proteins (SM proteins)), and Rab GTPases which catalyze the fusion events [222]. The unique interactions between the SNARE proteins found on vesicles (v-SNARE) and the SNARE proteins which they tether in target membranes (t-SNARE) define the specificity of the vesicle. Recently, this nomenclature has changed in favour of defining the SNARE by presence of a glutamine (q-SNARE) or an arginine (r-SNARE) within the hydrophobic pocket of the fully associated SNARE and SNAP complex prior to fusion. This region of co-ordinated hydrophilic bases within the hydrophobic pocket has been defined as the "zero ionic layer" and in mutational studies is required for proper dissociation of the fusion complex [223]. Many toxins have been discovered which inhibit a wide variety of these protein interactions; an example being Botulinum toxin which is able to cleave cytosolic SNAP 25 and inhibit acetylcholine release at the neuromuscular junction by abolishing proper SNARE complex assembly [224].

The SM group of proteins are essential for SNARE-mediated trafficking. As defined by studies of Munc18, this group of proteins recognizes a conserved N-terminal three helical domain responsible for proper localization (Habc) present in syntaxin-like SNAREs. Munc18

binding of the Habc domain results in a conformational stabilization, effectively extending the cellular half-lives of bound SNAREs [225]. Upon proper priming during membrane fusion, the SM protein is able to induce a conformational change in the Habc domain allowing it to either co-ordinate the fusion events in SNARE associated membrane docking, or actively participate in the process [226]. SM proteins are attractive candidates which when mutated or deleted result in a lowered abundance of the cognate SNARE proteins which they are able to bind. This is a useful strategy because many SNARE proteins serve essential functions. Thus, the analysis of null SM protein mutants can allow the investigation of the function of the interacting SNARE proteins.

Vps45p Function in *Saccharomyces cerevisiae*

Of particular interest is the trafficking of components to the vacuole, as studied in the model yeast *S. cerevisiae*. The vacuolar protein sorting class D gene *VPS45* encodes an SM family protein that encodes a product that participates in vacuolar protein sorting, by interacting with endosomal and Golgi apparatus derived vesicles via the SNARE protein assemblages at the PVC, and late Golgi network [227-229]. The effects on the cell are largely due to the breakdown of cellular trafficking and include class D like vacuolar phenotypes, temperature sensitivity, osmotic pressure sensitivity, cell wall stress sensitivity, and a variety of increased drug susceptibilities. Vps45p is atypical relative to other members of the SM family because it has two SNARE binding partners Tlg2p [227] and Pep12p [230]. Vps45p dependent functions are briefly summarized herein (Figure 2).

Tlg2p is a t-SNARE with high similarity to mammalian syntaxin 1 that is involved in late Golgi network trafficking in *S. cerevisiae*. Molecular characterization has shown that it interacts with the v-SNARE Vti1p and the SM protein Vps45p [227, 231]. Vps45p, Tlg2p and Vti1p participate in the fusion of endosome and PVC-derived vesicles at the late Golgi network [231]. Tlg2p shares amino acid sequence similarity to Tlg1p, a t-SNARE which interacts with Vti1p to fuse late Golgi network derived vesicles with the endosome, also known as anterograde transport. Intra-Golgi apparatus trafficking is managed by the t-SNARE protein Sed5p [232-234]. Membrane trafficking events require a proper balance of anterograde and retrograde traffic to maintain Golgi apparatus morphology, to return cargo proteins, and to maintain lipid composition of the network. These recycling steps are critical because if one direction of the

pathway is inhibited or lagging, the other can lag as a result. Vps45p maintains the stability of Tlg2p which decreases Tlg2p degradation, and primes membrane fusion events at the PVC [227, 228, 235]. It is through these actions that Vps45p appears to maintain the balance of trafficking events between the endosome and late Golgi network.

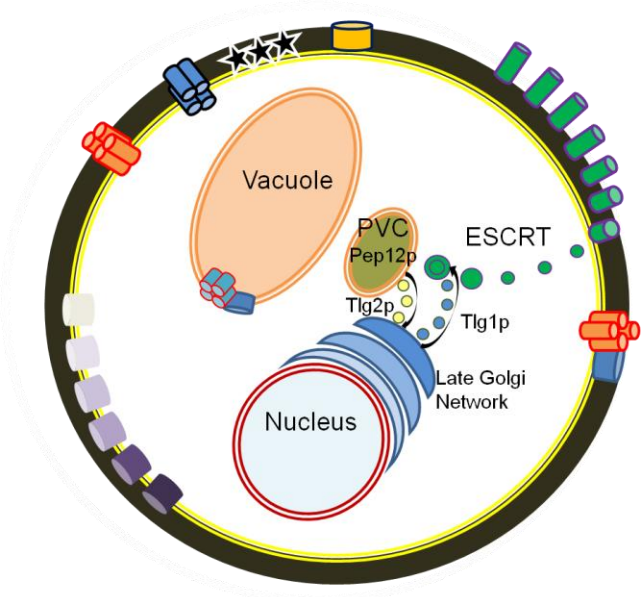

Figure 2. Vps45p dependent trafficking events in *Saccharomyces cerevisiae.* The t-SNARE's Tlg2p and Pep12p physically interact with Vps45p [227-229]. This interaction extends the half-lives of the t-SNARE's.Vps45p also facilitates fusion reactions with Tlg2p, and Pep12p assembled SNARE complexes [235]. Loss-of-function mutations in *VPS45* have shown that these mutants have class D-like vacuolar morphology. Tlg2p is a resident t-SNARE of the late Golgi network responsible for fusion of recycled cargo from the PVC and plasma membrane [231]. Tlg1p is a v-SNARE responsible for anterograde protein sorting from the late Golgi network to the developing endosome. In *tlg2*Δ mutants similar defects to *tlg1*Δ are observed indicating that these processes are linked [231]. Pep12p is a resident PVC t-SNARE that interacts with a wide array of endosomal and Golgi apparatus-related trafficking proteins and is responsible for fusion events with endosomal, Golgi apparatus, and vacuolar-derived vesicles [230, 236-238].

Pep12p is a t-SNARE with high similarity to mammalian syntaxin 1, and was first identified in a mutational screen for defective vacuolar transport of Cpy1p (the pep designation

originates from carboxypeptidase Y). Pep12p is the resident t-SNARE of the PVC, and is required for tethering and fusion of vesicles derived from the Golgi apparatus, endosomes, and the vacuole [228]. *PEP12* mutants have a class D vacuole morphology, and closely phenocopy *vps45*Δ strains. Pep12p interacts with Vps45p, Sec18p, and Pep7p *in vitro* [230]. Sec18p is an NSF-like protein that is required for SNARE fusion complex priming and disassociation at the vacuolar face and for homotypic vacuolar fusion [236]. Pep7p is an adaptor protein capable of binding both phosphatidylinositol 3-phosphate, an important surface marker of the endosome and vacuolar compartment during logarithmic growth [237], and protein components of the PVC SNARE fusion complex [235]. Pep12p also physically interacts with Vps21p, a Rab GTPase required for Golgi-PVC transport [238]. In a *vps45*Δ *pep12* temperature-sensitive mutant the vacuolar sorting defects are greatly intensified: 100% of Cpy1p is secreted and vacuolar targeting of Vph1p is abolished, however, Pho8p was unaffected and able to localize to the vacuole [230]. Further characterization of Pep12p has shown physical interactions with Vti1p, integrating the function of Pep12p PVC fusion of Golgi-derived vesicles [228]. Pep12p is positioned at the entrance point into the vacuole from both endocytotic movement and Golgi-derived vesicles.

Vps45p Function in *Homo sapiens*

Congenital neutropenias are genetic disorders wherein the circulating neutrophil count is substantially lower than in a healthy individual [239]. Neutrophils are a constituent of innate immunity, and are the primary circulating monocytes responsible for the phagocytosis of invading pathogens. The significance of neutropenia is a marked decrease in innate immunity, thus presentation of severe acute infections by bacteria and fungi are common. Patients are also at risk of developing myelodysplastic syndrome and acute myeloblastic leukemia [239]. There are a broad range of genetic factors which can result in neutropenia presentation, and as such the risk factors of acute infection or long-term disease state progression are variable. Recently, several unique point mutations in the human gene encoding Vps45p have been correlated with severe congenital neutropenia type 5 [240, 241]. Initial analysis of the *H. sapiens VPS45* gene locus was done by complementation experiments in *S. cerevisiae*. Complementation of *vps45*Δ *S. cerevisiae* with *H. sapiens VPS45* cDNA taken from a disease carrier and a healthy control implicate that Vps45p is non-functional in the disease condition [240]. Phenotypically, yeast

cells appear to have disrupted vacuolar transport consistent with the background *S. cerevisiae vps45*Δ mutant. These experiments were repeated in a Zebra fish model of *VPS45* and were congruent [241]. Mechanistically, the evidence suggests that defective endosomal membrane trafficking results in impaired cell line development, impaired cell type mobility, and increased apoptosis of neutrophils, fibroblasts, and bone marrow [240, 241]. Specifically, β1-integrin cell surface display is decreased in mutant fibroblast and neutrophil cell lines, which may explain defective signalling, and motility [241]. Therefore, direct treatment of cryptococcosis with a Vps45p specific drug would be deleterious to the patient, and may cause immunosuppression. However, the conservation of the important role of Vps45p in humans does illuminate the physiological importance of protein trafficking within the endosome membrane system, and potential for new drug development exists if a unique fungal process is discovered.

Thesis Objective

In *C. neoformans*, global regulators of gene expression have been extensively examined because they can be quickly identified by protein identity and can prove highly informative when describing adaptive responses. HapXp has been shown to be an up-stream regulator of the transcriptional response to extracellular iron composition [242]. Within the regulatory network of HapXp is a gene with high similarity to *S. cerevisiae VPS45*. Specifically, the transcript levels of this open reading frame, CNAG_03628.2, were reduced in a *hapx*Δ mutant with respect to wild-type transcription in low iron (~3-fold) and high iron (~5-fold) conditions. Interestingly, the mutant *hapx*Δ strain was hypovirulent in a murine model and was unable to utilize heme when supplemented. We aim to investigate the role of vacuolar protein trafficking on the uptake of iron, the expression of virulence factors, and the pathogenic growth of *C. neoformans*. This will be done by analyzing a deletion mutant of the predicted *C. neoformans* ortholog of Vps45p. If the gene product is functionally conserved deletion of the chromosomal locus will yield class D-like vacuolar morphology by breakdown of transit through the PVC. There is strong evidence to suggest that iron acquisition will be affected, as implicated by HapXp regulation [242] and in the ESCRT-I *vps23*Δ mutant [179]. Furthermore, this mutation may affect virulence factor elaboration, as seen in V-ATPase studies [207, 243]. Therefore, our primary goal is to explore the possibility that vacuolar trafficking plays a necessary role in the establishment of virulence in the human fungal pathogen *C. neoformans*.

Brief Summary

A chromosomal deletion of the *VPS45* locus was successfully performed in strain H99 of the *C. neoformans* var. *grubii* (serotype A) background. Phenotypic analysis showed that mutants were unable to grow robustly in minimal media supplemented with heme as a sole iron source, and utilization of $FeCl_3$ was also reduced. These mutants also had aberrant vacuolar morphology, and mislocalized a vacuolar green fluorescent protein. Sensitivity to cell wall integrity agonists was increased, as was osmotic stress, and mutants had an increased susceptibility to chloroquine and quinacrine. No distinguishable virulence factor defect was observed because mutants were melanized at near wild-type levels, growth at 37°C was not reduced, and mutant cells produced a polysaccharide capsule. Finally, macrophage survival after 24 hours was significantly decreased in both human and mouse macrophage cell lines. These results indicate that vacuolar trafficking is required for appropriate utilization of extracellular iron, tolerance to cell wall stressors, and for intracellular growth.

Materials and Methods

Growth Media

Fungal growth is performed predominantly in YPD rich media [1.0 % yeast extract (w/v), 2 % peptone (w/v), and 2.0 % dextrose (w/v), pH 7.4 (BD 242810), in ddH_2O. If solid media is needed, 2 % agar (Sigma A1296) is added before sterilization by autoclaving, and Petri dish plates are filled with 25 mL agar. For selection of mutants resistant to the antifungal drugs nourseothricin[NAT (GoldBiotech N500-5)] or geneticin [Neo (Sigma A1720-1G) after biolistic transformation, selective solid media are produced by mixing 50°C YPD agar with drug to yield a final concentration of 100 μg/mL and 2 μg/mL, respectively. Recovery media is supplemented with 1M D-sorbitol (Fischer Scientific 10293805). YPD agar base is used to generate a series of plates containing chemicals to generate cell wall and other stresses: sodium dodecyl sulphate [SDS (Sigma L3771)] at concentrations of 0.01 %, 0.02 %, 0.03 %, 0.04 %, and 0.05 % (w/v), NaCl (Fisher Scientific S271-10) at concentrations of 0.5 M, 1.0 M, 1.5 M, and 2.0 M, 0.5 mg/mL Congo red (Sigma C6767-25G), and 0.5 mg/mL caffeine (Sigma C0750). The synthetic minimal media yeast nitrogen base [YNB (BD 239210)] is prepared according to manufacturer's instructions; D-glucose (Sigma G8270-10KG) is used as a carbon source (0.5 % w/v), adjusted to pH 7.4, and 2% w/v agar is added if desired. Amino acid depleted YNB is prepared by mixing YNB minus amino acid base mix (BD 291940) with added carbon source, and the pH of the medium is adjusted as described above. Low iron YNB is prepared as above except that iron-chelated ddH_2O is used. Iron-chelated ddH_2O is produced by flowing ddH_2O through a Chelex (Bio-Rad 142-2832) matrix on a gravity column, at a ratio of 5 g Chelex for 3 L of ddH_2O. The drugs chloroquine and quinacrine are used to supplement solid and liquid culture media. Chloroquine and quinacrine stock solutions are generated by solvation in ddH2O, YNB or YPD to a final concentration of 20mg/mL or 40mg/mL, respectively, and filter sterilized using 0.40 μm Luer lock syringe filters (Sarstedt 83.1826). These stock solutions are then used to supplement prepared media. Chloroquine (Sigma C6628-25G) concentrations in YNB and YPD agar media are 2.0 mM, 3.0 mM, 4.0 mM, 5.0 mM, 6.0 mM, and 7.0 mM; liquid YNB cultures are set at 0.50 mM, 0.75 mM, 1.0 mM, 1.5 mM, 2.0 mM, 2.5 mM, 3.0 mM, 3.5 mM, and 4.0 mM. Quinacrine (Sigma Q3251-25G) concentrations utilized on YNB and YPD plates are 0.4mM, 0.5 mM, 0.6 mM, 0.7 mM, 0.8mM, and 0.9mM; liquid YNB cultures are set at 500 μM

and 1 mM. Fluorescent brightener 28, or calcofluor white [CFW (Sigma F3543-5G)] is added to YNB media before autoclaving at final concentrations of 0.5 mg/mL or 1.0 mg/mL.

Iron-dependent growth is assayed on both defined low iron media (LIM) and YNB prepared with chelated ddH_2O, with the additional iron chelating agent bathophenanthroline disulfonate [BPS (Sigma B1375-5G)]. LIM is prepared according to a standard protocol and contains sterile chelated ddH_2O, 0.5% w/v glucose, 0.5 % w/v L-asparagine (Sigma A8381), 2.3 mM K_2HPO_4 (Sigma P3786-500G), 1.7 mM $CaCl_2$-$2H_2O$ (Sigma 22,350-6), 189 μM $MgSO_4$-$7H_2O$ (Mallinckrodt AR 6066), 20 mM HEPES (Fisher Scientific BP310-500), 21 mM $NaHCO_3$ (Fisher Scientific S271-10), and with pH adjustment to 7.4 with low iron KOH (Sigma D1767). BPS is first suspended in chelated ddH_2O to a working concentration of 150 mM, filter sterilized and stored at 4°C in the absence of light. Hemin (Sigma 51280-5G) is dissolved in 0.2 M NaOH (Fisher Scientific 5318-1) to a final stock concentration of 50mM and stored at 4°C in the absence of light. $FeCl_3$ (Acros Organics 169430010) is dissolved in 0.1 M HCl (Fisher Scientific 381285-212) to a final stock concentration of 100 mM, syringe tip filter sterilized, and stored at 4°C in the absence of light. These chemicals are then added to low iron YNB or LIM (with additional 2 % agarose w/v). The final working concentration of BPS is 150 μM in the low iron YNB plates only, hemin and $FeCl_3$ are used at 10 μM and 100 μM in both YNB + 150 μM BPS and LIM agar media.

Melanization is observed by growth on agar plates containing L-dopa. This medium is prepared with a 10X nutrient broth consisting of 1.0 % w/v glucose, 1 % w/v L-asparagine, 3.0 % w/v KH_2PO_4, 0.25% w/v $MgSO_4$, and 0.2% w/v L-dopa [3,4-dihydroxyphenylalanine (Sigma D9628-25G)] in ddH_2O at a pH of 5.6. 1.0 mg of thiamine HCl (Sigma T4625) and 5.0 μg of biotin (Sigma B4501) are then added and the broth is vacuum filter sterilized (Sarstedt 83.1823). This solution is then mixed with 900 mL ddH2O containing 20 g of melted agar at pH 5.6, and 25 mL plates are prepared from this mixture.

DNA Isolation

DNA isolation from *C. neoformans* is performed utilizing two strategies, a "smash and grab" protocol which yields a high quantity of sheared DNA, and a "gentle extraction"

cetrimonium bromide (CTAB)-mediated cell lysis which yields a low quantity of high quality DNA.

"Smash and grab" lysis is performed by collecting cells from 2 mL of YPD medium overnight growth at 30°C with shaking. Cells are washed once in sterile ddH_2O water and then the pellet is suspended in 400 µL of ten minute buffer [2% Triton X 100 v/v (Sigma T8787-100mL), 1% SDS, 100 mM NaCl, 100 mM Tris-HCl pH 8.0 (Fisher Scientific BP152-10), 1 mM EDTA (Sigma ED255)]. Once resuspended, the mixture is transferred to a conical 2 mL screw cap O-ring microcentrifuge tube (Sarstedt 72.693.005). Mechanical digestion of cells for DNA isolation is performed by adding 600µL of 425-600 µm glass beads (Sigma G8772-1KG) with 400 µL of phenol:chloroform:isoamyl alcohol [25:24:1 (Sigma P3803-400mL)]. The suspension is mixed briefly by vortexing and followed by bead beating for three minutes. Immediately following the bead beating lysis, the mixture is cooled by transferring the tube to an ice bath for five minutes. The DNA-containing aqueous phase is separated by transferring the cooled tubes to a microcentrifuge (Eppendorf 5424) and applying maximum speed (15,000 rpm) for 10 minutes. The upper aqueous phase is transferred to a clean 2 mL microcentrifuge tube (Sarstedt 72.695.500) with 1 mL of ice cold 100% ethanol, mixed by inversion, and incubated at -20°C for 20 minutes. The precipitated DNA is collected in a pellet by maximum speed centrifugation for five minutes and then the supernatant is removed. Contaminating salts are removed from the pellet by washing the DNA in 1mL of 70% ethanol.The DNA pellets are incubated at 37°C for 15 min to evaporate the remaining ethanol and then are resuspended in 50 µL of sterile ddH_2O. RNase (Qiagen 19101) is added to a final concentration of 20 µg/mL and incubated for 30 minutes at 37°C to digest contaminating RNA. The DNA concentration is determined by the absorbance of samples at 280 nm and 260 nm by using the NanoDrop (NanoDrop ND1000 spectrophotometer). .

"Gentle extraction" requires a greater initial cell volume so starter cultures of 5 mL YPD are inoculated and grown overnight at 30°C with shaking [244]. The next day the cell cultures are transferred into a 250 mL Erlenmeyer flask containing 100 mL of sterile YPD. On the third day, 50 mL of cells are collected by centrifugation in 50mL falcon tubes (Corning 0553855) at 4000 x *g* for 15 min at 4°C in a high-speed centrifuge (Beckman-Coulter Avanti J-E) capable of housing a JS 5.3 rotor (Beckman-Coulter). Cells are washed twice with sterile ddH_2O collected

at 4000 x *g* for 10 min at 4°C, and then incubated at -80°C for at least 2 hours. Cells are then lyophilized overnight until dry. The dried pellet is ground into a fine powder by vigorous vortexing with 5 mL of 4 mm glass beads (Sigma Z143936). The cell powder is gently mixed with 10 mL of extraction buffer [100mM Tris-HCl pH 7.5, 1% w/v CTAB (Sigma H9151) , 1% 2-mercaptoethanol v/v (Sigma M6250), 0.7M NaCl, and 10mM EDTA] until a homogenous mixture is obtained. The mixture is then transferred to a fresh 50 mL falcon tube to remove the 4 mm glass beads. Cell lysis is performed by incubation at 65°C for 30 minutes. After the incubation period, the sample is cooled by immersion in tepid tap water for 20 minutes. Equal volumes of phenol:chloroform:isoamyl alcohol (25:24:1) are added to the cell lysate suspension, mixed by inversion, and separated by centrifugation at 4000 x *g* for 10 min at 4°C as described above. The aqueous phase is transferred to a fresh 50mL conical tube where an equal volume of pure chloroform (Fisher Scientific C298-4) is added. The tubes are then inverted and separated by centrifugation as described above. The aqueous phase is collected again, transferred into a new 50 mL conical tube, an equal volume of isopropanol (A416-P4) is added, and mixed by inversion. The precipitated DNA is separated by centrifugation at 4000 x *g* for 10 min at 4°C as described above. The supernatant is decanted and the DNA pellet is washed with 5 mL of ice-cold 70% ethanol. The supernatant is discarded and the DNA pellet is suspended in 1 mL of ddH_2O. The solution is then transferred to a clean 2 mL microcentrifuge tube, RNase is added to a final concentration of 20 µg/mL, and the solution is incubated at 37°C for 30 minutes. DNA concentration is determined by NanoDrop spectrophotometer and quality is assessed by gel electrophoresis on a 0.5% agarose (Invitrogen 1551027)/1X TAE [pH 8.0, 40mM Tris, 20mM acetic acid (Fisher Scientific 351271-212), and 1mM EDTA] gel to visualize DNA size.

Gene Identification and Phylogeny Analysis

Identification of the *VPS45* locus in *C. neoformans* is performed using a BLASTp search of the *C. neoformans var. grubii* H99 genome sequence (http://www.broadinstitute.org/) with the amino acid sequence of YGL095C, encoding Vps45p, from *S. cerevisiae* (http://www.yeastgenome.org/) [245]. This sequence is then used as a query in a BLASTp search of the *S. cerevisiae* protein sequence. The query is then extended against all fungal databases in a WuBLAST2p protein search, and a representative sample of highly similar proteins sequence is obtained, including the proteins from *A. fumigatus* and *Ustilago maydis*. Finally, the *Shigella*

flexneri VpsBp amino acid sequence is obtained from the NCBI gene database, and used as a query against known bacterial genes. The most similar protein sequence is identified in *Escherichia coli* corresponding to the protein coding sequence of the *MIAE* gene, corresponding to locus tag B3194.

Phylogenetic analysis is performed utilizing the MEGA6 software platform. Initial protein sequences of *C. neoformans* VpsBp (CNAG_03628.2**), *S. cerevisiae* Vps45p (YGL095C***), *U. maydis* UM02249 (*), *A. fumigatus* VpsBp (AFUA_6G04870*), *Homo sapiens* Vps45p isoforms 1-4 (NP_009190.2*, NP_001266282.1*, NP_001266283.1*, and NP_001266284.1*), *E. coli* MiaEp (B3194*), and *S. flexneri VPSB* (NC_004741.1*) are obtained from the NCBI Gene database (*), Broad database (**), or *Saccharomyces* Genome database (***). These protein sequences are entered into MEGA6 and aligned via the ClustalW tool with the following parameters: pairwise gap opening penalty 10, pairwise gap extension penalty 0.1, multiple gap opening penalty 10, multiple gap extension penalty 0.2, Gonnet protein weight matrix, residue specific penalties, hydrophobic penalties, a gap separation distance of 4, no end gap separation, negative matrix is not utilized, and delay divergent cut-off is set to 30%. This alignment is then assembled into a bootstrapped phylogeny based on the maximum likelihood statistical method. The following parameters are used: Jones-Taylor-Thornton model of amino acid substitution type, rates and sites are set to uniform rates, gaps or missing data in the alignment is deleted, under the nearest neighbour interchange ML heuristic method, and strong branch filter. The reported bootstrap values are filtered out if they are lower than 50.

VPS45 Knockout Scheme

All positions described herein will be with respect to the adenosine residue in the translational start codon (refer to Figure 3). The deletion cassette integrates between the -8 bp site and +2255 bp site that corresponds to 224 bp upstream of the translational stop codon. This insertion truncates the majority of the open reading frame, although three potential peptides may be synthesized of 9, 12 and 13amino acids in length. The resulting insertional mutant has integration of the nourseothricin resistance (NAT) marker (1646 bases) between the -8 bp and +2255 bp sites. Confirmation of NAT deletion cassette at the *VPS45* locus is determined by PCR amplification (Figure 3A). The presence of wild-type *VPS45* would result in amplification of a 598 bp fragment corresponding to the region of DNA between sites +922 bp and +1520 bp.

Integration of the NAT cassette is confirmed by PCR amplification using two primer sets that bind within the cassette and at the -1500 bp site or the +3440 bp site, producing fragments of 2164 bp or 2957 bp, respectively.

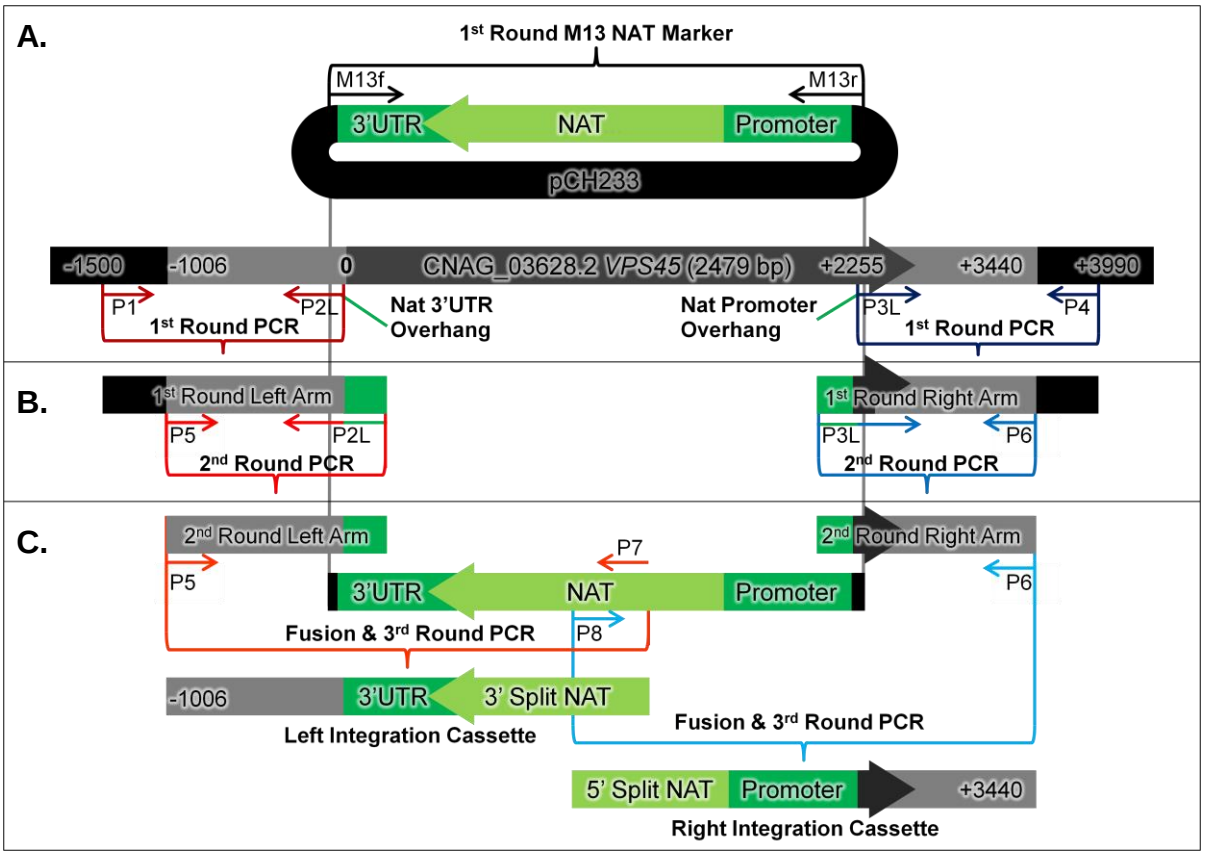

Figure 3. Schematic diagram of the *VPS45* locus and deletion cassette strategy. A) First round PCR reactions using the primer pairs that are colour-co-ordinated (refer to Table 1 for nucleotide sequence information). Amplification of the left and right arm included the addition of an overhanging fragment, pictured in green, for fusion reactions later in the protocol. B) Second round PCR reaction conditions using paired primers as indicated by colour. C) Fusion of NAT marker to Left and Right Arms to generate a split integration cassette.

Knockout Cassette Generation

Double-joint PCR split marker is utilized to generate two fragments for targeted gene deletion. This process, optimized for *C. neoformans*, relies primarily on PCR amplification of three regions: a left arm homology region, the marker, and a right arm homology region [246, 247] (Figure 3A). The left arm region is then fused to a segment of the marker by joint PCR, and the right arm to the reciprocal segment (Figure 3B). First round PCR is completed using primer pairs P1 + P2L and P3L + P4 d (refer to Table 1 for nucleotide sequence information) on 10 ng

Table 1. Primer list for targeted *VPS45* gene deletion, cassette generation, PCR confirmation, and Southern blot analysis. Listed abbreviations for primer names are referred to in Figures 3 and 4, and the Full Name is also provided. The DNA sequence is included and proceeds from the 5' to 3' end. All primers are synthesized, purified and quantified by Invitrogen.

Abbreviation	Full Name	DNA Sequence
P1	vps45ko1	gcccgcaaagaatgtcatgtc
P2L	vps45ko2long	gtttctacatctcttccgtgttaatacagatatgccctgtgggttgaacg
P3L	vps45ko3long	catgcttatgtgagtcctccccttcccgtgcaagcggagtgagtctaag
P4	vps45ko4	aagggcgatgagatcaagg
M13f	M13F	gtaaaacgacggccagt
M13r	M13R	aacagctatgaccatg
P5	vps45ko5	gacatctgtgcccatgac
P6	vps45ko6	cgttctccagcgagtaag
P7	natsplitleftarm	aaggtgttccccgacgacgaatcg
P8	natsplitrightarm	aactccgtcgcgagccccatcaac
P9	vps45negconf	gacccagtgacaccgttattg
P10	vps45negconr	tgatagcggagagcatagagg
P11	natconf	atgaccatgattacgccaag
P12	natconr	gttttcccagtcacgacgtt
P13	vps45southernprobefwd	cgaaagccaagatggatgag
P14	vps45southernproberev	cgacagtggtgatgaagaac

of *C. neoformans* wild-type DNA, with *Ex taq* polymerase (*TaKaRa* RR001C) (98°C for 5 min once; 98°C for 30 seconds, 55°C for 30 seconds, 72°C for 1.5 minutes 35 times; 72°C for 5 min once; then incubation at 10°C) (Figure 3A). The NAT marker is amplified using the primer pair, M13f and M13r, on 10 ng of purified pCH233 plasmid DNA template (Figure 3A), with *Ex taq* polymerase (98°C for 5 min once; 98°C for 30 seconds, 55°C for 30 seconds, 72°C for 2 minutes 35 times; 72°C for 5 min once; then incubation at 10°C). The products are analyzed on a 0.8% agarose TAE gel by electrophoresis, and subsequently gel purified with the QIAquick Gel extraction Kit™ (Qiagen 28706). Second round PCR is performed to purify the first round product from the left arm and right arm synthesis reactions (Figure 3B). 10 ng of gel-purified PCR product from round one is used as template, with corresponding primer pairs P5 + P2L and P3L + P6, with *Ex taq* polymerase (98°C for 5 min once; 98°C for 30 seconds, 55°C for 30 seconds, 72°C for one minute 35 times; 72°C for 10 min once; then incubation at 10°C) (Figure 3B). Fusion PCR is performed in a substrate ratio gradient set of homology arm:Nat marker at 1:1, 1:3, 1:9, 3:1, 9:1 with 1 corresponding to 50ng total DNA, with *Ex taq* polymerase (98°C for 5 min once; 98°C for 30 seconds, 55°C for 10 min, 72°C for 5 minutes 15 times; 72°C for 10 min once; then held at 10°C) (Figure 3C). The products are analyzed and purified as above. Third round PCR amplification is performed utilizing 10ng of isolated fusion fragments (corresponding primer pairs P5 + P7 and P6 + P8), with *Ex taq* polymerase (98°C for 5 min once; 98°C for 30 seconds, 55°C for 30 seconds, 72°C for 2.5 minutes 35 times; 72°C for 5 min once; then held at 10°C) (Figure 3C). The products are analyzed and purified as above. DNA concentration is determined by NanoDrop spectrophotometer as above.

Biolistic Bombardment for DNA Transformation

Biolistic bombardment is performed with recombination cassette DNA labelled-tungsten beadsthat are accelerated by an explosion of helium gas and then forced to penetrate fungal cells on a recovery plate. The beads deposit the DNA fragments as they pass through the cells; this approach has been optimized for *C. neoformans* [248]. To prepare target cells for transformation, a single isolated colony is transferred to 5 mL of YPD and incubated at 30°C with shaking overnight. This 5 mL starter culture is transferred to 50 mL of fresh YPD the next day in a 250 mL Erlenmeyer flask and is incubated overnight at 30°C with shaking. These cells are collected by centrifugation in a 50 mL falcon tube at 4000 x *g* for 10 min at 4°C on the third day, and

washed twice with sterile ddH_2O as above. The subsequent cell pellet is suspended in 5 mL of ddH_2O and 400 μL of these cells are transferred onto recovery plates (25mL of YPD, 1M sorbitol, and 2% w/v agar) to dry at 30°C.

Tungsten beads must be processed to allow recombination cassette DNA to adhere prior to bombardment. Processing starts by suspension of 60.0 mg of tungsten beads [0.6 μm diameter (Bio-Rad 1652266)] in 1 ml of absolute ethanol in a clean 1.5 mL microcentrifuge tube (Sarstedt 72.706). The beads are then collected by centrifugation at 12,000 x *g* for 1 minute and the ethanol is removed. The beads are washed once in 1 mL of ddH_2O before final suspension in 1.0 mL sterile ddH_2O for storage at 4°C until use. 10 μL of tungsten beads are loaded by stepwise addition of 2.0 μg of recombination cassette DNA (1 μg of each left and right fragments) suspended in ddH_2O, 10.0 μL of 2.5 mM $CaCl_2$, and 2.0 μL of 1.0 M spermidine [free base(Sigma S626)]. The solution is mixed by rapid pipette expulsion and left to precipitate onto the beads for 10 min at room temperature. The beads are then collected by centrifugation as described above, and the supernatant fully removed. The pellet is washed in 0.5 mL of absolute ethanol, without mixing, pulsed for 10 seconds in a microcentrifuge at maximum speed, and the supernatant decanted. The beads are then suspended in 10 μL of absolute ethanol, and transferred by micropipettor onto the centre of a sterile microcarrier membrane (Bio-Rad 1652335).

Biolistic bombardment is performed utilizing a helium particle delivery system [gene gun (Bio-Rad PDS100)] where helium pressure builds behind a rupture disc until the pressure exceeds 1,350 psi. Once the pressure is exceeded, the disc ruptures to release an explosive blast that pushes the microcarrier, and subsequently the beads, toward the target cells. The microcarrier abruptly stops as it hits the stainless steel stopping screen (Bio-Rad 1652336) releasing the beads. These particles continue toward the target cells, pass through them and lodge in the plate below. This process is done under a vacuum of 2800 psi, and in a sterile biological safety cabinet. The target cells then are allowed to grow and recover overnight at room temperature. 1350 rupture discs (Bio-Rad 1652330) are utilized to insure internal pressure greater than 1, 350 psi is achieved. Stainless steel stopping screens are used internally to prevent the microcarrier, and rupture disc from damaging the recovery plate and target cells below

After a single day of recovery, cells within the blast radius, visualized by the tungsten-stained media, are isolated using cell scrapers (Nunc 179707), and deposited into 1.5 mL microcentrifuge tubes. The cells are then washed with sterile ddH_20, and resuspended with sterile ddH_2O to 1 mL where 250 µL are then transferred to selective plate medium. In the case of the *vps45*Δ::NAT construct, 100 µg/mL nouroseothricin is used for selection. To generate the *vps45*Δ::NAT mutation in the *CFO1-GFP*: Neo background 2 µg/mL geneticin, and 100 µg/mL nourseothricin YPD agar is used. These selection media are incubated at 30°C until resistant colonies appear (typically within 3-5 days). A pure strain of these colonies is isolated by multiple rounds of selective streaking to isolate single clonal mutants.

PCR Confirmation

"Smash and grab" DNA extractions are performed on isolated colonies to be screened for correct integration of transforming DNA. DNA concentration is quantified by NanoDrop analysis, and adjusted to 10 ng/µL. Four PCR reactions are conducted on each isolated colony: one "negative" screen is performed to assay for the presence or absence of the deleted region of *VPS45* using primer pair P11+ P12, and two "positive" reactions are performed to confirm correct insertion of the left arm of the split NAT marker cassette (primers P1 + P10) and the right arm insertion (primers P4 + P9) (Figure 4A). PCR reaction conditions are performed using *Ex taq* DNA polymerase: 98°C for 5 minutes once; 98°C for 30 seconds, 55°C for 30 seconds, 72°C for 2.5 minutes 35 times; 72°C for 5 minutes once; then held at 10°C. PCR products are visualized by electrophoresis on a 0.8% agarose TAE gel.

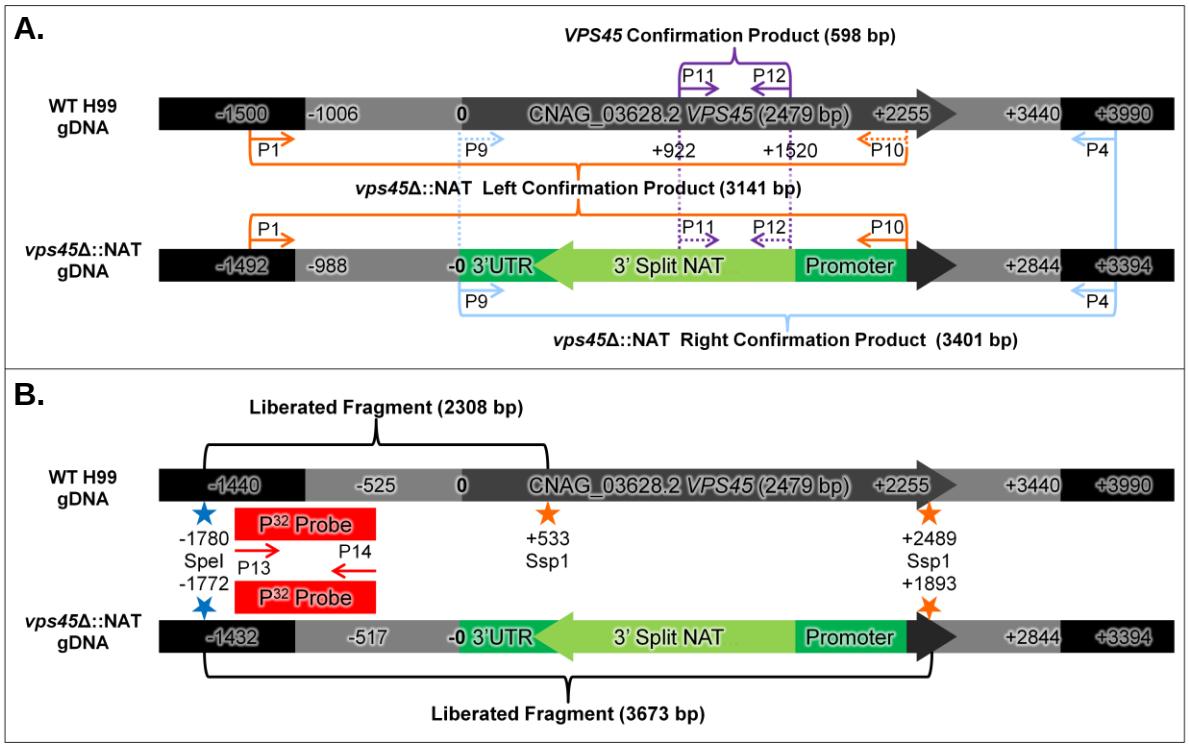

Figure 4. Schematic of the *VPS45* locus for PCR confirmation and Southern blot analysis of deletion. A) Primer combinations for PCR confirmation are colour coordinated; if a primer binding site is missing the corresponding line is dotted. A *VPS45* gene control is included, and PCR amplification with primers P11 + P12 yields a 598 bp fragment. In addition, confirmation of integration of the left arm of the integration cassette is performed using primer pair P1 + P10 with a predicted amplification length of 3141 bp. The right arm confirmation reaction is performed using primer pair P9 + P4, with a predicted product of 3401 bp. B) Schematic of the Southern blot for analyzing the structure of the *VPS45* locus. Genomic DNA is isolated and subsequently digested with two restriction enzymes, Spe1 (blue stars) and Ssp1 (orange stars). The specific recognition sites are listed relative to the first adenosine nucleotide residue of the first codon set to 0, and in the *vps45*Δ mutant to the first nucleotide residue of the NAT marker (-8 site in H99). A P^{32} labelled probe is synthesized from H99 genomic DNA utilizing primer pair P13 + P14, and used to detect digested DNA. It is predicted that H99 digestion will liberate a 2308 bp fragment that will allow probe annealing, and 3673 bp if the *vps45*Δ::NAT cassette integrate properly, due to the loss of the Ssp1 restriction enzyme binding site at +533 bp.

Southern Blot Preparation and Hybridization

The schematic for the *VPS45* Southern blot analysis is shown in Figure 4B. Three cut sites exist across the gene locus in wild-type strain H99 genomic DNA; SpeI at -1780 bp, and SspI at +533 bp and +2489 bp. In mutant clones, integration of the *vps45*Δ::NAT cassette replaces 2255 bp of genomic DNA with 1679 bp of marker DNA, and removes the SspI +533 site. Subsequently, double digestion of the genomic DNA is predicted to liberate a 2308 bp in wild-type strain H99 genomic DNA, and a 3678 bp fragment in mutant *vps45*Δ::NAT mutant genomic DNA.

Southern blot analysis is performed on DNA samples from both the "smash and grab", and "gentle extraction" protocols. Genomic DNA samples are digested using high fidelity restriction enzymes SpeI-HF (NEB R3133S) and SspI-HF (NEB R3132S). After digestion, DNA is purified via the QIAquick PCR purification kit (Lifetechnologies 28104), separated by gel electrophoresis, and transferred to a nylon membrane. Probe template is generated by PCR amplification (primer pair P13 + P14) of 10 ng of wild-type strain H99 genomic DNA with *Ex taq* polymerase (98°C for 5 min once; 98°C for 30 seconds, 55°C for 30 seconds, 72°C for one minute 35 times; 72°C for 5 min once; then held at 10°C). P^{32} radiolabelled probe is generated from Klenow DNA polymerase synthesis in the presence of P^{32}-dCTP nucleotides (Perkin Elmer BLU 513H500UC) using the DECAprime™ II kit (Life technologies AM1455). This probe is then hybridized to the DNA bound on the nylon membrane under stringent conditions. Detection of radiolabeled probe is done by visualization via Phosphor Screen, and the laser-scanning Pharos System. These images are then aligned with DNA ladder length standards from which the band size is calculated.

Specifically, 20 μg of cryptococcal DNA from wild-type strain H99 and the two *vps45*Δ::NAT mutants is digested using the enzymes Ssp1-HF and Spe1-HF overnight at 37°C. DNA digestion reactions are heat inactivated at 80°C for 15 minutes. The digestion products are precipitated with 100 % ethanol at 4°C for 30 min. Precipitated DNA is collected via centrifugation at maximum speed in a microcentrifuge, supernatant is discarded and DNA is suspended in 50 μL ddH_2O. DNA from this isolate is further purified utilizing the QIAquick PCR purification kit to remove any contaminating DNA. Eluted DNA samples are mixed with a proportionate amount of 6X DNA loading dye, to a final concentration of 1X, and samples are

loaded onto a 1 % agarose TAE gel to be run at 30 V overnight. Upon completion the gel is imaged with a reference ruler under UV light for an internal molecular size standard to be used later.

The DNA within the agarose gel matrix is then prepared for transfer to the nylon membrane by a stepwise process. First, the DNA within the gel matrix is depurinated via incubation at room temperature in 0.25 M HCl for 5 min. The DNA is denatured by washing in 0.5 M NaOH, and 1.5 M NaCl for 20 min. Neutralization is performed in a solution of 0.5 M Tris-HCl pH7.0, and 3 M NaCl for 20 min. For the DNA transfer sandwich assembly, a reservoir of 1X SSC [150 mM NaCl, 15mM $Na_3C_6H_5O_7$ (Fisher Scientific 5467-3)] is drawn and a plexiglass bridge is placed on top. A strip of Whatman paper (Fisher Scientific 05-714-5) the width of the gel and long enough to reach the bath at each end of the reservoir is then cut and placed with the ends soaking in buffer. Two Whatman paper blotting papers the same dimensions as the gel are bathed in 5X SSC (750mM NaCl, 75mM $Na_3C_6H_5O_7$) and placed atop the Whatman strip that is wicking buffer on the plexiglass bridge. The depurinated and neutralized gel is placed atop these papers with the loading wells facing down. Subsequently, a Hybond+ (GE Healthcare RPN305B) nylon membrane is cut to the exact dimensions of the gel, soaked in 5X SSC and placed on top of the gel. Two Whatman blotting papers bathed in 5X SSC are placed on the membrane followed by a large amount of dry paper towel. Finally, a weight is balanced on the paper towels to complete the transfer sandwich. After transferring overnight the Hybond+ membrane is removed from the sandwich and the DNA is cross-linked to the membrane by UV radiation. The membrane is transferred to a blocking solution [50mL of 1% BSA (w/v) (Sigma O5420), 1 mM EDTA, 7% SDS, 0.5 M Na_2PO_4 pH 7.2 (Fisher Scientific BP331-1)] and incubated for four hours at 60°C.

Radioactive probe is generated using the DECAprime™ II kit (Life technologies AM1455). First, linear DNA for probe generation is amplified by PCR (primer pair P13 + P14) from 10 ng of CTAB-extracted wild-type strain H99 DNA with *Ex taq* DNA polymerase (98°C for 5 min once; 98°C for 30 seconds, 55°C for 30 seconds, 72°C for 1 minutes 35 times; 72°C for 5 min once; then held at 10°C). PCR-amplified DNA is quantified to 25ng, denatured by heating at 95°C for 15 minutes, and cooled on ice for two minutes. Incorporation of radiation can now be completed utilizing the melted template DNA via Klenow polymerase, Decamer

solution, and dNTP's (including P^{32}-dCTP) and incubated for 30 min at 37°C. Upon completion of probe extension, 0.5M EDTA is added to halt the reaction. To remove any unincorporated P^{32}-dCTP, the reaction solution is applied to G25 columns (GE Healthcare 27-535-01) and eluted via microcentrifugation at 3000 rpm for two minutes. The eluted probe is then denatured by heating at 95°C for five minutes and cooled on ice for one minute. Immediately following this incubation the probe is transferred to the prehybridization solution, now designated the hybridization solution, and incubated at 60°C overnight.

Upon completion of hybridization, the buffer is discarded and the membrane is washed before exposure to the Phosphor Screen. Washing is performed by first incubating the membrane in 50 mL 2X SSC (300 mM NaCl, 30 mM $Na_3C_6H_5O_7$) with the addition of 0.1 % SDS w/v at 60°C for 15 minutes. The wash buffer is discarded and replaced with 50 mL 0.1X SSC (15mM NaCl, and 1.5mM $Na_3C_6H_5O_7$) with the addition of 0.1% SDS w/v at 60°C for 15 minutes. The membrane is then retrieved, wrapped in cellophane, and exposed to the Phosphor screen (Bio-Rad 170-7841) in the absence of light for a specific time interval (2 hr, or 21 hr). A Pharos FX plus scanning laser is used to image the Phosphor screen. Images collected in this way are then aligned with the UV image and ruler to determine specific band lengths using Adobe Photoshop CS3.

GFP Fusion Reporter

The *vps45*Δ::NAT cassette is generated by PCR amplification (primer pair P5 + P6)from 10 ng of Southern-confirmed *vps45*Δ::Nat 1-2 mutant strain genomic DNA with *Ex taq* DNA polymerase(98°C for 5 min once; 98°C for 30 seconds, 55°C for 30 seconds, 72°C for 4.5 minutes 35 times; 72°C for 5 min once; then held at 10°C). The products are analyzed on a 0.8% agarose TAE gel by gel electrophoresis, and subsequently gel purified with the QIAquick Gel extraction Kit™. DNA concentration is determined by NanoDrop.The cassette is then transformed by biolistic bombardment into a previously confirmed *CFO1-GFP*::Neo background [180]. PCR confirmation of candidate *vps45*Δ clonal isolates is performed as previously described herein.

Spot Plate

Spot plate analysis is used to visually compare sensitivity between strains across a variety of media including the presence of drug, small molecule uptake or utilization, carbon source, nitrogen source, amino acid auxotrophy, etc. Herein, spot plate analysis is used to visualize differential growth rates, as observed in growth curves from liquid cultures, in the presence of the antimicrobial compounds chloroquine and quinacrine. Additionally, this technique is applied to the cell wall stressors caffeine, Congo red, calcofluor white, and sodium dodecyl sulphate (SDS). Osmotic stress is determined by growth sensitivity to NaCl concentrations. First, 1 mL of cells from a 5 mL overnight starter culture is transferred into a sterile 1.5 mL microcentrifuge tube. Cells are then separated from the growth media by centrifugation at 8000 rpm for 3 min and the separated media is removed by decanting. The cell pellet is then washed twice in 1 mL of 4°C sterile ddH_2O, and placed on ice. Two ten-fold serial dilutions are performed into sterile water; cells numbers in these dilutions are estimated using a haemocytometer, from which the original count/mL is determined. A 96 well plate (Sarstedt 83.1835.500) is schematically prepared as follows: in column 1 strains to be applied to the plate media are deposited at 2.5×10^7 cells/mL in a volume of 200 µL with 180µL of sterile ddH_2O added to the wells in the next 5 columns. From column one, 20µL of the cell suspension is transferred into the second column of wells and mixed by pipetting. This process continues (ex: 20 µL of column two into column three), a serial dilution, until 20 µL of column five is mixed with column six. Four µL of cell suspension from columns two (10^4 cells total) through six (10^0 cells total) are applied row by row to the plate media, allowed to dry, and incubated for three to five days at either 30°C or 37°C. Images of the plates are taken every 24 hours utilizing either gel doc camera or a scanner.

Growth Assays

Growth assays in liquid media are performed with the infinite M200pro Tecan plate reader in conjunction with 96 well plates. Cells are prepared and counted as previously described, except that 4°C reference media is utilized in place of water during washes. For example, if cells are to be grown in YNB containing drug for 72 hours, they would be prepared in 4°C YNB media not ddH_2O. Cell suspensions are prepared to a final concentration of 2×10^6 cells/mL, and 100 µL (200 cells) are inoculated into 96 well plates. 100 µL of growth media is then added onto the cell suspensions as per experimental design. The 96-well plate is then

transferred into the infinite M200pro Tecan plate reader. Growth curve analysis is performed with the internal temperature at either 30°C or 37°C; and initial orbital shaking for 60 seconds at an amplitude of 2mm. Initial absorbance at 600nm is determined for all liquid cultures and recorded. Orbital shaking then recommences for 28 minutes at an amplitude of 2 mm and absorbance at 600 nm is determined for all liquid cultures and recorded; this is repeated for 144 cycles over approximately 72 hours. Upon completion of cycle 144 the infinite M200pro Tecan reader saved the data set and ended the experiment.

Microscopy

Capsule is induced by growth in liquid LIM (as defined above) at 30°C [described in [249]]. A YPD starter culture is used for the independent *vps45Δ* mutants and wild-type strain H99. Cells are collected in 1 mL of media and washed 3 times in LIM. The washed cells are then resuspended in 5 mL of LIM and incubated at 30°C for two days. Capsule is stained using super black India Ink (Speedball 21104-2004) by mixing at a ratio 2:1 (ink:cell volume). Microscopic examination is carried out using differential interference microscopy (DIC, Zeiss Axioplan 2 imaging system, 100× magnification).

To determine the localization of the Cfo1-GFPp by fluorescence microscopy. gene expression is induced by growth in LIM (modified from[180]). To achieve this overnight 5 mL starter cultures of the *vps45Δ* mutants and wild-type strain H99 expressing the Cfo1-GFPp fusion protein are inoculated. The following day, cells are washed 3 times in LIM, suspended in 1 mL LIM, and inoculated into 5 mL of LIM supplemented with $FeCl_3$ at a final concentration of 10 μM or 100 μM at 30°C for one and two days. Cell suspensions are mounted onto microscope slides and visualized using a Zeiss Axioplan 2 imaging system under 100× magnification. LysoTracker Red DND-99 (LifeTechnologies L-7528) staining is performed by incubating a 200 μL aliquot of cell suspensions in the presence of 150 nM LysoTracker red at 30°C with shaking for 90 min.

Macrophage Survival Assays

Macrophage survival assays are conducted to determine average fitness of independent *vps45*Δ mutants when compared to wild-type strain H99 during intracellular growth of both differentiated murine J774A.1 (ATCC® TIB-67™) and human THP-1 (ATCC® TIB-202™)

macrophage-like cells [249]. This assay quantifies macrophage uptake of opsonised cryptococcal cells, as well as intracellular survival by comparing counts of cryptococcal uptake at 2 hours with counts of the remaining fungal cell population after 24 hr of co-incubation with macrophage. J774.1, and THP-1tissue cultures are seeded on 24 well plates and grown at 37°C with 5 % CO_2 to 80% confluence in DMEM (Gibco 11960-044), or RPMI (Gibco 31800-089) respectively. Both media are supplemented with 10% fetal bovine serum [FBS (Gibco 12483-020)], 1 % non-essential amino acids (Gibco 11140-050), 4 mM L-glutamine (Gibco 25030-081), and penicillin-streptomycin [final concentration 100 U/ml penicillin, 100 μg/ml streptomycin (Gibco 15140-122)]. Differentiation is induced by introduction of 150 nM phorbol myristate acid [PMA(Sigma p8139)] during incubation. J774.1 cells are incubated in DMEM (as described above) with PMA for 2 hours previous to fungal inoculation. THP-1 cultures are incubated for 24 hours with RPMI (as described above) and PMA. Media is then removed, cells are washed using PBS (Gibco 10010-023), fresh RPMI (as described above) is added and differentiation is continued for 48 hours prior to fungal inoculation.

Fungal cultures are grown overnight in YPD media at 30°C with shaking and washed the following day in PBS. Fungal cell counts are enumerated with a haemocytometer and 100 μL aliquots of 2 X 10^6 cells are opsonised in fresh DMEM or RPMI with 0.5 μg/mL of the monoclonal antibody 18B7[250] for 30 min at 37°C. Macrophage cultures are then inoculated with the opsonised aliquots at a multiplicity of infection of 1:1. To determine fungal uptake cultures are first incubated for 2 hours at 37°C with 5 % CO_2 and then rinsed four times with PBS to remove any non-macrophage associated fungal cells. At this point, microscopic images of the co-cultured cells are also taken to enumerate the number of cryptococcal cells engulfed by macrophage in at least 10 fields of view. Macrophage cell populations containing *C. neoformans* cells are then lysed by incubation with sterile ddH_2O for 30 minutes at room temperature. Cell counts in the lysate are determined by serial dilutions of the lysate, of which 200 μL is taken and allowed to dry on YPD agar media containing chloramphenicol (25 μg/mL) and incubated at 30°C for 48 hours. Colony forming units (CFU) are counted on each plate from lysate samples taken at two and 24 hours. All experiments are carried out in triplicate. Statistical significance of intracellular survival and uptake rates are determined by unpaired two-tailed Student's t-tests, under the assumption of unequal variance. Control for growth in media is performed by growth

curve analysis in a Tecan plate reader (as described): cells are pre-grown in YPD overnight, rinsed with ice cold sterile media (RPMI or DMEM), and OD_{600nm} is reported. As an alternate approach, wild-type and *vps45*Δ mutants are grown in DMEM and RPMI with 10% fetal bovine serum, 1 % non-essential amino acids, 4 mM L-glutamine, and penicillin-streptomycin (100 U/mL penicillin, 100 μg/mL streptomycin) at 37°C with 5 % CO_2. CFU plate counts are taken at two and 24 hours, as described above.

Results

Identification of *VPS45* in *C. neoformans*

Given the importance of Vps45p in vacuolar function in other organisms, we initially set out to identify the gene encoding the protein in *C. neoformans.* The product of the *C. neoformans* gene locus, CNAG_03628.2, was identified as the best match to the *S. cerevisiae* Vps45p protein with a BLASTp score of 332.413 bits, an alignment length of 592 amino acids (with 204 identical and 324 similar residues) and an E-value of 0. A reciprocal BLASTp search using the predicted CNAG_03628.2 protein sequence against *S. cerevisiae* found that the initial query, Vps45p, was the most probable match. When the protein coding sequence of CNAG_03628.2 was used as a query of the entire fungal protein collection (WU-BLAST2p), a variety of annotated matches including Vps45p, "conserved hypothetical proteins," or "VpsBp," were obtained. Interestingly, although the best match for CNAG_03628.2 locus in *S. cerevisiae* was Vps45p, the current annotation in the BROAD database is VPSB. Therefore, we had to confirm which protein our gene of interest was more closely related to, VpsBp or Vps45p. The ancestry of the VpsBp annotation appears to be rooted in a bacterial protein from *S. flexneri* that has similarity to our initial query Vps45p protein sequence from *S. cerevisiae*. Given the evolutionary distance between bacteria and fungi, we were very confident that the fungal protein would be distinct from the bacterial protein.

Phylogenetic analysis (Figure 5) was completed to determine the relatedness between the annotation groups. Included within are four fungal protein sequences from similar predicted proteins as determined by WU-BLAST2. These fungal groups have separate annotations and are from two divisions, Ascomycota (*A. fumigatus*, and *S. cerevisiae*) and Basidiomycota (*U. maydis* and *C. neoformans*). Two Proteobacteria VpsBp sequences were included from *S. flexneri* and *E. coli* (annotated as B3194). As an out-group four *H. sapiens* Vps45p isoforms were included. In our model of 1000 possible trees the bacterial protein is never considered to be similar, or related to the eukaryotic sub-population. Furthermore, the included out-group of *H. sapiens* is more closely related to fungal Vps45p sequence. This observation indicates that the current annotations are incorrect. It is interesting that the fungal species appear to have increased diversity between the Ascomycete and Basidomycete sub-populations included. This may

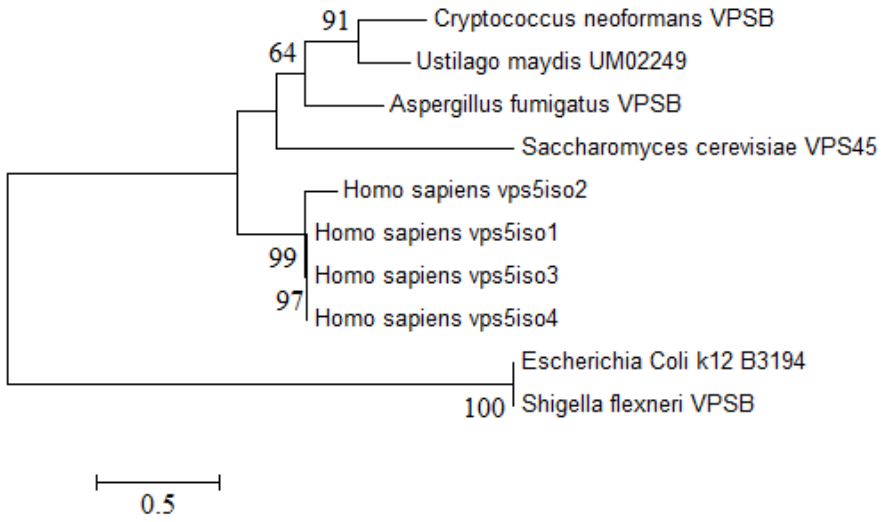

Figure 5. Molecular phylogenetic analysis of the predicted Vps45p or VpsB amino acid sequence by the maximum likelihood method. The evolutionary history was inferred by using the Maximum Likelihood method based on the JTT matrix-based model [1]. The tree with the highest log likelihood (-3498.8405) is shown. Only values greater than 50% were reported for the percentage of trees in which the associated taxa clustered together is shown next to the branches.. Initial tree(s) for the heuristic search were obtained automatically by applying Neighbor-Join and BioNJ algorithms to a matrix of pairwise distances estimated using a JTT model, and then selecting the topology with superior log likelihood value. The tree is drawn to scale, with branch lengths measured in the number of substitutions per site. The analysis involved 10 amino acid sequences. All positions containing gaps and missing data were eliminated. There were a total of 257 positions in the final dataset. Evolutionary analyses were conducted in MEGA6 [2].

however be an artifact of performing gap deletion during the alignment. If highly conserved sequences between fungi are not shared with *H. sapiens* or the Proteobacteria then they will be removed from the alignment. Although this may lead to incorrect inferences within the fungal kingdom, this method provides the most strict criteria for analyzing relatedness between kingdoms because only related sequences are compared. This is strong evidence that the protein encoded by the cryptococcal gene locus of CNAG_03628.2 is more closely related to *S. cerevisiae* Vps45p than *S. flexneri* VpsBp. We suggest the annotation of CNAG_03628.2 be changed from *VPSB* to *VPS45* because the protein sequence is more similar to that of *S. cerevisiae* Vps45p. Since neither gene product has been functionally characterized in either *A. fumigatus* or *U. maydis* this rationale could be expanded to these organisms as well upon further study. Overall, these observations have strongly suggested that CNAG_03628.2 gene product is orthologous to the *S. cerevisiae* protein Vps45p.

Chromosomal Deletion of the *VPS45* Locus

After identification of the best candidate gene encoding Vps45p in *C. neoformans,* we constructed a deletion mutant lacking the gene so that the phenotypic impact could be assessed. Deletion was performed utilizing a split NAT marker protocol, as explained in the Materials and Methods section. This split marker was transformed into *C. neoformans* by biolistic bombardment, and drug resistant clones were screened for positive integration of the marker at the chromosomal *VPS45* locus. Screening was done on clonal isolates by specific PCR amplification of extracted genomic DNA. Upon analysis by gel electrophoresis (Figure 6A), *VPS45* disruption by NAT resistance marker integration was confirmed in two independent mutants, designated *vps45*Δ::NAT 1:2, and 3:4 (lane 6, 7, 9, 10). These reactions confirmed that at least 593bp of the *VPS45* locus had been deleted in the potential mutants (lane 5, 6). A Southern blot was used to confirm the deletion of the gene and to rule out ectopic insertion of transforming DNA at another site in the genome (Figure 6B). Digestion of chromosomal DNA with SspI and SpeI is expected to liberate a 2308 bp fragment if the cassette has not integrated correctly, or a 3673 bp fragment if the NAT cassette has integrated at the proper locus. A 2308 bp fragment was identified from digested wild-type strain H99 chromosomal DNA, and a 3673 bp fragment was found for the chromosomal DNA from two independent mutants. However, a secondary band in the wild-type strain H99 DNA lane was observed with an approximately equal

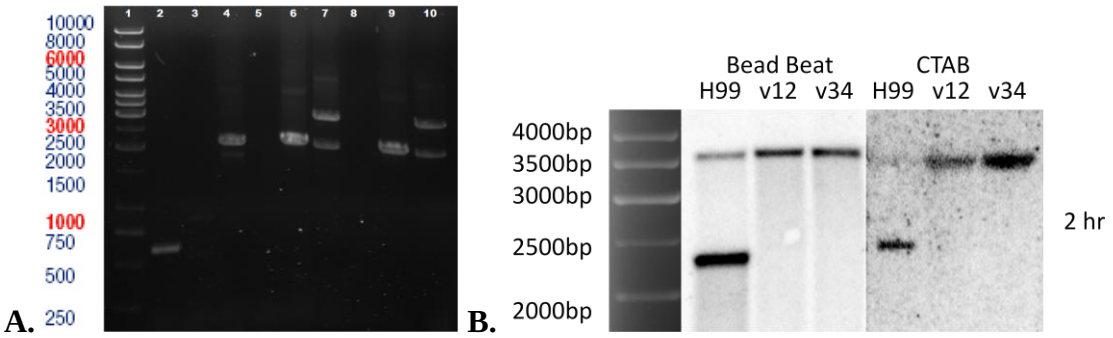

Figure 6. Confirmation of the *VPS45* chromosomal deletion in *C. neoformans* strain H99. A. PCR confirmation of the *VPS45* deletion. GeneRuler 1 kb DNA ladder was used in lane 1. Wild-type strain H99 DNA was used as a template in reactions visualised in lanes 2-4. *vps45*Δ 1:2 mutant reactions were in lanes 5-7. *vps45*Δ 3:4 reactions were in lanes 8-10. Reactions in lanes 2, 5, and 8 amplify a 593 bp fragment of the *VPS45* gene. Reactions in lanes 3, 6, and 9 confirmed integration of the 5' region of the NAT cassette. Reactions in lanes 4, 7, and 10 confirmed integration of the 3' region of the resistance cassette. Non-specific PCR amplification was observed in the right confirmation reaction and was removed at an annealing temperature of 63°C. **B.** Southern blot analysis of the *VPS45* gene locus. Chromosomal DNA was collected via bead beating and CTAB extraction from either H99 or listed strain. Dna samples were digested utilizing the restriction enzymes SpnI and SpeI. DNA samples were probed with a radioactive P^{32} labeled probe created from the 5' region of the locus. NAT cassette integration results in a band shift from 2038 bp to 3673 bp. The wild-type strain H99 lanes show a fragment at 2038 bp and background binding at 3671bp, the *vps45*Δ 1:2 and 3:4 mutants have lost the wild-type band of the locus at 2038 bp, and have a shifted band size of 3673 bp, indicating chromosomal integration of the deletion cassette at the *VPS45* locus. A schematic diagram of the confirmation reactions is included in Figure 4.

length of the mutant DNA. This corresponds to a region outside of the gene locus that has homology to 374 bp of the 915 bp probe used for hybridization in the Southern blot. When wild-type strain H99 chromosomal DNA is cleaved with SspI and SpeI a predicted 3671 bp fragment capable of binding the probe outside of the *VPS45* locus is released. We believe that this contaminating band corresponds to this predicted fragment. We can say with confidence that the deletion construct has successfully integrated in two mutants, *vps45*Δ::NAT 1:2, and *vps45*Δ::NAT 3:4. These mutants were used for subsequent phenotypic assessment of the contribution of the associated gene product.

Iron Utilization is Negatively Affected in *vps45*Δ Mutants

We had previously identified HapXp, an iron responsive transcriptional regulator of *C. neoformans*, as an upstream regulator of *VPS45* gene expression in response to iron limitation and in media supplemented with 100 μM $FeCl_3$ [242]. We therefore investigated the potential for our deletion mutant to grow in the controlled presence of different iron sources. The uptake of exogenous iron sources was assayed by serial dilution analysis of growth on solid medium, and by growth in liquid cultures. Two types of solid media, LIM and YNB, were utilized to examine growth fitness (Figure 7). Mutant strains had reduced growth on LIM (Figure 7A) supplemented with 10 or 100 μM of hemin when compared to the wild-type strain H99. In a more complete medium background, YNB (Figure 7B), *vps45*Δ mutants were still challenged when grown in the presence of 10 or 100 μM of hemin as the sole iron source. These phenotypes were exacerbated when growth temperature was increased from 30°C to 37°C. Strains were also iron-starved by growth in LIM for 2 days and applied to the same media and growth conditions. No additional growth defects were observed, although growth rates were decreased in all strains. Since LIM is not supplemented with complete amino acids, the growth difference between LIM, and YNB media supplemented with 10 or 100 μM $FeCl_3$ may be attributed to an auxotrophic sensitivity of the *vps45*Δ strain. This hypothesis is consistent with the known function of the yeast vacuole as a store of excess cytosolic amino acids. To test this YNB media was prepared without amino acid supplementation, and iron was added as above. Growth of the *vps45*Δ mutants on YNB with or without amino acid supplementation did not vary, indicating that an amino acid auxotrophy did not exist.

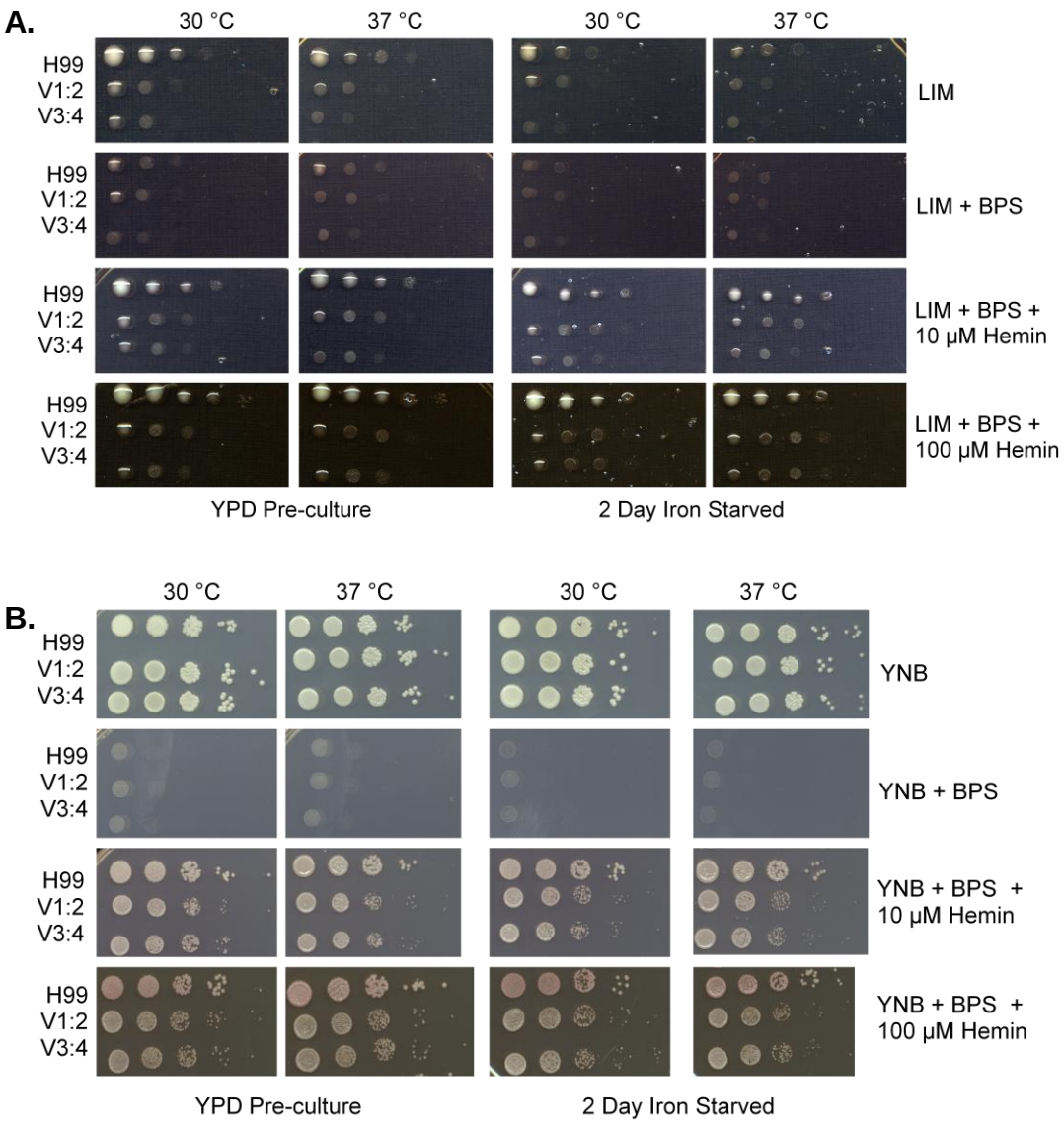

Figure 7. *VPS45* is required for growth when hemin is the sole extracellular iron source on solid media. A. Ten-fold serial dilutions of cells (starting at 10^4 cells) were spotted onto solid LIM medium (control), iron-chelated LIM medium with 150 µM BPS, low iron (LIM with 150 µM BPS, and 10 µM hemin), and high-iron (LIM supplemented with 150 µM BPS-100 µM hemin). Plates were incubated at 30°C or 37°C for 3 days. Strains are indicated by genotypes. Pre-culture conditions were either overnight in YPD or two days growth in LIM to deplete intercellular iron. **B.** Tenfold serial dilutions were performed as described above, although YNB media was used in place of LIM.

Analysis of growth in liquid cultures was performed to assay microaerophilic growth in a liquid medium at 30°C when iron source was controlled in LIM (Figure 8). As with the plate assays, the *vps45*Δ mutant exhibited retarded growth as determined by OD_{600} in LIM when compared with the wild-type strain H99; similarly, reduced growth was observed in media supplemented with 10 μM of $FeCl_3$, 100 μM of $FeCl_3$, 10 μM of hemin, and 100 μM of hemin. These observations were also consistent if the mutant was precultured in rich media or iron starved in minimal LIM. These data suggest that Vps45p function is required for growth when challenged with nutrient stress and limited iron availability or variety. Furthermore, the acquisition of iron by *C. neoformans* from hemin may require transit through the PVC in a Vps45p dependent manner.

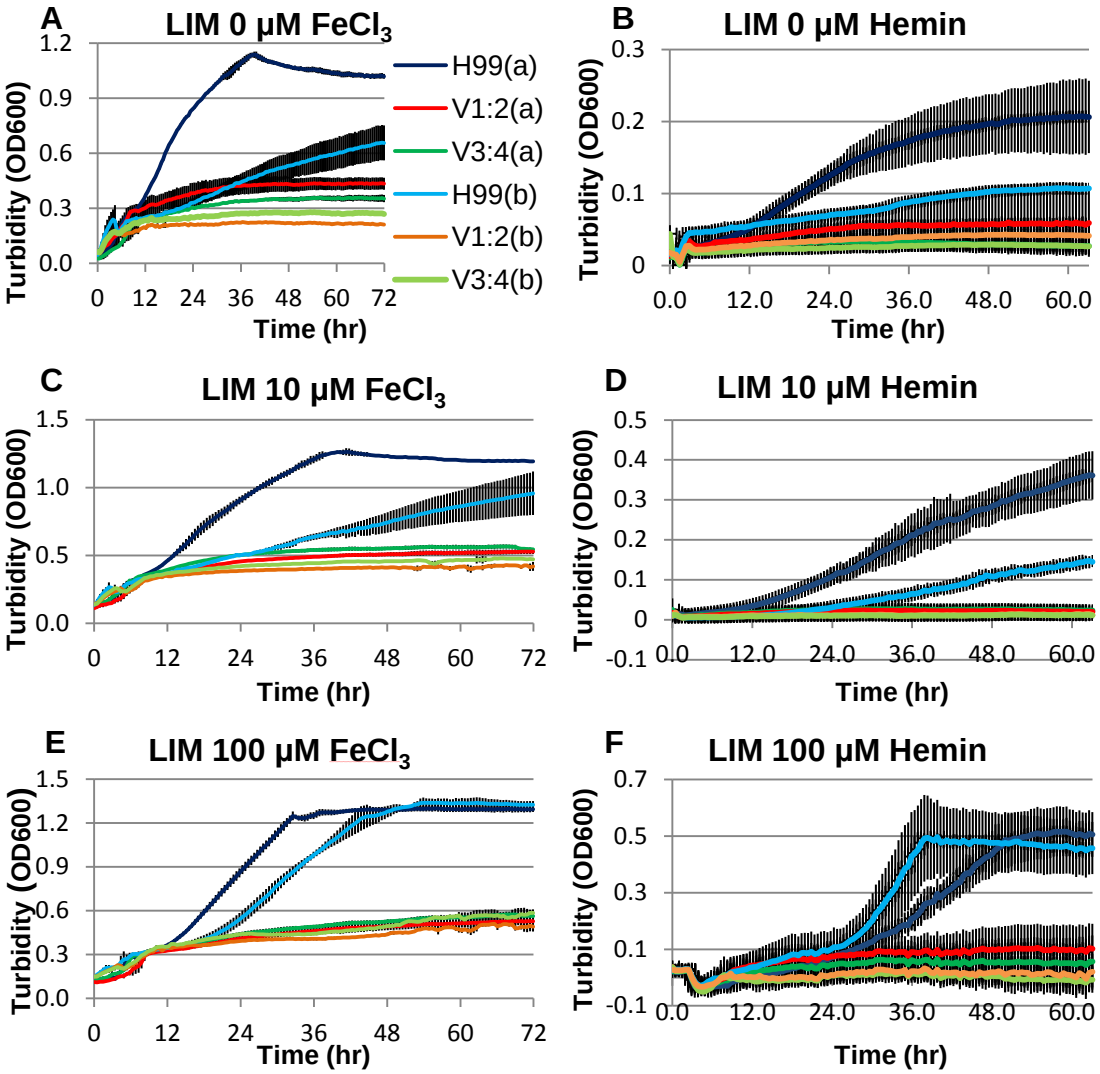

Figure 8. *VPS45* is required for growth when in iron limited conditions during microaerophilic growth. Cells were inoculated into defined liquid low iron medium (LIM) (A, B), LIM containing 10 µM $FeCl_3$ (C), or 100 µM $FeCl_3$ (E), or LIM containing hemin 10 µM (D) or 100 µM hemin (F). Cultures were incubated at 30°C, and optical densities at 600 nm (OD_{600}) were measured in a Tecan M200 infinite pro. Note that all assays were performed in triplicate, and that data collected for $FeCl_3$ (A, C, E) and hemin (B, D, F) were taken in separate experiments. Cells were either pre-cultured in YPD overnight [(a) in legend], or in LIM for 2 days [(b) in legend] prior to inoculation into the 96-well microplate.

Vacuolar Accumulation of CFO1-GFP is Disrupted by Deletion of *VPS45*

To further examine iron-dependent growth, a set of *vps45Δ* mutants were created in a *CFO1:GFP:Neo* H99 background. CFO1p has been characterized as a requisite component of high-affinity iron-uptake, and deletion mutants are hypovirulent [180]. Previously unpublished work in our laboratory showed that growth for 24 hours or longer in LIM causes Cfo1-GFPp to primarily localize to the vacuole, when compared to the plasma membrane at 6 hr. Additionally the CFO1-GFP fusion construct was able to successfully complement a *cfo1*Δ strain, meaning that it is functional [180]. Confirmation of *vps45*Δ in the *CFO1-GFP*:Neo background was performed by PCR amplification (Figure 9). We observe no amplification of confirmation products in wild-type background conditions (lane 2, and 3). However, amplification products of the same length as compared to Southern blot confirmed *vps45*Δ::NAT 1:2 mutant (lane 4 and 5) are detected in all potential *CFO1-GFP*:Neo *vps45*Δ::NAT mutant chromosomal DNA samples (lanes 6-13). We can therefore confirm that integration was successful and these mutants are *vps45*Δ strains.

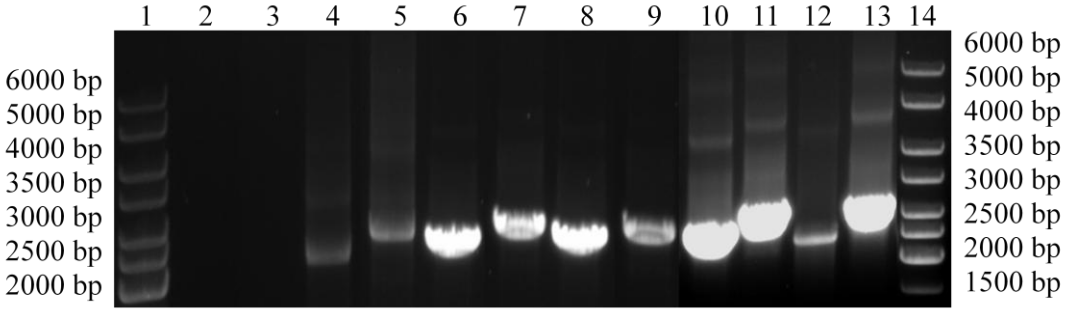

Figure 9: PCR confirmation of *vps45*Δ::NAT integration in a *CFO1-GFP*::Neo strain of H99. PCR amplification products were separated by electrophoresis on a 0.8 % agarose TAE gel. PCR amplification was performed to confirm integration of the 5' region of the Nat cassette (even numbered lanes, except 14) and 3’ region of the Nat cassette (odd numbered lanes except 1). Wild-type strain H99 genomic DNA was used as template in lanes 2 and 3. *vps45*Δ 1:2 DNA was used as a positive control in lane 4 and 5. Confirmation reactions were performed on isolates *CFO1-GFP*:Neo *vps45*Δ::NAT 2:3 (lane 6 and 7), 2:4 (lane 8 and 9), 1:9 (10 and 11), and 1:14 (12 and 13). 2164 bp fragments were observed in lanes 4, 6, 8, 10, and 12, and 2957 bp fragments were observed in lanes 5, 7, 9, 11, and 13.

In order to determine if cellular localization of the Cfo1-GFPp was affected by deletion of *VPS45* cells were incubated in LIM with or without the addition of 100 μM $FeCl_3$ to induce gene expression of the ferroxidase. After two days of accumulation, cells were stained with LysoTracker Red for one hour and images were captured by fluorescence microscopy (Figure 10). LysoTracker Red selectively stains acidic compartments typically below pH 5.2, and as such can be used as a vacuolar stain. In the *CFO1-GFP*:Neo wild-type control strain, all GFP fluorescence appeared to be localized to LysoTracker Red-stained vacuolar structures. Whereas, Cfo1-GFPp localization in the *vps45*Δ mutants appeared to be dispersed in the cytosol, plasma membrane, and into LysoTracker Red stained vacuolar compartments with aberrant morphology. These data suggest that vacuolar sorting of Cfo1-GFP is strongly affected by the deletion of *VPS45*. Furthermore, the fractured vacuolar morphology suggests that these mutants may have impacted functions beyond iron acquisition and heme accumulation in the vacuole.

Interestingly, vacuolar accumulation of the Cfo1-GFPp occurs in wild-type cryptococcal cells regardless of extracellular iron presence. This observation is seen in the *vps45*Δ mutants as well, although because of vacuolar fragmentation and mislocalization of the reporter this trend is less clear. These observations suggest that Cfo1p could have a function in the vacuole of *C. neoformans*. Additionally, LysoTracker Red fluorescence was less intense in *vps45*Δ mutants which may indicate that vacuolar pH is affected in the *vps45*Δ strain. However these observations could not be quantified because photobleaching of the LysoTracker Red fluorophore occurs rapidly and data readings would not be consistent within each sample. Thus no conclusion can be drawn, but these observations should be noted.

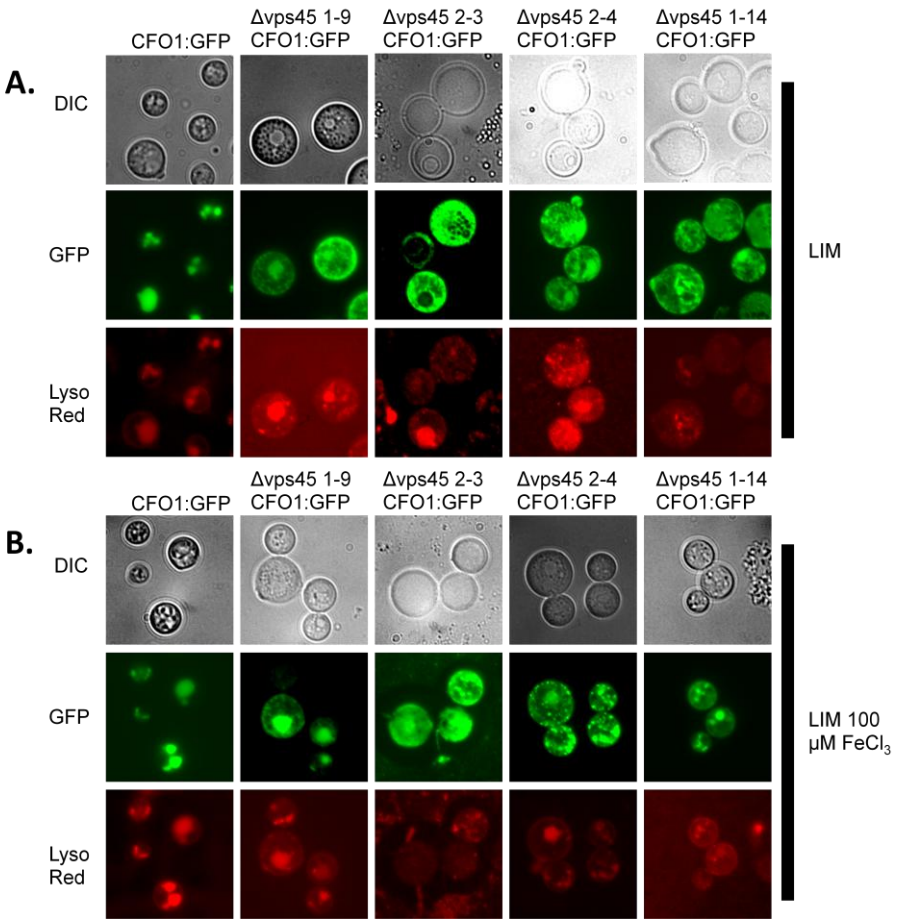

Figure 10. Localization of Cfo1-GFP in iron-starved *C. neoformans* strains requires *VPS45* for proper compartmentalization. Cells were grown in LIM (A), or LIM + 100 μM $FeCl_3$ (B) at 30°C for 48 hr and visualized. The Cfo1-GFP fusion is localized to vacuolar structures in wild-type strain H99 background, while the GFP signal is more dispersed in *vps45Δ* mutants. No difference is observed between media culture conditions. LysoTracker Red was used to stain the vacuolar compartment. The cells were observed with a Zeiss Axioplan 2 imaging microscope and the images were processed as described in Materials and Methods. DIC; differential interference contrast.

Phenotypic Characterization of Stress Response in *vps45*Δ Mutants

In *S. cerevisiae*, *vps45*Δ results in susceptibilities to numerous extracellular stressors including NaCl hyperosmotic stress [251], and the cell wall stressors calcofluor white [252] and caffeine [253]. These susceptibilities were investigated in our *C. neoformans vps45*Δ mutants and were found to be similar to those seen in *S. cerevisiae* (Figure 11). Cryptococcal *VPS45* was required for resistance against hyperosmotic stress from 1.5 M NaCl at 30 °C, and 1 M NaCl at 37 °C. The cell wall of *vps45*Δ mutants was sensitive to stressors such as 0.5 mg/mL and 1 mg/mL calcofluor white, 0.5 mg/mL caffeine, and low concentrations of SDS stress (0.01 - 0.03 %). Glucan fibril synthesis was not affected in *vps45*Δ strains because mutants grown on media supplemented with Congo red appeared close to wild-type strain H99 in growth rate [254]. The congruency between *S. cerevisiae* and *C. neoformans* phenotypic response to extracellular stressors strengthens the phylogenetic argument that *S. cerevisiae VPS45* functions are conserved in *C. neoformans*.

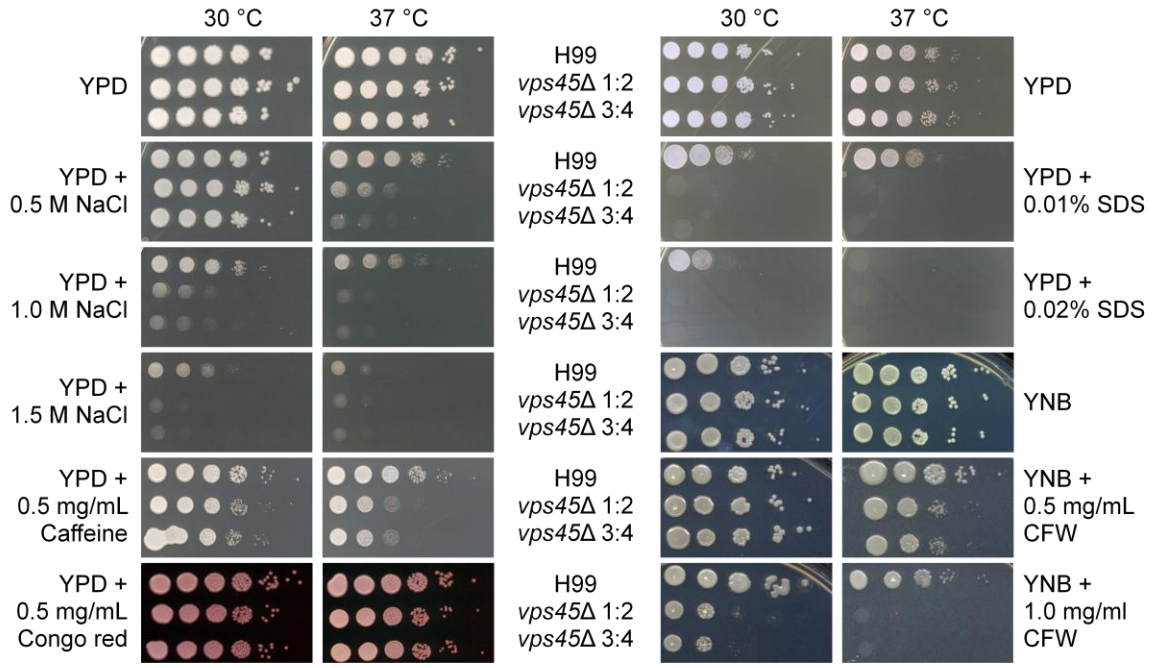

Figure 11. *VPS45* is required for protection against extracellular stressors. Ten-fold serial dilutions of cells (starting at 10^5 cells) were spotted onto solid YPD or YNB medium (controls), YPD with NaCl (0.5 M, 1.0 M, or 1.5 M), YPD with caffeine (0.5 mg/mL), YPD with Congo red (0.5 mg/mL), YPD with SDS (0.01 %, and 0.02 %), and YNB with calcofluor white (0.5, and 1.0 mg/mL). Plates were incubated at 30°C or 37°C for 3 days. Strains are indicated by genotypes, wild-type control strain H99 was included for reference. Strains were pre-cultured in YPD overnight before spotting.

Vacuolar Accumulated Drug has Increased Toxicity in *vps45*Δ Background

Further investigation of the defective vacuolar homeostasis in the *vps45*Δ mutant background required additional stressors. Vacuolar pH has been manipulated by various methods including deletion of *VPH1*, pH-gradient destabilization with weak bases, and trafficking inhibition by treatment with brefeldin A; this feature is also essential for *C. neoformans* virulence [207, 217, 243, 255, 256]. We hypothesized that the *vps45*Δ mutant would have an increased sensitivity to similar stressors. The vacuolar antagonists, quinacrine and chloroquine, were chosen as they have been previously shown to accumulate in the cryptococcal vacuole and also to modulate *C. neoformans* virulence, intracellular survival, and virulence factor expression, as (Figure 12). These drugs were originally developed as anti-malarial therapies, but have since

been shown to have broad-spectrum toxicity against viruses, bacteria, fungi, and in cancer therapeutics [257]. On solid YPD medium (Figure 12A), *vps45*Δ strains were sensitive to 3mM chloroquine with diminished growth at 7mM, a concentration that is almost completely toxic at 30°C. When grown on solid YNB medium (Figure 12C), or at 37°C (Figure 12A) chloroquine toxicity increases. Quinacrine, a more potent drug, has antifungal activity at 0.4 mM when tested on YPD solid medium at 30°C (Figure 12B). Similar to chloroquine, growth on YNB (Figure 12C) or at 37°C (Figure 12B) also increases the effectiveness of the drug.

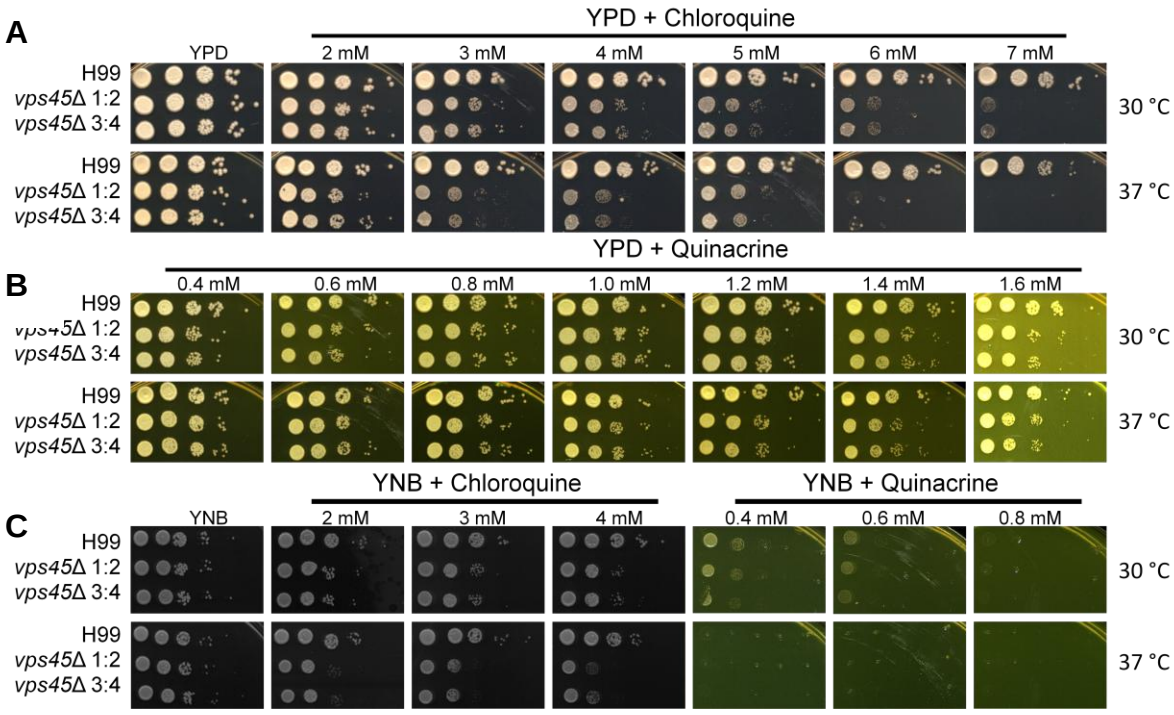

Figure 12. Deletion of *VPS45* increases sensitivity to antimalarial drugs. (A) Ten-fold serial dilutions of cells (starting at 10^4 cells) were spotted onto solid YPD medium containing chloroquine at indicated concentrations. (B) Ten-fold serial dilutions of cells (starting at 10^4 cells) were spotted onto solid YPD medium, and YPD medium-containing quinacrine at the concentrations listed (C) Ten-fold serial dilutions of cells (starting at 10^4 cells) were spotted onto solid YNB medium and YNB medium-containing chloroquine, or quinacrine at the listed concentrations. Plates were incubated at 30°C or 37 °C for 3 days as indicated.

Microaerophilic liquid culture growth curve data was collected to investigate the effect of chloroquine and quinacrine on the growth kinetics of fungal cells. It was seen that liquid growth

increased dose-sensitivity for *vps45*Δ mutants (Figure 13). When grown in the presence of chloroquine (Figure 13A), fungistatic effects can be observed in the wild-type strain and mutants. Primarily, chloroquine appears to increase the lag phase during adaptation, and this effect is more pronounced in the *vps45*Δ mutants. A secondary lag phase appears only in the wild-type strain H99 when grown in 3.5 mM and 4 mM of chloroquine resembling a classic diauxic shift. This lag phase may be experienced by mutants initially, which may explain the extended lag phase observed before exponential growth. When quinacrine is present in YNB, microaerophilic growth is severely impacted. Resistance to quinacrine was more robust in cells that were pre-cultured in rich YPD medium (Figure 13B) than those pre-cultured in LIM (Figure 13C). YPD pre-cultured *vps45*Δ mutants were susceptible to quinacrine concentrations as low as 500 μM (Figure 13B). Comparatively, wild-type growth was unaffected by quinacrine concentration at 500 μM, growth-inhibition of wild-type was seen at a two-fold increase of 1 mM quinacrine. Maximal OD_{600} for wild-type cells grown in the presence of all quinacrine concentrations assayed was between 1 and 1.5. However, *vps45*Δ deletion mutants grown in the presence of quinacrine were able to reach a maximal OD_{600} of approximately 0.5, if growth occurred at all. Iron-starvation by two day LIM pre-culture increased sensitivity of wild-type strain H99 to 1 mM quinacrine while the *vps45*Δ mutant strains were completely non-viable in the presence of quinacrine at concentrations as low as 500 μM. It appears that the vacuolar accumulation of chloroquine and quinacrine has increased toxicity in the *vps45*Δ mutant when compared to wild-type strain H99 *C. neoformans*. Although the precise mechanisms of anti-cryptococcal activity of these drugs are unknown, a loss of Vps45p function decreases innate resistance. These observations indicate that fungal resistance to chloroquine and quinacrine is mediated in some way by Vps45p.

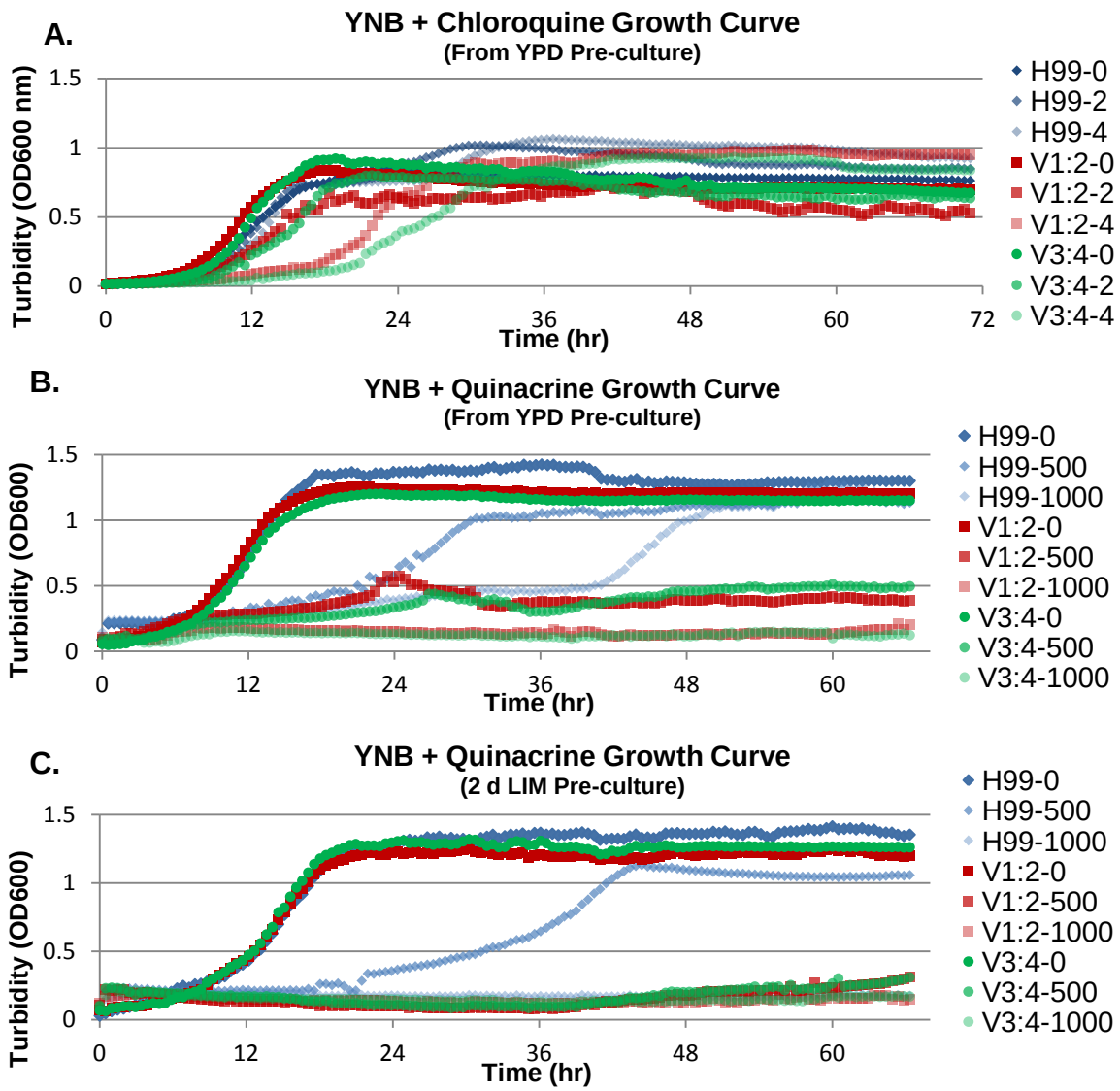

Figure 13. *VPS45* is required for resistance to antimalarial drugs in liquid microaerophilic growth cultures. A) Growth curve analysis of *C. neoformans* strains in YNB culture media with 0 mM, 2 mM, and 4 mM chloroquine. B) Growth curve analysis of *C. neoformans* strains pre-cultured in YPD overnight with 0 μM, 500 μM and 1000 μM quinacrine. C) Growth curve analysis of *C. neoformans* strains iron starved by pre-culture in LIM for 2 days at 30 °C cells resuspended in YNB with addition of 0 μM, 500 μM and 1000 μM quinacrine. Cells were grown at 30 °C with shaking in a Tecan M200 Infinite Pro for the indicated time. Strain is indicated in the legend first (H99=wild type, V1:2 = *vps45*Δ::NAT 1:2, V3:4 = *vps45*Δ::NAT 3:4), with concentration beside it. Chloroquine is listed in mM, quinacrine listed in μM.

Virulence Factor Expression is Unaffected by *vps45*Δ

The elaboration of virulence factors was investigated. Previous studies had shown that vacuole acidification was required for elaboration of capsule and melanization, mutants were also attenuated for virulence in a murine model [207]. Thus, there was reason to suspect that *VPS45* may phenocopy these traits. The wild-type strain H99 and the *vps45*Δ mutants were grown in capsule-inducing media for two days and stained with India ink to visualize the capsule by dye exclusion. No difference in capsule size was observed after two days incubation (Figure 14A). Addition of 0.25 mM chloroquine to the induction media was sufficient to impair capsule elaboration. Melanisation was induced on specific media in the presence of L-dopa and near wild-type pigmentation was observed after 3 days of incubation (Figure 14B). Growth at 37°C was not perturbed in spot plate analysis when grown on both YPD and YNB solid media (Figure 14B). Although the cryptococcal *VPS45* is involved in a wide array of cellular processes, such as iron utilization, trafficking events, and environmental response, there is no associated loss of virulence factor elaboration in the methods we analyzed.

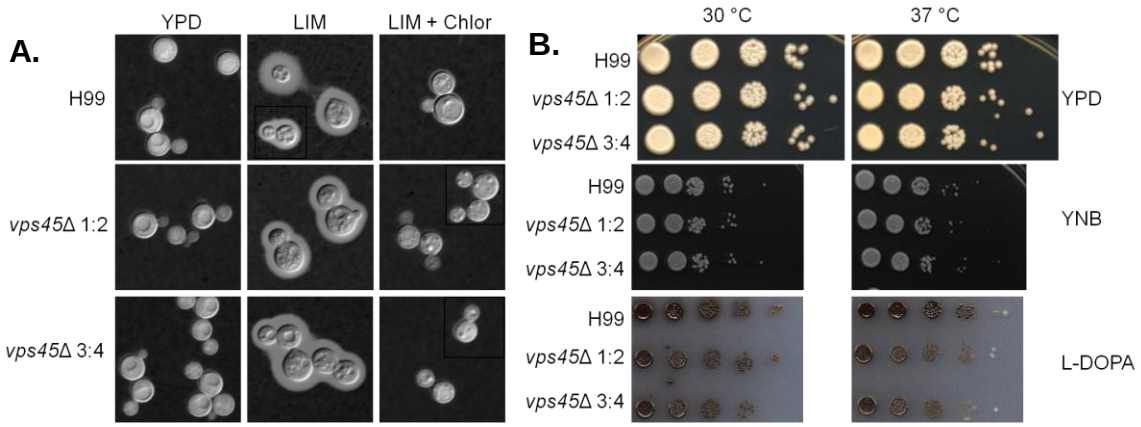

Figure 14. Deletion of *VPS45* does not influence the major virulence factors. A) Capsule formation was examined by YPD overnight growth (negative control) 2 day growth in LIM, and LIM containing 250 μM chloroquine followed by staining with India ink and visualization by DIC microscopy. B) Temperature stress was analyzed by spotting a dilution series (starting at 10^4 cells) on YPD or YNB and growth was monitored at 30 °C and 37 °C after 3 days. Melanin production was tested by spotting a dilution series (starting with 10^4) of cells on L-dopa medium for 3 days at 30°C.

In vitro Macrophage Clearance of a *vps45*Δ Mutant of *C. neoformans* is Increased

C. neoformans is able to persist in the phagolysosomal compartment of macrophages and the growth in lungs and blood is dependent on the initial outcome of macrophage interaction. Therefore, characterizing the outcome of this interaction can be predictive of infection in murine models, which can then be extrapolated to human disease. Since we observed that the *vps45*Δ mutant has a wide array of phenotypic defects which appear to be related to adaptation in response to extracellular cues, such as shifted iron source or introduction of cell wall stressors, it was expected that these mutants would be susceptible to macrophage killing. Thus, macrophage-uptake and survival measurements were taken to determine relative fitness of the infective yeast *in vitro*. In two independent observations, as determined by DIC microscopic count of intracellular *C. neoformans* after 2 hr of co-incubation, uptake was not affected by *VPS45* in J774a.1 (Figure 15A). These results are disputed by CFU counts of *C. neoformans* taken after 2 hrs of co-incubation (Figure 15B). A statistically significant reduction of viable *vps45*Δ mutant cells with respect to wild type was observed after two hours of co-incubation in three trials, although in all but one of these trials an independent vps45Δ mutant subjected to identical treatment had no statistically significant reduction in uptake. The pooled data set of all four trials (n=12) suggests that no statistical significant difference in uptake exists between *vps45*Δ independent mutant strains and wild-type strain H99. Survival of cryptococcal strains was determined as a percentage CFU count at 24 hours with respect to 2 hrs (Figure 15C). In every trial the *vps45*Δ strains had significantly lower survival (40-75%) when compared to the wild-type strain H99 (100-215 %).

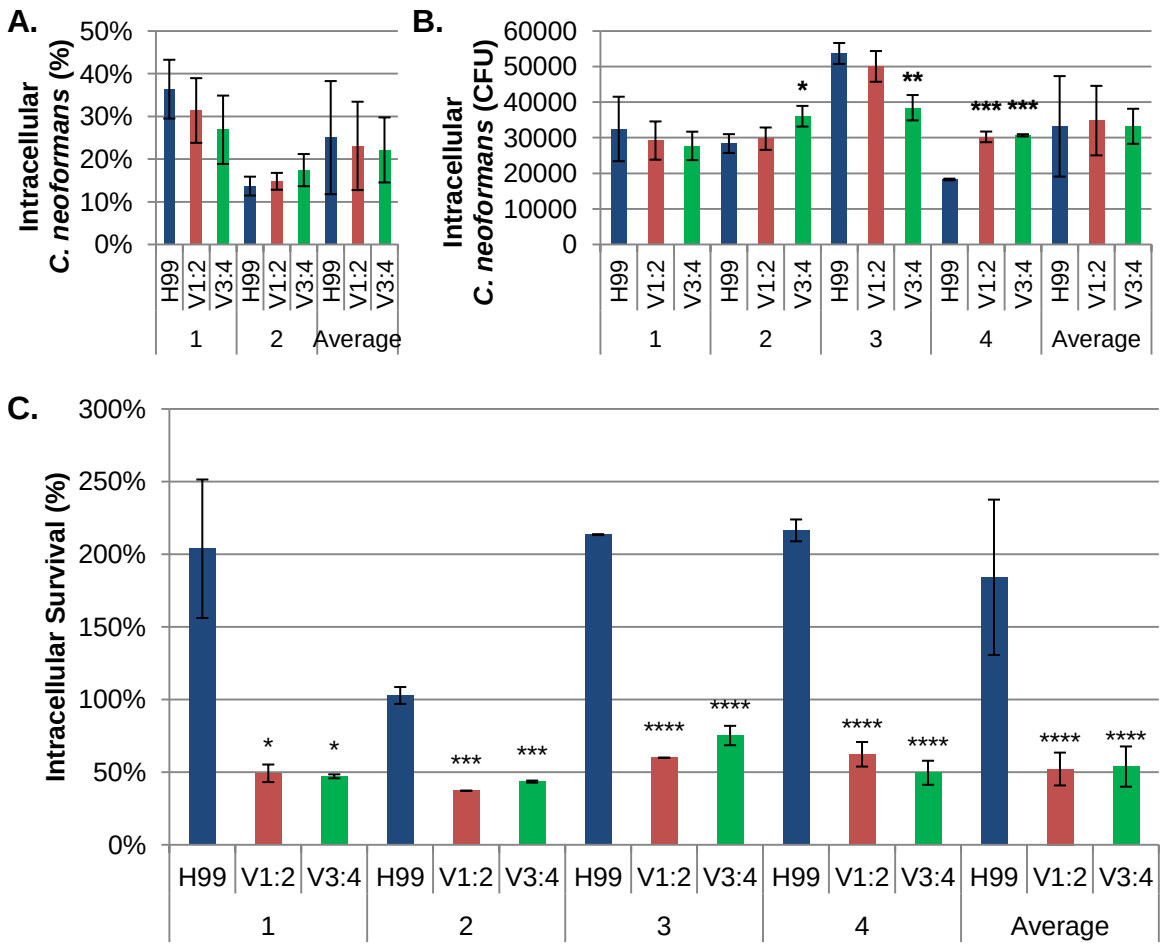

Figure 15. *VPS45* is required for intracellular survival within stimulated J774a.1 macrophages. A) Percent of macrophage observed with intracellular *C. neoformans* as determined by DIC microscopy at 2 hr of co-incubation. B) Uptake of *C. neoformans* at 2 hr as determined by CFU count analysis of washed and lysed macrophages. C) Survival percent determined by CFU count of *C. neoformans* at 24 hr divided by CFU count of *C. neoformans* at 2 hr. Cryptococcal strains and J774a.1 macrophages were incubated in DMEM at a MOI of 1:1 at 37 °C with 5 % CO_2 for 2, or 24 hrs. p-value determined by student's unpaired two tailed t-test with respect to H99 of the experiment, 1 asterisk indicates $0.05<p<0.01$, 2 indicates $0.01<p<0.005$, three indicates $0.005<p<0.001$, four indicates $p<0.001$. Experiments were performed in triplicate. Error bars are calculated standard deviations.

These experiments were recapitulated in the THP1 human cell line (Figure 16). Uptake of *C. neoformans* was determined at two hours of co-incubation, and no statistical difference was observed between wild-type strain H99 and the *vps45*Δ mutants (Figure 16A). Survival was severely inhibited by deletion of *VPS45* (Figure 16B), wild-type survival within macrophage was 109% and was reduced to 14-12 % in mutant strains. The tissue culture media was assayed for potential toxic effect on H99 and *vps45*Δ mutants (Table 2). Percent survival was determined by CFU count at 24 hours with respect to two hours. Percentage growth was determined by CFU count at 24 hours minus CFU count at two hours with respect to CFU count at 2 hours. These two parameters were utilized as measures of cryptococcal resilience in the assayed media. When compared to wild-type strain H99 the mutant *vps45*Δ strains had significantly reduced survival percentage and percent growth in DMEM, culture medium utilized for J774a.1. These observations had a similar trend in THP1 culture media, RPMI, but had much greater variance and as such no statistical significance could be determined. These data imply a marked reduction in fitness for the *vps45*Δ mutants when grown in mammalian tissue culture media and may account for a portion of the defects in macrophage survival. Despite the fitness loss in the tissue culture media, the decreased ability for *vps45*Δ mutants to survive macrophage dependent killing after 24 hours is relevant.

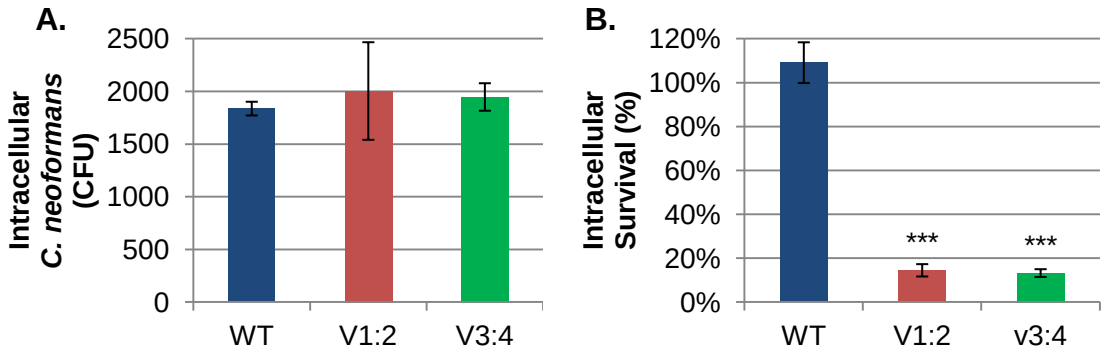

Figure 16. *VPS45* is required for intracellular survival within stimulated THP1 macrophages. A) Uptake of *C. neoformans* at 2 hr was determined by CFU count analysis of washed and lysed macrophages. B) Survival percent determined by CFU count of *C. neoformans* at 24 hr divided by CFU count of *C. neoformans* at 2 hr. Cryptococcal strains and THP1 macrophages were incubated in DMEM at a MOI of 1:1 at 37 °C with 5 % CO_2 for 2 or 24 hrs. p-value determined by student's unpaired two tailed t-test with respect to H99 of the experiment, 1 asterisk indicates $0.05<p<0.01$, 2 indicates $0.01<p<0.005$, 3 indicates $0.005<p<0.001$. Experiments were performed in triplicate and error bars are standard deviations.

Table 2. A *vps45*Δ is susceptible to growth inhibition in tissue culture media. Percent survival was determined as a ratio of CFU count at 24 hr with respect to CFU count at 2 hr. Percentage growth was determined as the ratio of the difference in CFU at 24 hr and 2 hr with respect to the CFU count at 2 hr. p-values were calculated by Student's unpaired two tailed t-test with respect to wild-type H99 in the experiment. DMEM and RPMI media were supplemented with 1% fetal bovine serum, and incubated at 37°C with 5% CO_2.

Media	Strain	Percentage Survival at 24 hr	p-value	Percentage Growth at 24 hr	p-value
DMEM	H99	1794.42 % ± 134.74 %	1	1694.42% ± 134.74%	1
	V1:2	28.61 % ± 7.14 %	0.00189	-71.39% ± 7.14%	0.00189
	V3:4	23.01 % ± 1.65 %	0.00192	-76.99% ± 1.65%	0.00192
RPMI	H99	515 % ± 892 %	1	415 % ± 892 %	1
	V1:2	15.53 ± 27 %	0.435	-83 % ± 27 %	0.433

Discussion

Previous work in the Kronstad laboratory has identified many iron responsive networks. Initial studies utilizing SAGE analysis of transcript populations from *C. neoformans* grown in defined iron media showed similarity to those isolated from *in vitro* macrophage culture and fungal cells recovered from *in vivo* murine models [258]. This work led to the development of a broader understanding of iron responsive gene networks by focusing on the regulatory transcription factors involved in this network. Several transcription factors have been implicated in iron response thus far including Cir1p, HapXp, Gat201p, Rim101p, and Nrg1p. However, the enrichment for genes that are predicted to play a role in iron function is best seen in experiments with HapXp and Cir1p.

Cir1p differentially regulates 2311 genes under iron limitation and 1623 upon iron repletion, of those the two most common gene ontology (GO) terms identified were in iron transport and siderophore transport [63]. HapXp was identified based on sequence similarity to a known iron regulatory complex in *A. nidulans* [259]. Mutational analysis of this component in *C. neoformans* showed that in differential iron media 2224 genes are down regulated and 2222 genes were up regulated [242]. The most significant defect in regulation was seen in LIM without iron supplementation where there were 1131 down and 910 up-regulated genes. Within these differentially regulated genes, GO term enrichment was observed in iron transport and siderophore transport. Among these differentially regulated genes, was *CIR1* and a gene, CNAG_03628.2, that was predicted to encode a protein involved in vacuolar protein sorting [242].

Specifically, the transcript levels of the open reading frame, CNAG_03628.2, were positively regulated by HapXp under low iron (~3X) and high iron (~5X) conditions. In addition, the gene is annotated as *VPSB* but has high amino acid sequence similarity to the *S. cerevisiae* protein Vps45p. Interestingly, *VPSB* is a gene within an operon of the bacterial pathogen *S. flexneri*, and the gene is implicated in the infection and invasion of host cells, maintenance of cytoplasmic membrane stability, and protein secretion [260]. We have determined by phylogenetic analysis that this annotation is incorrect, and indeed the best possible annotation at this time is *VPS45*; although it is striking to see that both *S. flexneri* VpsBp, and *C. neoformans*

Vps45p have roles in virulence. We suggest that the *C. neoformans* annotation be updated to *VPS45*, and that these qualifications be applied to other fungal genomes that are currently annotated with the misnomer of *VPSB* following adequate functional characterization.

In *S. cerevisiae,* Vps45p is an SM protein that mediates the SNARE activities and protein half-lives of Tlg2p [227]and Pep12p[230]. Tlg2p is responsible for vesicular traffic between the late Golgi and the endosome or PVC [231]. Pep12p is responsible for recognition of anterograde and retrograde vesicular trafficking at the PVC, including ESCRT pathway-generated endosomes [228, 230]. Targeted deletion of the chromosomal *C. neoformans VPS45* gene was performed to examine the role of the gene in virulence-related phenotypes, with the prediction that the phenotypes would result from impaired anterograde and retrograde vacuolar trafficking based on the observations in *S. cerevisiae*.

Iron utilization was assayed in our *vps45*Δ mutant with both liquid and solid media. In liquid culture, the *vps45*Δ strains were unable to grow with comparable kinetics to the wild-type strain in the presence of 10 μM and 100 μM $FeCl_3$. These growth deficiencies may be a result of an overload of free cytosolic iron because of impaired vacuolar storage of free iron resulting in [261]. An increase in cytosolic iron may continue until toxic, or fungistatic level is reached, as a result of defective signalling responses to iron accumulation. A distinct growth defect in liquid culture and in spot assays on solid medium was present when the extracellular iron source was limited to hemin, although this growth defect was not as prominent when cells were grown on solid YNB medium. Iron limitation can influence iron dependent processes such as DNA synthesis and repair, protein translation, and metabolic catalysis. Therefore under iron-starvation conditions the cell must prioritize essential iron-dependent processes. LIM is a minimal media with trace amount of minerals, 0.5% glucose, 0.5% L-asparagine, and 2.3 mM phosphate, and as such iron-dependent processes are all essential for cell survival. However in YNB amino acids are supplemented and glucose concentration is brought to 2% which may ease the metabolic constraints of LIM growth. Thus, it may be that these processes allow an increased basal level of growth irrespective of iron concentration. The iron-related growth phenotype defects of the *vps45*Δ mutant are similar to the hemin-deficient growth seen in *hapx*Δ and *vps23*Δ mutants [179, 242]. These phenotypes prompted a closer investigation of the subcellular localization of components utilized in the uptake of extracellular iron.

Impaired vacuolar trafficking of a reporter protein with clear vacuolar accumulation was observed in the *vps45*Δ mutant by microscopic analysis. In wild type cells, the Cfo1-GFPp fusion protein localizes to the plasma membrane within six hours of growth in iron-depleted conditions [63, 64], but vacuolar accumulation of the GFP signal is prominent by 2 days of growth. Co-localization with the pH sensitive LysoTracker Red revealed that the GFP signal is indeed vacuolar. The trends for localization in the *vps45*Δ mutant were markedly different as the GFP signal was present in a diffuse cytosolic pattern, associated with the plasma membrane, seen in punctuate cytosolic structures, and presumed endosomes due to lack of LysoTracker Red staining. However, multiple LysoTracker Red positive compartments that had positive co-localization with GFP signal indicated that a percentage of Cfo1-GFPp is able to reach the vacuole. These data indicate that vacuolar localization of the Cfo1-GFPp reporter was impaired in these mutants. These observations are consistent with the vacuolar structures and protein sorting defects observed in the deletion studies of *S. cerevisiae VPS45* [190]. Iron acquisition and utilization is dramatically affected in the *C. neoformans vps45*Δ mutant, and the localization of the ferroxidase, Cfo1p, is similarly affected. We propose that the utilization of heme in *C. neoformans* requires uptake of bound extracellular heme in an ESCRT-dependent process followed by trafficking to the PVC prior to an undescribed vacuolar metabolic process to liberate iron sequestered by heme that may utilize Cfo1p.

Cfo1p is utilized by *C. neoformans* in the high affinity uptake of extracellular soluble iron and deletion mutants have sustained growth defects when extracellular iron is limited to $FeCl_3$ or transferrin [64, 180]. In the *vps45*Δ mutant, the intracellular localization of Cfo1p is affected, as previously described. This may illustrate a dual role for Cfo1p: i.e., initially it may be utilized by the cell in iron uptake and then later in intracellular iron homeostasis by regulating cytosolic concentrations via vacuolar uptake or release. It is important to note that in liquid culture, the *vps45*Δ mutants also show reduced growth in the presence of $FeCl_3$ and hemin. These growth defects may be, as previously suggested, due to an accumulation of cytosolic iron to toxic levels. This suggestion correlates nicely with the observed localization pattern of Cfo1p in the wild-type strain, and the loss of proper localization in the *vps45*Δ mutant. Although these findings are an attractive rationale for the iron sensitive growth phenotypes, no characterized vacuolar iron transporters have been studied in *C. neoformans* and many genes have been

implicated in iron-sensitive growth. These include *FRE2, CFO2, CFT1*, *CIG1*, and a putative siderophore transporter *SIT1* [64, 177, 178, 180, 262].

Alternate cellular defects also exist beyond vacuolar morphology and protein trafficking in *vps45*Δ mutants. Cell wall integrity is also compromised in the *vps45*Δ mutants based on the observation that growth in the presence of cell wall and hyperosmotic stressors is reduced. These results are congruent with what has been observed in *vps45*Δ mutants of *S. cerevisiae* [251-253]. Vacuolar composition can alter the dynamics of the cell wall by affecting turgor pressure of the cell, and by influencing membrane protein turnover from recycling events. The cell wall integrity (CWI) pathway is responsible for mediating cellular response to extracellular stressors. Briefly, in *S. cerevisiae* the plasma transmembrane receptors Wsc1-3p, Mid1p, and Mtl1p sense extracellular stressors and activate G-protein Rho1 which activates protein kinase c (PKC) [263]. Subsequently PKC signals through a MAPK cascade by activating Bck1 (MAPKKK) that activates Mkk1p and Mkk2p (MAPKK's) which activates the MAPKs Mpk1p, and Slt2p [263]. In terms of cell wall stressors, calcofluor white antagonizes chitin synthesis, Congo red antagonizes glucan fibril growth, and the influence of caffeine is undetermined, but all three influence the CWI pathway.

A mutant in *Aspergillus niger* was isolated in a subunit of the V-ATPase which had similar cell wall sensitivities to the *vps45*Δ mutant in *C. neoformans* [264]. When wild-type *A. niger* cells were treated with bafilomycinB(1), a V-ATPase inhibitor, CWI-associated gene transcription was increased. These results serve to correlate increased cell wall stress sensitivity with vacuolar proton pump activity and acidification of the vacuole. In *C. neoformans*, the *vps45*Δ mutant V-ATPase activity is unaffected, as determined by positive LysoTracker red staining, but the vacuole is fragmented and localization of V-ATPase or associated cell wall machinery may be affected. Two *S. cerevisiae* studies have identified Slt2p as an inhibitor of non-apoptotic yeast cell death as a result of ER stress [265, 266]. One study showed that vacuolar permeablization by V-ATPase activity was the causative agent of cell death in a process similar to neuron necrosis [266]. If vacuolar trafficking is reduced in conjunction with late Golgi protein efflux while cells are undergoing a cell wall stress event, then ER stress is expected to occur. Perhaps, this may be an additional rationale for an increased susceptibility to cell wall stressors in vacuolar mutants.

The antimalarial drugs chloroquine and quinacrine are weak bases which are lysosomotropic and that preferentially accumulate in acidic environments. Studies in *C. neoformans* have shown that these drugs are effective in reducing intracellular macrophage survival *in vitro*, as well as decreased fungal burden during murine *in vivo* infection [217]. These drugs are known to inhibit heme utilization in the vacuoles of *Plasmodium* spp. by sequestering monomeric and dimeric heme to terminate hemozoin crystal formation [267, 268]; they also cause DNA damage by intercalating into DNA, by inhibiting DNA topoisomerase and helicase, and by inhibiting DNA and RNA polymerases [269]. DNA damage has been associated with autophagy in *S. cerevisiae* such that inhibition of the cytoplasm-to-vacuole pathway inhibits cell cycle progression [270]. Iron-deprivation by chloroquine and quinacrine during intracellular growth has been observed in *Legionella pneumophila* [271] and *Histoplasma capsulatum* [272], although no defect in iron utilization was observed in *C. neoformans*. Therefore, a general toxicity model including DNA damage and disruption of vacuolar acidification has been proposed [256].

Disruption of the arachidonic acid pathway by inhibition of phospholipase A2 is correlated with plasma membrane association of quinacrine [273]. *C. neoformans* utilizes arachidonic acid during pathogenesis via Lac1p-dependent metabolism to generate prostaglandin E2 which inhibits IL-17 induction of T-cells during differentiation [274, 275]. It is important to note that *vps45*Δ mutants have decreased ability to utilize extracellular heme, and show increased susceptibility to chloroquine and quinacrine treatment. It is apparent that Vps45p control of trafficking through the PVC is necessary for wild-type levels of resistance to the drugs. This may be a result of defective transport of a resident vacuolar efflux protein such as the observations in the mutated drug efflux protein in *Plasmodium falciparum* encoded by the gene *PfCRT* [276]. Perhaps the vacuole is compromised in some other way and susceptible to vacuolar loading of the drugs. The interpretation is however the same in thatthe vacuole is compromised in these mutants as a result of the loss of *VPS45*, and observations strongly phenocopy the orthologous gene described in *S. cerevisiae VPS45*. This conclusion is supported by phylogenetic analysis, similar stress phenotypes, and the aberrant localization of Cfo1-GFPp.

The phenotypic characterization of mutants lacking *VPS45* prompted us to also analyze the role of vacuolar trafficking in virulence. As mentioned previously the three primary virulence

factors of *C. neoformans* are the ability to proliferate at 37°C, melanin formation via the action of Lac1p and Lac2p on host-derived precursors, and production of an immunomodulatory polysaccharide capsule. No correlation between thermal sensitivity and the status of *VPS45* was observed upon growth on YPD or YNB media at 37°C, although toxicity of all stressors was increased when cells were assayed at 37°C. Previous work suggests that Vps23p and mutants in other ESCRT complexes (G. Hu, unpublished data) were acapsular and had defective melanization [179]. In the *vps23*Δ mutants, capsule polymer was secreted, but elaboration of cellular capsule never occurred. We therefore expected the null *vps45*Δ mutant to be defective in the establishment of the polysaccharide capsule and melanin. However, there were no observed differences in the ability of the *vps45*Δ mutant to produce cell-associated polysaccharide capsule, and near wild-type levels of melanin were observed. Thus, Vps45p-dependent transit processes are not required for capsule elaboration or melanin biosynthesis.

Previous reports have shown that drugs like bafilomycin A, chloroquine, quinacrine, and small molecules like ammonium chloride which disrupt pH gradients in *C. neoformans* have a negative effect on melanization, or capsule establishment [207, 217, 218, 256]. Consistent with these observations, we found that the *vps45*Δ mutant and the wild-type strain H99 showed reduced cell-associated capsule upon challenge with 250 μM chloroquine. Although, these effects may be due to vesicular accumulation of chloroquine, as many exocytic and endocytic vesicles maintain a low pH, the majority of the drug is localized to the vacuolar compartment. We conclude that although trafficking of capsule requires endocytic components for elaboration, these reactions are not dependent of Vps45p prevacuolar trafficking, but may still transit through the vacuole or PVC because they appear to be sensitive to weak bases, vacuolar drugs, and V-ATPase inhibitors.

In our deletion strains, we observed significant loss of growth capability during interactions with the J774a.1 and THP1 macrophage-like cell line. On average, *vps45*Δ mutants do not appear to have significant losses when compared to wild type in measurement of CFU at 2 hr of co-incubation. These data indicate that macrophages are able to detect and ingest both the mutant and wild-type strains with near equal efficiency. However a significant defect is observed in fungal counts after 24 hours of co-incubation with macrophages. Specifically, it appears that Vps45p functions are required to survive the phagolysosome.

Further study of the culture conditions showed that *vps45*Δ mutants are unable to persist in DMEM or RPMI media, with or without the addition of FBS, as determined by CFU counts. In this media nutrients are optimized for the growth of mammalian cells, and as such growth limitations for *C. neoformans* may be found in mutants defective in vacuolar storage or release of phosphates, metals, and amino acids. Tissue culture media sensitivity may be a result of defective signalling response to the extracellular milieu. The *vps45*Δ mutants have shown defective CWI response and these defects may not be limited solely to cell wall agonists. If these cells were unable to sense nutrient limitations this could inhibit adaptation to the media and may induce alternate survival programs [197, 270]. In this scenario a starvation response would be triggered, and cells would begin to undergo autophagy. If the *vps45*Δ mutant was non-responsive to autophagy induction, cell death could occur. As seen in yeast stress conditions, permeablization of the vacuole is required for non-apoptotic death [266]. Ergo, if the *C. neoformans* vacuole is as highly disordered as believed in the *vps45*Δ mutant it may be primed for cell death responses. Alternatively, if vacuolar inheritance is negatively affected by the *vps45*Δ mutant in *C. neoformans* cell division could be impacted, a process that would drastically affect CFU counts [277]. The compliment present in the supplemented FBS used in the tissue culture media may be functional and result in lysis of mutant strains which are defective in osmotolerance, polysaccharide capsule, and cell wall stressors. Importantly, these observations indicate that vacuolar function is crucial for intracellular survival, and within tissue culture growth media conditions.

Collectively these data suggest a wide variety of physiological and pathogenesis-related roles for the vacuole in the opportunistic pathogen *C. neoformans*. It is clear that vacuolar protein trafficking is responsible for a wide variety of phenotypic properties including iron utilization from soluble free iron and heme, CWI stress response, and intracellular survival in macrophages. We believe that these phenotypes strongly imply that these mutants will be avirulent in a murine infection model and these experiments will be performed in future work on this project. The evidence collected and referenced in this thesis supports a focused future effort to study vacuolar development and associated implications of virulence in fungi. As a direct extension of our analyses, we believe that it will be important to characterize the vacuolar protein sorting defects of *vps45*Δ mutants with respect to the classical studies performed in *S. cerevisiae*.

These would include analyzing the localization and maturation of Cpy1p, Pho8p and Vph1p in the *vps45*Δ background. Further analysis can be performed on the exopolysaccharide fraction associated and shed from the cell via antibody blotting, and the ratio of sugars within the capsule by immunofluorescence. These studies would determine whether vacuolar function is important for capsule synthesis and export. Secretion of associated virulence factors such as secreted proteinases, urease, and the phospholipase Plb1p may help explain the phenotypes observed in macrophage uptake. Further work can be performed with the cognate SNARE proteins to prove interactions with Vps45p as well as individual deletion studies to analyze the impact each of these factors has on cell physiology and virulence.

Fungal pathogens represent a significant global health, economic, and ecological burden. The development of new antifungal drugs to combat these outbreaks represents a prominent scientific and social concern. Recent work has illustrated that fungal physiology is reliant on a functional vacuole because it is a central component of biosynthetic, endocytic and autophagic traffic [184-186, 197, 270]. By developing this organelle as a biological model future discoveries may be made which can be leveraged as future drug targets. For example, comparison of the V-ATPase organization in mammals and fungi have identified significant differences between structure, regulation and disassembly that it is being utilized in drug development screens as a therapeutic target in the model fungal pathogen *C. albicans* [278]. We strongly believe that the pursuit to understand physiological vacuolar function in *C. neoformans* will lead to similar discoveries, and potential avenues of therapeutic applications within and outside of the genus *Cyrptococcus*.

References

1. Jones, D.T., W.R. Taylor, and J.M. Thornton, *The rapid generation of mutation data matrices from protein sequences.* Comput Appl Biosci, 1992. **8**(3): p. 275-82.
2. Tamura, K., et al., *MEGA6: Molecular Evolutionary Genetics Analysis version 6.0.* Mol Biol Evol, 2013. **30**(12): p. 2725-9.
3. Cogliati, M., *Global Molecular Epidemiology of Cryptococcus neoformans and Cryptococcus gattii: An Atlas of the Molecular Types.* Scientifica (Cairo), 2013. **2013**: p. 675213.
4. Steenbergen, J.N., H.A. Shuman, and A. Casadevall, *Cryptococcus neoformans Interactions with Amoebae Suggest an Explanation for its Virulence and Intracellular Pathogenic Strategy in Macrophages.* Proceedings of the National Academy of Sciences, 2001. **98**(26): p. 15245-15250.
5. Derengowski Lda, S., et al., *The transcriptional response of Cryptococcus neoformans to ingestion by Acanthamoeba castellanii and macrophages provides insights into the evolutionary adaptation to the mammalian host.* Eukaryot Cell, 2013. **12**(5): p. 761-74.
6. Velagapudi, R., et al., *Spores as infectious propagules of Cryptococcus neoformans.* Infect Immun, 2009. **77**(10): p. 4345-55.
7. Botts, M.R., et al., *Isolation and characterization of Cryptococcus neoformans spores reveal a critical role for capsule biosynthesis genes in spore biogenesis.* Eukaryot Cell, 2009. **8**(4): p. 595-605.
8. Geunes-Boyer, S., et al., *Surfactant protein D facilitates Cryptococcus neoformans infection.* Infect Immun, 2012. **80**(7): p. 2444-53.
9. Hartl, D. and M. Griese, *Surfactant protein D in human lung diseases.* Eur J Clin Invest, 2006. **36**(6): p. 423-35.
10. Nicola, A.M. and A. Casadevall, *In vitro measurement of phagocytosis and killing of Cryptococcus neoformans by macrophages.* Methods Mol Biol, 2012. **844**: p. 189-97.
11. Sabiiti, W. and R.C. May, *Mechanisms of infection by the human fungal pathogen Cryptococcus neoformans.* Future Microbiol, 2012. **7**(11): p. 1297-313.
12. McQuiston, T.J. and P.R. Williamson, *Paradoxical roles of alveolar macrophages in the host response to Cryptococcus neoformans.* J Infect Chemother, 2012. **18**(1): p. 1-9.
13. Alvarez, M. and A. Casadevall, *Phagosome Extrusion and Host-Cell Survival after Cryptococcus neoformans Phagocytosis by Macrophages.* Current Biology, 2006. **16**(21): p. 2161-2165.
14. Bolaños, B. and T.G. Mitchell, *Phagocytosis of Cryptococcus neoformans by Rat Alveolar Macrophages.* Medical Mycology, 1989. **27**(4): p. 203-217.
15. Goldman, D.L., et al., *Persistent Cryptococcus neoformans pulmonary infection in the rat is associated with intracellular parasitism, decreased inducible nitric oxide synthase expression, and altered antibody responsiveness to cryptococcal polysaccharide.* Infect Immun, 2000. **68**(2): p. 832-8.
16. Crabtree, J.N., et al., *Titan cell production enhances the virulence of Cryptococcus neoformans.* Infect Immun, 2012. **80**(11): p. 3776-85.
17. Zaragoza, O., et al., *Fungal cell gigantism during mammalian infection.* PLoS Pathog, 2010. **6**(6): p. e1000945.

18. Barbosa, F.M., et al., *Glucuronoxylomannan-mediated interaction of Cryptococcus neoformans with human alveolar cells results in fungal internalization and host cell damage.* Microbes Infect, 2006. **8**(2): p. 493-502.
19. Merkel, G.J. and B.A. Scofield, *The in vitro interaction of Cryptococcus neoformans with human lung epithelial cells.* FEMS Immunol Med Microbiol, 1997. **19**(3): p. 203-13.
20. Shao, X., et al., *An innate immune system cell is a major determinant of species-related susceptibility differences to fungal pneumonia.* J Immunol, 2005. **175**(5): p. 3244-51.
21. Kechichian, T.B., J. Shea, and M. Del Poeta, *Depletion of alveolar macrophages decreases the dissemination of a glucosylceramide-deficient mutant of Cryptococcus neoformans in immunodeficient mice.* Infect Immun, 2007. **75**(10): p. 4792-8.
22. Nicola, A.M., et al., *Nonlytic exocytosis of Cryptococcus neoformans from macrophages occurs in vivo and is influenced by phagosomal pH.* MBio, 2011. **2**(4).
23. Alvarez, M. and A. Casadevall, *Cell-to-cell spread and massive vacuole formation after Cryptococcus neoformans infection of murine macrophages.* BMC Immunol, 2007. **8**: p. 16.
24. Ma, H., et al., *Expulsion of Live Pathogenic Yeast by Macrophages.* Current Biology, 2006. **16**(21): p. 2156-2160.
25. García-Rodas, R. and O. Zaragoza, *Catch Me if You Can: Phagocytosis and Killing Avoidance by Cryptococcus neoformans.* FEMS Immunology & Medical Microbiology, 2011: p. n/a-n/a.
26. Tabassum, S., et al., *Cryptococcal meningitis with secondary cutaneous involvement in an immunocompetent host.* J Infect Dev Ctries, 2013. **7**(9): p. 680-5.
27. Zacharia, A., et al., *A case of disseminated cryptococcosis with skin manifestations in a patient with newly diagnosed HIV.* J La State Med Soc, 2013. **165**(3): p. 171-4.
28. Alhaji, M. and R.T. Sadikot, *Cryptococcal endocarditis.* South Med J, 2011. **104**(5): p. 363-4.
29. Zhang, C., et al., *Isolated hepatobiliary cryptococcosis manifesting as obstructive jaundice in an immunocompetent child: case report and review of the literature.* Eur J Pediatr, 2013.
30. Lin, X. and J. Heitman, *The biology of the Cryptococcus neoformans species complex.* Annu Rev Microbiol, 2006. **60**: p. 69-105.
31. Kronstad, J.W., et al., *Expanding Fungal Pathogenesis: Cryptococcus Breaks out of the Opportunistic Box.* Nat Rev Microbiol, 2011. **9**(3): p. 193-203.
32. Casadevall, A., *Cryptococci at the brain gate: break and enter or use a Trojan horse?* J Clin Invest, 2010. **120**(5): p. 1389-92.
33. O'Shea, E., et al., *Current preclinical studies on neuroinflammation and changes in blood-brain barrier integrity by MDMA and methamphetamine.* Neuropharmacology, 2014.
34. Pulzova, L., M.R. Bhide, and K. Andrej, *Pathogen translocation across the blood-brain barrier.* FEMS Immunol Med Microbiol, 2009. **57**(3): p. 203-13.
35. Charlier, C., et al., *Evidence of a role for monocytes in dissemination and brain invasion by Cryptococcus neoformans.* Infect Immun, 2009. **77**(1): p. 120-7.
36. Chang, Y.C., et al., *Cryptococcal Yeast Cells Invade the Central Nervous System via Transcellular Penetration of the Blood-Brain Barrier.* Infect. Immun., 2004. **72**(9): p. 4985-4995.

37. Maruvada, R., et al., *Cryptococcus neoformans phospholipase B1 activates host cell Rac1 for traversal across the blood-brain barrier.* Cell Microbiol, 2012. **14**(10): p. 1544-53.
38. Griffiths, E.J., M. Kretschmer, and J.W. Kronstad, *Aimless mutants of Cryptococcus neoformans: failure to disseminate.* Fungal Biol Rev, 2012. **26**(2-3): p. 61-72.
39. Ikeda, R. and T. Ichikawa, *Interaction of surface molecules on Cryptococcus neoformans with plasminogen.* FEMS Yeast Res, 2013.
40. Shi, M., et al., *Real-time imaging of trapping and urease-dependent transmigration of Cryptococcus neoformans in mouse brain.* J Clin Invest, 2010. **120**(5): p. 1683-93.
41. Stie, J.T. and D.S. Fox, *Blood-brain Barrier Invasion by Cryptococcus neoformans is Enhanced by Functional Interactions with Plasmin.* Microbiology, 2011.
42. Kanmogne, G.D., et al., *HIV-1 gp120 compromises blood-brain barrier integrity and enhances monocyte migration across blood-brain barrier: implication for viral neuropathogenesis.* J Cereb Blood Flow Metab, 2007. **27**(1): p. 123-34.
43. Park, B.J., et al., *Estimation of the Current Global Burden of Cryptococcal Meningitis Among Persons Living with HIV/AIDS.* AIDS, 2009. **23**(4): p. 525-30.
44. Prevention, C.f.D.C.a. *C. neoformans cryptococcosis*. 2012 May 6, 2013 [cited 2014 February 20]; Available from: http://www.cdc.gov/fungal/cryptococcosis-neoformans/.
45. Kausik Datta, K.H.B., Rebecca Baer, Edmond Byrnes, Eleni Galanis, Joseph Heitman, Linda Hoang, Mira J. Leslie, Laura MacDougall, Shelley S. Magill, Muhammad G. Morshed, Kieren A. MarrComments to Author , and for the Cryptococcus gattii Working Group of the Pacific Northwes *Spread of Cryptococcus gattii into Pacific Northwest Region of the United States*. Emerging Infectious Diseases, 2009. **15**.
46. Leongson, K., et al., *Altered immune response differentially enhances susceptibility to Cryptococcus neoformans and Cryptococcus gattii infection in mice expressing the HIV-1 transgene.* Infect Immun, 2013. **81**(4): p. 1100-13.
47. Kwon-Chung, K.J. and J.E. Bennett, *High prevalence of Cryptococcus neoformans var. gattii in tropical and subtropical regions.* Zentralbl Bakteriol Mikrobiol Hyg A, 1984. **257**(2): p. 213-8.
48. Kwon-Chung, K.J. and J.E. Bennett, *Epidemiologic differences between the two varieties of Cryptococcus neoformans.* Am J Epidemiol, 1984. **120**(1): p. 123-30.
49. Prevention, C.f.D.C.a., *Emergence of Cryptococcus gattii—Pacific Northwest.* MMWR Morb Mortal Wkly Rep, 2010. **59**(28): p. 865–868.
50. Zaragoza, O., et al., *Capsule Enlargement in Cryptococcus neoformans Confers Resistance to Oxidative Stress Suggesting a Mechanism for Intracellular Survival.* Cellular Microbiology, 2008. **10**(10): p. 2043-2057.
51. Chang, Y.C. and K.J. Kwon-Chung, *Complementation of a Capsule-deficient Mutation of Cryptococcus neoformans Restores its Virulence.* Mol. Cell. Biol., 1994. **14**(7): p. 4912-4919.
52. Dong, Z. and J. Murphy, *Effects of the Two Varieties of Cryptococcus neoformans Cells and Culture Filtrate Antigens on Neutrophil Locomotion.* Infect. Immun., 1995. **63**(7): p. 2632-2644.
53. Lipovsky, M.M., et al., *Cryptococcal Glucuronoxylomannan Induces Interleukin (IL)-8 Production by Human Microglia but Inhibits Neutrophil Migration toward IL-8.* Journal of Infectious Diseases, 1998. **177**(1): p. 260-263.

54. Vecchiarelli, A., et al., *Purified Capsular Polysaccharide of Cryptococcus neoformans Induces Interleukin-10 Secretion by Human Monocytes.* Infect. Immun., 1996. **64**(7): p. 2846-2849.
55. Wang, Y., P. Aisen, and A. Casadevall, *Cryptococcus neoformans melanin and virulence: mechanism of action.* Infect Immun, 1995. **63**(8): p. 3131-6.
56. Aubry, A.F., *Applications of affinity chromatography to the study of drug-melanin binding interactions.* J Chromatogr B Analyt Technol Biomed Life Sci, 2002. **768**(1): p. 67-74.
57. Kwon-Chung, K.J., I. Polacheck, and T.J. Popkin, *Melanin-lacking mutants of Cryptococcus neoformans and their virulence for mice.* J Bacteriol, 1982. **150**(3): p. 1414-21.
58. Eisenman, H.C., et al., *Cryptococcus neoformans laccase catalyses melanin synthesis from both D- and L-DOPA.* Microbiology, 2007. **153**(Pt 12): p. 3954-62.
59. Kraus, P.R., C.B. Nichols, and J. Heitman, *Calcium- and calcineurin-independent roles for calmodulin in Cryptococcus neoformans morphogenesis and high-temperature growth.* Eukaryot Cell, 2005. **4**(6): p. 1079-87.
60. Glazier, V.E. and J.C. Panepinto, *The ER stress response and host temperature adaptation in the human fungal pathogen Cryptococcus neoformans.* Virulence, 2013. **5**(2).
61. Fu, J., I.R. Morris, and B.L. Wickes, *The production of monokaryotic hyphae by Cryptococcus neoformans can be induced by high temperature arrest of the cell cycle and is independent of same-sex mating.* PLoS Pathog, 2013. **9**(5): p. e1003335.
62. Jung, W.H. and J.W. Kronstad, *Iron and fungal pathogenesis: a case study with Cryptococcus neoformans.* Cell Microbiol, 2008. **10**(2): p. 277-84.
63. Jung, W.H., et al., *Iron Regulation of the Major Virulence Factors in the AIDS-Associated Pathogen <named-content xmlns:xlink="http://www.w3.org/1999/xlink" content-type="genus-species" xlink:type="simple">Cryptococcus neoformans</named-content>.* PLoS Biol, 2006. **4**(12): p. e410.
64. Jung, W.H., et al., *Iron Source Preference and Regulation of Iron Uptake in Cryptococcus neoformans.* PLoS Pathog, 2008. **4**(2): p. e45.
65. Jakobsen, H. and I. Jonsdottir, *Mucosal vaccination against encapsulated respiratory bacteria--new potentials for conjugate vaccines?* Scand J Immunol, 2003. **58**(2): p. 119-28.
66. Garcia-Rodas, R. and O. Zaragoza, *Catch me if you can: phagocytosis and killing avoidance by Cryptococcus neoformans.* FEMS Immunol Med Microbiol, 2012. **64**(2): p. 147-61.
67. O'Meara, T.R. and J.A. Alspaugh, *The Cryptococcus neoformans capsule: a sword and a shield.* Clin Microbiol Rev, 2012. **25**(3): p. 387-408.
68. Monari, C., et al., *Differences in outcome of the interaction between Cryptococcus neoformans glucuronoxylomannan and human monocytes and neutrophils.* Eur J Immunol, 2003. **33**(4): p. 1041-51.
69. Yauch, L.E., M.K. Mansour, and S.M. Levitz, *Receptor-mediated clearance of Cryptococcus neoformans capsular polysaccharide in vivo.* Infect Immun, 2005. **73**(12): p. 8429-32.

70. Grinsell, M., et al., *In vivo clearance of glucuronoxylomannan, the major capsular polysaccharide of Cryptococcus neoformans: a critical role for tissue macrophages.* J Infect Dis, 2001. **184**(4): p. 479-87.
71. Hansen, J., et al., *Large-scale evaluation of the immuno-mycologics lateral flow and enzyme-linked immunoassays for detection of cryptococcal antigen in serum and cerebrospinal fluid.* Clin Vaccine Immunol, 2013. **20**(1): p. 52-5.
72. Jain, N., A. Guerrero, and B.C. Fries, *Phenotypic switching and its implications for the pathogenesis of Cryptococcus neoformans.* FEMS Yeast Res, 2006. **6**(4): p. 480-8.
73. Feldmesser, M., et al., *Cryptococcus neoformans is a facultative intracellular pathogen in murine pulmonary infection.* Infect Immun, 2000. **68**(7): p. 4225-37.
74. Naslund, P.K., W.C. Miller, and D.L. Granger, *Cryptococcus neoformans fails to induce nitric oxide synthase in primed murine macrophage-like cells.* Infect Immun, 1995. **63**(4): p. 1298-304.
75. Walenkamp, A.M., et al., *Cryptococcus neoformans and its cell wall components induce similar cytokine profiles in human peripheral blood mononuclear cells despite differences in structure.* FEMS Immunol Med Microbiol, 1999. **26**(3-4): p. 309-18.
76. Vecchiarelli, A., et al., *The polysaccharide capsule of Cryptococcus neoformans interferes with human dendritic cell maturation and activation.* J Leukoc Biol, 2003. **74**(3): p. 370-8.
77. Coenjaerts, F.E., et al., *Potent inhibition of neutrophil migration by cryptococcal mannoprotein-4-induced desensitization.* J Immunol, 2001. **167**(7): p. 3988-95.
78. Monari, C., et al., *Cryptococcus neoformans capsular glucuronoxylomannan induces expression of fas ligand in macrophages.* J Immunol, 2005. **174**(6): p. 3461-8.
79. Villena, S.N., et al., *Capsular polysaccharides galactoxylomannan and glucuronoxylomannan from Cryptococcus neoformans induce macrophage apoptosis mediated by Fas ligand.* Cell Microbiol, 2008. **10**(6): p. 1274-85.
80. Piccioni, M., et al., *A critical role for FcgammaRIIB in up-regulation of Fas ligand induced by a microbial polysaccharide.* Clin Exp Immunol, 2011. **165**(2): p. 190-201.
81. Monari, C., et al., *A microbial polysaccharide reduces the severity of rheumatoid arthritis by influencing Th17 differentiation and proinflammatory cytokines production.* J Immunol, 2009. **183**(1): p. 191-200.
82. Kwon-Chung, K.J., I. Polacheck, and J.E. Bennett, *Improved diagnostic medium for separation of Cryptococcus neoformans var. neoformans (serotypes A and D) and Cryptococcus neoformans var. gattii (serotypes B and C).* J Clin Microbiol, 1982. **15**(3): p. 535-7.
83. Boekhout, T., et al., *Molecular typing of Cryptococcus neoformans: taxonomic and epidemiological aspects.* Int J Syst Bacteriol, 1997. **47**(2): p. 432-42.
84. Franzot, S.P., I.F. Salkin, and A. Casadevall, *Cryptococcus neoformans var. grubii: separate varietal status for Cryptococcus neoformans serotype A isolates.* J Clin Microbiol, 1999. **37**(3): p. 838-40.
85. Cordero, R.J., et al., *Chronological aging is associated with biophysical and chemical changes in the capsule of Cryptococcus neoformans.* Infect Immun, 2011. **79**(12): p. 4990-5000.
86. Jain, N. and B.C. Fries, *Phenotypic switching of Cryptococcus neoformans and Cryptococcus gattii.* Mycopathologia, 2008. **166**(4): p. 181-8.

87. Chang, Y.C., L.A. Penoyer, and K.J. Kwon-Chung, *The second capsule gene of cryptococcus neoformans, CAP64, is essential for virulence.* Infect Immun, 1996. **64**(6): p. 1977-83.
88. Chang, Y.C. and K.J. Kwon-Chung, *Isolation of the third capsule-associated gene, CAP60, required for virulence in Cryptococcus neoformans.* Infect Immun, 1998. **66**(5): p. 2230-6.
89. Chang, Y.C. and K.J. Kwon-Chung, *Isolation, characterization, and localization of a capsule-associated gene, CAP10, of Cryptococcus neoformans.* J Bacteriol, 1999. **181**(18): p. 5636-43.
90. Vaishnav, V.V., et al., *Structural characterization of the galactoxylomannan of Cryptococcus neoformans Cap67.* Carbohydr Res, 1998. **306**(1-2): p. 315-30.
91. Jesus, M.D., et al., *Glucuronoxylomannan, galactoxylomannan, and mannoprotein occupy spatially separate and discrete regions in the capsule of Cryptococcus neoformans.* Virulence, 2010. **1**(6): p. 500-8.
92. McFadden, D.C., et al., *Capsule structural heterogeneity and antigenic variation in Cryptococcus neoformans.* Eukaryot Cell, 2007. **6**(8): p. 1464-73.
93. Moyrand, F. and G. Janbon, *UGD1, encoding the Cryptococcus neoformans UDP-glucose dehydrogenase, is essential for growth at 37 degrees C and for capsule biosynthesis.* Eukaryot Cell, 2004. **3**(6): p. 1601-8.
94. Wills, E.A., et al., *Identification and characterization of the Cryptococcus neoformans phosphomannose isomerase-encoding gene, MAN1, and its impact on pathogenicity.* Mol Microbiol, 2001. **40**(3): p. 610-20.
95. Moyrand, F., et al., *UGE1 and UGE2 regulate the UDP-glucose/UDP-galactose equilibrium in Cryptococcus neoformans.* Eukaryot Cell, 2008. **7**(12): p. 2069-77.
96. Bar-Peled, M., C.L. Griffith, and T.L. Doering, *Functional cloning and characterization of a UDP- glucuronic acid decarboxylase: the pathogenic fungus Cryptococcus neoformans elucidates UDP-xylose synthesis.* Proc Natl Acad Sci U S A, 2001. **98**(21): p. 12003-8.
97. Klutts, J.S. and T.L. Doering, *Cryptococcal xylosyltransferase 1 (Cxt1p) from Cryptococcus neoformans plays a direct role in the synthesis of capsule polysaccharides.* J Biol Chem, 2008. **283**(21): p. 14327-34.
98. Klutts, J.S., S.B. Levery, and T.L. Doering, *A beta-1,2-xylosyltransferase from Cryptococcus neoformans defines a new family of glycosyltransferases.* J Biol Chem, 2007. **282**(24): p. 17890-9.
99. Sommer, U., H. Liu, and T.L. Doering, *An alpha-1,3-mannosyltransferase of Cryptococcus neoformans.* J Biol Chem, 2003. **278**(48): p. 47724-30.
100. Janbon, G., et al., *Cas1p is a membrane protein necessary for the O-acetylation of the Cryptococcus neoformans capsular polysaccharide.* Mol Microbiol, 2001. **42**(2): p. 453-67.
101. Panepinto, J., et al., *Sec6-dependent Sorting of Fungal Extracellular Exosomes and Laccase of Cryptococcus neoformans.* Molecular Microbiology, 2009. **71**(5): p. 1165-1176.
102. Yoneda, A. and T.L. Doering, *An unusual organelle in Cryptococcus neoformans links luminal pH and capsule biosynthesis.* Fungal Genet Biol, 2009. **46**(9): p. 682-7.
103. Kmetzsch, L., et al., *Role for Golgi reassembly and stacking protein (GRASP) in polysaccharide secretion and fungal virulence.* Mol Microbiol, 2011. **81**(1): p. 206-18.

104. Casadevall, A., *Amoeba provide insight into the origin of virulence in pathogenic fungi.* Adv Exp Med Biol, 2012. **710**: p. 1-10.
105. Robert, V.A. and A. Casadevall, *Vertebrate endothermy restricts most fungi as potential pathogens.* J Infect Dis, 2009. **200**(10): p. 1623-6.
106. Hu, G., et al., *Metabolic adaptation in Cryptococcus neoformans during early murine pulmonary infection.* Mol Microbiol, 2008. **69**(6): p. 1456-75.
107. Kozubowski, L., et al., *Association of calcineurin with the COPI protein Sec28 and the COPII protein Sec13 revealed by quantitative proteomics.* PLoS One, 2011. **6**(10): p. e25280.
108. Odom, A., et al., *Calcineurin is required for virulence of Cryptococcus neoformans.* EMBO J, 1997. **16**(10): p. 2576-89.
109. Havel, V.E., et al., *Ccr4 promotes resolution of the endoplasmic reticulum stress response during host temperature adaptation in Cryptococcus neoformans.* Eukaryot Cell, 2011. **10**(7): p. 895-901.
110. Shapiro, R.S. and L. Cowen, *Coupling temperature sensing and development: Hsp90 regulates morphogenetic signalling in Candida albicans.* Virulence, 2010. **1**(1): p. 45-8.
111. Shapiro, R.S., et al., *Hsp90 orchestrates temperature-dependent Candida albicans morphogenesis via Ras1-PKA signaling.* Curr Biol, 2009. **19**(8): p. 621-9.
112. Shapiro, R.S., et al., *The Hsp90 co-chaperone Sgt1 governs Candida albicans morphogenesis and drug resistance.* PLoS One, 2012. **7**(9): p. e44734.
113. Senn, H., R.S. Shapiro, and L.E. Cowen, *Cdc28 provides a molecular link between Hsp90, morphogenesis, and cell cycle progression in Candida albicans.* Mol Biol Cell, 2012. **23**(2): p. 268-83.
114. Shapiro, R.S., et al., *Pho85, Pcl1, and Hms1 signaling governs Candida albicans morphogenesis induced by high temperature or Hsp90 compromise.* Curr Biol, 2012. **22**(6): p. 461-70.
115. Lamoth, F., et al., *Heat shock protein 90 is required for conidiation and cell wall integrity in Aspergillus fumigatus.* Eukaryot Cell, 2012. **11**(11): p. 1324-32.
116. Lamoth, F., et al., *In vitro activity of calcineurin and heat shock protein 90 Inhibitors against Aspergillus fumigatus azole- and echinocandin-resistant strains.* Antimicrob Agents Chemother, 2013. **57**(2): p. 1035-9.
117. Singh, S.D., et al., *Hsp90 governs echinocandin resistance in the pathogenic yeast Candida albicans via calcineurin.* PLoS Pathog, 2009. **5**(7): p. e1000532.
118. Sanglard, D., et al., *Calcineurin A of Candida albicans: involvement in antifungal tolerance, cell morphogenesis and virulence.* Mol Microbiol, 2003. **48**(4): p. 959-76.
119. Lamoth, F., et al., *Transcriptional Activation of Heat Shock Protein 90 Mediated Via a Proximal Promoter Region as Trigger of Caspofungin Resistance in Aspergillus fumigatus.* J Infect Dis, 2014. **209**(3): p. 473-81.
120. Ji, Y., et al., *HOG-MAPK signaling regulates the adaptive responses of Aspergillus fumigatus to thermal stress and other related stress.* Mycopathologia, 2012. **174**(4): p. 273-82.
121. Feng, X., et al., *HacA-independent functions of the ER stress sensor IreA synergize with the canonical UPR to influence virulence traits in Aspergillus fumigatus.* PLoS Pathog, 2011. **7**(10): p. e1002330.
122. Richie, D.L., et al., *A role for the unfolded protein response (UPR) in virulence and antifungal susceptibility in Aspergillus fumigatus.* PLoS Pathog, 2009. **5**(1): p. e1000258.

123. Miyazaki, T. and S. Kohno, *ER stress response mechanisms in the pathogenic yeast Candida glabrata and their roles in virulence.* Virulence, 2013. **5**(2).
124. Krishnan, K. and D.S. Askew, *The fungal UPR: A regulatory hub for virulence traits in the mold pathogen.* Virulence, 2013. **5**(2).
125. Heimel, K., et al., *Crosstalk between the unfolded protein response and pathways that regulate pathogenic development in Ustilago maydis.* Plant Cell, 2013. **25**(10): p. 4262-77.
126. Bates, S., et al., *Candida albicans Pmr1p, a secretory pathway P-type Ca2+/Mn2+-ATPase, is required for glycosylation and virulence.* J Biol Chem, 2005. **280**(24): p. 23408-15.
127. Tsai, H.F., et al., *Pentaketide melanin biosynthesis in Aspergillus fumigatus requires chain-length shortening of a heptaketide precursor.* J Biol Chem, 2001. **276**(31): p. 29292-8.
128. Taylor, B.E., M.H. Wheeler, and P.J. Szaniszlo, *Evidence for Pentaketide Melanin Biosynthesis in Dematiaceous Human Pathogenic Fungi.* Mycologia, 1987. **79**(2): p. 320-322.
129. Wheeler, M.H., *Comparisons of fungal melanin biosynthesis in ascomycetous, imperfect and basidiomycetous fungi.* Transactions of the British Mycological Society, 1983. **81**(1): p. 29-36.
130. Romero-Martinez, R., et al., *Biosynthesis and functions of melanin in Sporothrix schenckii.* Infect Immun, 2000. **68**(6): p. 3696-703.
131. Zhu, X. and P.R. Williamson, *Role of laccase in the biology and virulence of Cryptococcus neoformans.* FEMS Yeast Res, 2004. **5**(1): p. 1-10.
132. Eisenman, H.C. and A. Casadevall, *Synthesis and assembly of fungal melanin.* Appl Microbiol Biotechnol, 2012. **93**(3): p. 931-40.
133. Bell, A.A. and M.H. Wheeler, *Biosynthesis and Functions of Fungal Melanins.* Annual Review of Phytopathology, 1986. **24**(1): p. 411-451.
134. Ito, S. and K. Wakamatsu, *Quantitative analysis of eumelanin and pheomelanin in humans, mice, and other animals: a comparative review.* Pigment Cell Res, 2003. **16**(5): p. 523-31.
135. Pukkila-Worley, R., et al., *Transcriptional network of multiple capsule and melanin genes governed by the Cryptococcus neoformans cyclic AMP cascade.* Eukaryot Cell, 2005. **4**(1): p. 190-201.
136. Missall, T.A., et al., *Distinct stress responses of two functional laccases in Cryptococcus neoformans are revealed in the absence of the thiol-specific antioxidant Tsa1.* Eukaryot Cell, 2005. **4**(1): p. 202-8.
137. Frases, S., et al., *Cryptococcus neoformans can utilize the bacterial melanin precursor homogentisic acid for fungal melanogenesis.* Appl Environ Microbiol, 2007. **73**(2): p. 615-21.
138. Fowler, Z.L., et al., *Melanization of flavonoids by fungal and bacterial laccases.* Yeast, 2011. **28**(3): p. 181-8.
139. Vidotto, V., et al., *A new caffeic acid minimal synthetic medium for the rapid identification of Cryptococcus neoformans isolates.* Rev Iberoam Micol, 2004. **21**(2): p. 87-9.

140. Zhu, X. and P.R. Williamson, *A CLC-type chloride channel gene is required for laccase activity and virulence in Cryptococcus neoformans.* Mol Microbiol, 2003. **50**(4): p. 1271-81.
141. Mauch, R.M., O. Cunha Vde, and A.L. Dias, *The copper interference with the melanogenesis OF Cryptococcus neoformans.* Rev Inst Med Trop Sao Paulo, 2013. **55**(2): p. 117-20.
142. Silva, F.D., et al., *Effects of microplusin, a copper-chelating antimicrobial peptide, against Cryptococcus neoformans.* FEMS Microbiol Lett, 2011. **324**(1): p. 64-72.
143. Nosanchuk, J.D. and A. Casadevall, *Budding of melanized Cryptococcus neoformans in the presence or absence of L-dopa.* Microbiology, 2003. **149**(Pt 7): p. 1945-51.
144. Dalisay, D.S., J.P. Saludes, and T.F. Molinski, *Ptilomycalin A inhibits laccase and melanization in Cryptococcus neoformans.* Bioorg Med Chem, 2011. **19**(22): p. 6654-7.
145. Nosanchuk, J.D., R. Ovalle, and A. Casadevall, *Glyphosate inhibits melanization of Cryptococcus neoformans and prolongs survival of mice after systemic infection.* J Infect Dis, 2001. **183**(7): p. 1093-9.
146. Rosas, A.L., J.D. Nosanchuk, and A. Casadevall, *Passive immunization with melanin-binding monoclonal antibodies prolongs survival of mice with lethal Cryptococcus neoformans infection.* Infect Immun, 2001. **69**(5): p. 3410-2.
147. Hamilton, A.J. and M.D. Holdom, *Antioxidant systems in the pathogenic fungi of man and their role in virulence.* Med Mycol, 1999. **37**(6): p. 375-89.
148. Jacobson, E.S. and J.D. Hong, *Redox buffering by melanin and Fe(II) in Cryptococcus neoformans.* J Bacteriol, 1997. **179**(17): p. 5340-6.
149. Rosas, A.L. and A. Casadevall, *Melanization decreases the susceptibility of Cryptococcus neoformans to enzymatic degradation.* Mycopathologia, 2001. **151**(2): p. 53-6.
150. Mohagheghpour, N., et al., *Synthetic melanin suppresses production of proinflammatory cytokines.* Cell Immunol, 2000. **199**(1): p. 25-36.
151. Eisenman, H.C., et al., *Vesicle-associated melanization in Cryptococcus neoformans.* Microbiology, 2009. **155**(Pt 12): p. 3860-7.
152. Nicola, A.M., S. Frases, and A. Casadevall, *Lipophilic dye staining of Cryptococcus neoformans extracellular vesicles and capsule.* Eukaryot Cell, 2009. **8**(9): p. 1373-80.
153. van Duin, D., A. Casadevall, and J.D. Nosanchuk, *Melanization of Cryptococcus neoformans and Histoplasma capsulatum reduces their susceptibilities to amphotericin B and caspofungin.* Antimicrob Agents Chemother, 2002. **46**(11): p. 3394-400.
154. Wang, Y. and A. Casadevall, *Susceptibility of melanized and nonmelanized Cryptococcus neoformans to the melanin-binding compounds trifluoperazine and chloroquine.* Antimicrob Agents Chemother, 1996. **40**(3): p. 541-5.
155. Rosas, A.L., et al., *Activation of the alternative complement pathway by fungal melanins.* Clin Diagn Lab Immunol, 2002. **9**(1): p. 144-8.
156. Gomez, B.L., et al., *Detection of melanin-like pigments in the dimorphic fungal pathogen Paracoccidioides brasiliensis in vitro and during infection.* Infect Immun, 2001. **69**(9): p. 5760-7.
157. Nosanchuk, J.D., et al., *Histoplasma capsulatum synthesizes melanin-like pigments in vitro and during mammalian infection.* Infect Immun, 2002. **70**(9): p. 5124-31.
158. Wang, Y. and A. Casadevall, *Decreased susceptibility of melanized Cryptococcus neoformans to UV light.* Appl Environ Microbiol, 1994. **60**(10): p. 3864-6.

159. Rosas, A.L. and A. Casadevall, *Melanization affects susceptibility of Cryptococcus neoformans to heat and cold.* FEMS Microbiol Lett, 1997. **153**(2): p. 265-72.
160. Wang, Y. and A. Casadevall, *Susceptibility of melanized and nonmelanized Cryptococcus neoformans to nitrogen- and oxygen-derived oxidants.* Infect Immun, 1994. **62**(7): p. 3004-7.
161. Steenbergen, J.N., H.A. Shuman, and A. Casadevall, *Cryptococcus neoformans interactions with amoebae suggest an explanation for its virulence and intracellular pathogenic strategy in macrophages.* Proc Natl Acad Sci U S A, 2001. **98**(26): p. 15245-50.
162. Dadachova, E., et al., *Ionizing Radiation Changes the Electronic Properties of Melanin and Enhances the Growth of Melanized Fungi.* PLoS One, 2007. **2**(5): p. e457.
163. Turick, C.E., et al., *Gamma radiation interacts with melanin to alter its oxidation-reduction potential and results in electric current production.* Bioelectrochemistry, 2011. **82**(1): p. 69-73.
164. Saini, A.S. and J.S. Melo, *Biosorption of uranium by melanin: kinetic, equilibrium and thermodynamic studies.* Bioresour Technol, 2013. **149**: p. 155-62.
165. Ball, V., J. Bour, and M. Michel, *Step-by-step deposition of synthetic dopamine-eumelanin and metal cations.* J Colloid Interface Sci, 2013. **405**: p. 331-5.
166. Schaible, U.E. and S.H. Kaufmann, *Iron and microbial infection.* Nat Rev Microbiol, 2004. **2**(12): p. 946-53.
167. Vartivarian, S.E., et al., *Regulation of cryptococcal capsular polysaccharide by iron.* J Infect Dis, 1993. **167**(1): p. 186-90.
168. Jacobson, E.S. and G.M. Compton, *Discordant regulation of phenoloxidase and capsular polysaccharide in Cryptococcus neoformans.* J Med Vet Mycol, 1996. **34**(4): p. 289-91.
169. Klee, C.B., H. Ren, and X. Wang, *Regulation of the Calmodulin-stimulated Protein Phosphatase, Calcineurin.* Journal of Biological Chemistry, 1998. **273**(22): p. 13367-13370.
170. Fox, D.S., et al., *Calcineurin regulatory subunit is essential for virulence and mediates interactions with FKBP12-FK506 in Cryptococcus neoformans.* Mol Microbiol, 2001. **39**(4): p. 835-49.
171. Lian, T., et al., *Iron-regulated transcription and capsule formation in the fungal pathogen Cryptococcus neoformans.* Mol Microbiol, 2005. **55**(5): p. 1452-72.
172. Jung, W.H., et al., *HapX Positively and Negatively Regulates the Transcriptional Response to Iron Deprivation in Cryptococcus neoformans.* PLoS Pathog, 2010. **6**(11): p. e1001209.
173. O'Meara, T.R., et al., *Interaction of Cryptococcus neoformans Rim101 and Protein Kinase A Regulates Capsule.* PLoS Pathog, 2010. **6**(2): p. e1000776.
174. Lee, H., et al., *Regulatory Diversity of TUP1 in Cryptococcus neoformans.* Eukaryot Cell, 2009. **8**(12): p. 1901-1908.
175. Cramer, K.L., et al., *Transcription factor Nrg1 mediates capsule formation, stress response, and pathogenesis in Cryptococcus neoformans.* Eukaryot Cell, 2006. **5**(7): p. 1147-56.
176. Nyhus, K.J., A.T. Wilborn, and E.S. Jacobson, *Ferric iron reduction by Cryptococcus neoformans.* Infect Immun, 1997. **65**(2): p. 434-8.
177. Saikia, S., et al., *Role of Ferric Reductases in Iron Acquisition and Virulence in the Fungal Pathogen Cryptococcus neoformans.* Infect Immun, 2014. **82**(2): p. 839-50.

178. Cadieux, B., et al., *The Mannoprotein Cig1 supports iron acquisition from heme and virulence in the pathogenic fungus Cryptococcus neoformans.* J Infect Dis, 2013. **207**(8): p. 1339-47.
179. Hu, G., et al., *Cryptococcus neoformans requires the ESCRT protein Vps23 for iron acquisition from heme, for capsule formation, and for virulence.* Infect Immun, 2013. **81**(1): p. 292-302.
180. Jung, W.H., et al., *Role of ferroxidases in iron uptake and virulence of Cryptococcus neoformans.* Eukaryot Cell, 2009. **8**(10): p. 1511-20.
181. Jacobson, E.S. and M.J. Petro, *Extracellular iron chelation in Cryptococcus neoformans.* J Med Vet Mycol, 1987. **25**(6): p. 415-8.
182. Vanden Bossche, H., et al., *Antifungal drug resistance in pathogenic fungi.* Med Mycol, 1998. **36 Suppl 1**: p. 119-28.
183. Tangen, K.L., et al., *The iron- and cAMP-regulated gene SIT1 influences ferrioxamine B utilization, melanization and cell wall structure in Cryptococcus neoformans.* Microbiology, 2007. **153**(1): p. 29-41.
184. Klionsky, D.J., P.K. Herman, and S.D. Emr, *The fungal vacuole: composition, function, and biogenesis.* Microbiol Rev, 1990. **54**(3): p. 266-92.
185. Reggiori, F. and D.J. Klionsky, *Autophagic processes in yeast: mechanism, machinery and regulation.* Genetics, 2013. **194**(2): p. 341-61.
186. Bryant, N.J. and T.H. Stevens, *Vacuole biogenesis in Saccharomyces cerevisiae: protein transport pathways to the yeast vacuole.* Microbiol Mol Biol Rev, 1998. **62**(1): p. 230-47.
187. Yamashiro, C.T., et al., *Role of vacuolar acidification in protein sorting and zymogen activation: a genetic analysis of the yeast vacuolar proton-translocating ATPase.* Mol Cell Biol, 1990. **10**(7): p. 3737-49.
188. Takegawa, K., et al., *Vesicle-mediated protein transport pathways to the vacuole in Schizosaccharomyces pombe.* Cell Struct Funct, 2003. **28**(5): p. 399-417.
189. Iwaki, T., et al., *Characterization of Schizosaccharomyces pombe mutants defective in vacuolar acidification and protein sorting.* Mol Genet Genomics, 2004. **271**(2): p. 197-207.
190. Robinson, J.S., et al., *Protein sorting in Saccharomyces cerevisiae: isolation of mutants defective in the delivery and processing of multiple vacuolar hydrolases.* Mol Cell Biol, 1988. **8**(11): p. 4936-48.
191. Raymond, C.K., et al., *Morphological classification of the yeast vacuolar protein sorting mutants: evidence for a prevacuolar compartment in class E vps mutants.* Mol Biol Cell, 1992. **3**(12): p. 1389-402.
192. Klionsky, D.J. and S.D. Emr, *Membrane protein sorting: biosynthesis, transport and processing of yeast vacuolar alkaline phosphatase.* EMBO J, 1989. **8**(8): p. 2241-50.
193. Anraku, Y., et al., *Structure and function of the yeast vacuolar membrane proton ATPase.* J Bioenerg Biomembr, 1989. **21**(5): p. 589-603.
194. Coonrod, E.M. and T.H. Stevens, *The yeast vps class E mutants: the beginning of the molecular genetic analysis of multivesicular body biogenesis.* Mol Biol Cell, 2010. **21**(23): p. 4057-60.
195. Hedman, J.M., et al., *Prevacuolar compartment morphology in vps mutants of Saccharomyces cerevisiae.* Cell Biol Int, 2007. **31**(10): p. 1237-44.
196. Veses, V., A. Richards, and N.A.R. Gow, *Vacuoles and fungal biology.* Curr Opin Microbiol, 2008. **11**(6): p. 503-510.

197. Bartoszewska, M. and J.A. Kiel, *The role of macroautophagy in development of filamentous fungi.* Antioxid Redox Signal, 2011. **14**(11): p. 2271-87.
198. Palmer, G.E., *Vacuolar trafficking and Candida albicans pathogenesis.* Commun Integr Biol, 2011. **4**(2): p. 240-2.
199. Patenaude, C., et al., *Essential role for vacuolar acidification in Candida albicans virulence.* J Biol Chem, 2013. **288**(36): p. 26256-64.
200. Rane, H.S., et al., *Candida albicans VMA3 is necessary for V-ATPase assembly and function and contributes to secretion and filamentation.* Eukaryot Cell, 2013. **12**(10): p. 1369-82.
201. Johnston, D.A., et al., *Three prevacuolar compartment Rab GTPases impact Candida albicans hyphal growth.* Eukaryot Cell, 2013. **12**(7): p. 1039-50.
202. Abenza, J.F., et al., *Long-distance movement of Aspergillus nidulans early endosomes on microtubule tracks.* Traffic, 2009. **10**(1): p. 57-75.
203. Abenza, J.F., et al., *Aspergillus RabB Rab5 integrates acquisition of degradative identity with the long distance movement of early endosomes.* Mol Biol Cell, 2010. **21**(15): p. 2756-69.
204. Calcagno-Pizarelli, A.M., et al., *Rescue of Aspergillus nidulans severely debilitating null mutations in ESCRT-0, I, II and III genes by inactivation of a salt-tolerance pathway allows examination of ESCRT gene roles in pH signalling.* J Cell Sci, 2011. **124**(Pt 23): p. 4064-76.
205. de Gouvea, P.F., et al., *Functional characterization of the Aspergillus fumigatusPHO80 homologue.* Fungal Genet Biol, 2008. **45**(7): p. 1135-46.
206. Gsaller, F., et al., *The interplay between vacuolar and siderophore-mediated iron storage in Aspergillus fumigatus.* Metallomics, 2012. **4**(12): p. 1262-70.
207. Erickson, T., et al., *Multiple virulence factors of Cryptococcus neoformans are dependent on VPH1.* Mol Microbiol, 2001. **42**(4): p. 1121-31.
208. Liu, X., et al., *Role of a VPS41 homologue in starvation response, intracellular survival and virulence of Cryptococcus neoformans.* Mol Microbiol, 2006. **61**(5): p. 1132-46.
209. Narasipura, S.D., et al., *Characterization of Cu,Zn superoxide dismutase (SOD1) gene knock-out mutant of Cryptococcus neoformans var. gattii: role in biology and virulence.* Mol Microbiol, 2003. **47**(6): p. 1681-94.
210. Kmetzsch, L., et al., *The vacuolar Ca(2)(+) exchanger Vcx1 is involved in calcineurin-dependent Ca(2)(+) tolerance and virulence in Cryptococcus neoformans.* Eukaryot Cell, 2010. **9**(11): p. 1798-805.
211. Kmetzsch, L., et al., *The calcium transporter Pmc1 provides Ca2+ tolerance and influences the progression of murine cryptococcal infection.* FEBS J, 2013. **280**(19): p. 4853-64.
212. Kronstad, J.W., G. Hu, and J. Choi, *The cAMP/Protein Kinase A Pathway and Virulence in Cryptococcus neoformans.* Mycobiology, 2011. **39**(3): p. 143-50.
213. Choi, J., A.W. Vogl, and J.W. Kronstad, *Regulated expression of cyclic AMP-dependent protein kinase A reveals an influence on cell size and the secretion of virulence factors in Cryptococcus neoformans.* Mol Microbiol, 2012. **85**(4): p. 700-15.
214. Wilson, M.S., T.M. Livermore, and A. Saiardi, *Inositol pyrophosphates: between signalling and metabolism.* Biochem J, 2013. **452**(3): p. 369-79.
215. Xue, C., *Cryptococcus and beyond--inositol utilization and its implications for the emergence of fungal virulence.* PLoS Pathog, 2012. **8**(9): p. e1002869.

216. Lev, S., et al., *Phospholipase C of Cryptococcus neoformans regulates homeostasis and virulence by providing inositol trisphosphate as a substrate for Arg1 kinase.* Infect Immun, 2013. **81**(4): p. 1245-55.
217. Harrison, T.S., G.E. Griffin, and S.M. Levitz, *Conditional Lethality of the Diprotic Weak Bases Chloroquine and Quinacrine against Cryptococcus neoformans.* Journal of Infectious Diseases, 2000. **182**(1): p. 283-289.
218. Mazzolla, R., et al., *Enhanced resistance to Cryptococcus neoformans infection induced by chloroquine in a murine model of meningoencephalitis.* Antimicrob Agents Chemother, 1997. **41**(4): p. 802-7.
219. Popova, N.V., I.E. Deyev, and A.G. Petrenko, *Clathrin-mediated endocytosis and adaptor proteins.* Acta Naturae, 2013. **5**(3): p. 62-73.
220. Viotti, C., *ER and vacuoles: never been closer.* Front Plant Sci, 2014. **5**: p. 20.
221. Brandizzi, F. and C. Barlowe, *Organization of the ER-Golgi interface for membrane traffic control.* Nat Rev Mol Cell Biol, 2013. **14**(6): p. 382-92.
222. Duman, J.G. and J.G. Forte, *What is the role of SNARE proteins in membrane fusion?* Am J Physiol Cell Physiol, 2003. **285**(2): p. C237-49.
223. Scales, S.J., B.Y. Yoo, and R.H. Scheller, *The ionic layer is required for efficient dissociation of the SNARE complex by α-SNAP and NSF.* Proceedings of the National Academy of Sciences, 2001. **98**(25): p. 14262-14267.
224. Blasi, J., et al., *Botulinum neurotoxin A selectively cleaves the synaptic protein SNAP-25.* Nature, 1993. **365**(6442): p. 160-3.
225. Struthers, M.S., et al., *Functional homology of mammalian syntaxin 16 and yeast Tlg2p reveals a conserved regulatory mechanism.* Journal of Cell Science, 2009. **122**(13): p. 2292-2299.
226. MacDonald, C., M. Munson, and N.J. Bryant, *Autoinhibition of SNARE complex assembly by a conformational switch represents a conserved feature of syntaxins.* Biochem Soc Trans, 2010. **38**(Pt 1): p. 209-12.
227. Bryant, N.J. and D.E. James, *Vps45p stabilizes the syntaxin homologue Tlg2p and positively regulates SNARE complex formation.* EMBO J, 2001. **20**(13): p. 3380-8.
228. Bryant, N.J., et al., *Traffic into the prevacuolar/endosomal compartment of Saccharomyces cerevisiae: a VPS45-dependent intracellular route and a VPS45-independent, endocytic route.* Eur J Cell Biol, 1998. **76**(1): p. 43-52.
229. Piper, R.C., E.A. Whitters, and T.H. Stevens, *Yeast Vps45p is a Sec1p-like protein required for the consumption of vacuole-targeted, post-Golgi transport vesicles.* Eur J Cell Biol, 1994. **65**(2): p. 305-18.
230. Burd, C.G., et al., *A novel Sec18p/NSF-dependent complex required for Golgi-to-endosome transport in yeast.* Mol Biol Cell, 1997. **8**(6): p. 1089-104.
231. Holthuis, J.C., et al., *Two syntaxin homologues in the TGN/endosomal system of yeast.* EMBO J, 1998. **17**(1): p. 113-26.
232. Weinberger, A., et al., *Control of Golgi morphology and function by Sed5 t-SNARE phosphorylation.* Mol Biol Cell, 2005. **16**(10): p. 4918-30.
233. Hardwick, K.G. and H.R. Pelham, *SED5 encodes a 39-kD integral membrane protein required for vesicular transport between the ER and the Golgi complex.* J Cell Biol, 1992. **119**(3): p. 513-21.
234. Wooding, S. and H.R. Pelham, *The dynamics of golgi protein traffic visualized in living yeast cells.* Mol Biol Cell, 1998. **9**(9): p. 2667-80.

235. Peterson, M.R., C.G. Burd, and S.D. Emr, *Vac1p coordinates Rab and phosphatidylinositol 3-kinase signaling in Vps45p-dependent vesicle docking/fusion at the endosome.* Curr Biol, 1999. **9**(3): p. 159-62.
236. Hong, W., *SNAREs and traffic.* Biochim Biophys Acta, 2005. **1744**(2): p. 120-44.
237. Obara, K., et al., *Transport of phosphatidylinositol 3-phosphate into the vacuole via autophagic membranes in Saccharomyces cerevisiae.* Genes Cells, 2008. **13**(6): p. 537-47.
238. Gerrard, S.R., N.J. Bryant, and T.H. Stevens, *VPS21 controls entry of endocytosed and biosynthetic proteins into the yeast prevacuolar compartment.* Mol Biol Cell, 2000. **11**(2): p. 613-26.
239. Hauck, F. and C. Klein, *Pathogenic mechanisms and clinical implications of congenital neutropenia syndromes.* Curr Opin Allergy Clin Immunol, 2013. **13**(6): p. 596-606.
240. Stepensky, P., et al., *The Thr224Asn mutation in the VPS45 gene is associated with the congenital neutropenia and primary myelofibrosis of infancy.* Blood, 2013. **121**(25): p. 5078-87.
241. Vilboux, T., et al., *A congenital neutrophil defect syndrome associated with mutations in VPS45.* N Engl J Med, 2013. **369**(1): p. 54-65.
242. Jung, W.H., et al., *HapX positively and negatively regulates the transcriptional response to iron deprivation in Cryptococcus neoformans.* PLoS Pathog, 2010. **6**(11): p. e1001209.
243. Harrison, T.S., G.E. Griffin, and S.M. Levitz, *Conditional lethality of the diprotic weak bases chloroquine and quinacrine against Cryptococcus neoformans.* J Infect Dis, 2000. **182**(1): p. 283-9.
244. Pitkin, J.W., D.G. Panaccione, and J.D. Walton, *A putative cyclic peptide efflux pump encoded by the TOXA gene of the plant-pathogenic fungus Cochliobolus carbonum.* Microbiology, 1996. **142 (Pt 6)**: p. 1557-65.
245. Altschul, S.F., et al., *Basic local alignment search tool.* J Mol Biol, 1990. **215**(3): p. 403-10.
246. Yu, J.H., et al., *Double-joint PCR: a PCR-based molecular tool for gene manipulations in filamentous fungi.* Fungal Genet Biol, 2004. **41**(11): p. 973-81.
247. Kim, M.S., et al., *Targeted gene disruption in Cryptococcus neoformans using double-joint PCR with split dominant selectable markers.* Methods Mol Biol, 2012. **845**: p. 67-84.
248. Toffaletti, D.L., et al., *Gene transfer in Cryptococcus neoformans by use of biolistic delivery of DNA.* J Bacteriol, 1993. **175**(5): p. 1405-11.
249. Griffiths, E.J., et al., *A defect in ATP-citrate lyase links acetyl-CoA production, virulence factor elaboration and virulence in Cryptococcus neoformans.* Mol Microbiol, 2012. **86**(6): p. 1404-23.
250. Casadevall, A., et al., *Characterization of a murine monoclonal antibody to Cryptococcus neoformans polysaccharide that is a candidate for human therapeutic studies.* Antimicrob Agents Chemother, 1998. **42**(6): p. 1437-46.
251. Auesukaree, C., et al., *Genome-wide identification of genes involved in tolerance to various environmental stresses in Saccharomyces cerevisiae.* J Appl Genet, 2009. **50**(3): p. 301-10.
252. Ando, A., et al., *Identification and classification of genes required for tolerance to freeze-thaw stress revealed by genome-wide screening of Saccharomyces cerevisiae deletion strains.* FEMS Yeast Res, 2007. **7**(2): p. 244-53.

253. Banuelos, M.G., et al., *Genomic analysis of severe hypersensitivity to hygromycin B reveals linkage to vacuolar defects and new vacuolar gene functions in Saccharomyces cerevisiae.* Curr Genet, 2010. **56**(2): p. 121-37.
254. Kopecka, M. and M. Gabriel, *The influence of congo red on the cell wall and (1----3)-beta-D-glucan microfibril biogenesis in Saccharomyces cerevisiae.* Arch Microbiol, 1992. **158**(2): p. 115-26.
255. Weber, S.M., S.M. Levitz, and T.S. Harrison, *Chloroquine and the fungal phagosome.* Curr Opin Microbiol, 2000. **3**(4): p. 349-53.
256. Levitz, S.M., et al., *Chloroquine induces human mononuclear phagocytes to inhibit and kill Cryptococcus neoformans by a mechanism independent of iron deprivation.* J Clin Invest, 1997. **100**(6): p. 1640-6.
257. Rolain, J.M., P. Colson, and D. Raoult, *Recycling of chloroquine and its hydroxyl analogue to face bacterial, fungal and viral infections in the 21st century.* Int J Antimicrob Agents, 2007. **30**(4): p. 297-308.
258. Larraya, L.M., et al., *Serial Analysis of Gene Expression Reveals Conserved Links between Protein Kinase A, Ribosome Biogenesis, and Phosphate Metabolism in Ustilago maydis.* Eukaryotic Cell, 2005. **4**(12): p. 2029-2043.
259. Hortschansky, P., et al., *Interaction of HapX with the CCAAT-binding complex--a novel mechanism of gene regulation by iron.* EMBO J, 2007. **26**(13): p. 3157-68.
260. Hong, M., et al., *Identification of two Shigella flexneri chromosomal loci involved in intercellular spreading.* Infect Immun, 1998. **66**(10): p. 4700-10.
261. Park, J., et al., *The lack of synchronization between iron uptake and cell growth leads to iron overload in Saccharomyces cerevisiae during post-exponential growth modes.* Biochemistry, 2013. **52**(52): p. 9413-25.
262. Tangen, K.L., et al., *The iron- and cAMP-regulated gene SIT1 influences ferrioxamine B utilization, melanization and cell wall structure in Cryptococcus neoformans.* Microbiology, 2007. **153**(Pt 1): p. 29-41.
263. Levin, D.E., *Cell wall integrity signaling in Saccharomyces cerevisiae.* Microbiol Mol Biol Rev, 2005. **69**(2): p. 262-91.
264. Schachtschabel, D., et al., *Vacuolar H(+)-ATPase plays a key role in cell wall biosynthesis of Aspergillus niger.* Fungal Genet Biol, 2012. **49**(4): p. 284-93.
265. Bonilla, M. and K.W. Cunningham, *Mitogen-activated protein kinase stimulation of Ca(2+) signaling is required for survival of endoplasmic reticulum stress in yeast.* Mol Biol Cell, 2003. **14**(10): p. 4296-305.
266. Kim, H., A. Kim, and K.W. Cunningham, *Vacuolar H+-ATPase (V-ATPase) promotes vacuolar membrane permeabilization and nonapoptotic death in stressed yeast.* J Biol Chem, 2012. **287**(23): p. 19029-39.
267. Egan, T.J., D.C. Ross, and P.A. Adams, *Quinoline anti-malarial drugs inhibit spontaneous formation of beta-haematin (malaria pigment).* FEBS Lett, 1994. **352**(1): p. 54-7.
268. Leed, A., et al., *Solution structures of antimalarial drug-heme complexes.* Biochemistry, 2002. **41**(32): p. 10245-55.
269. Ehsanian, R., C. Van Waes, and S.M. Feller, *Beyond DNA binding - a review of the potential mechanisms mediating quinacrine's therapeutic activities in parasitic infections, inflammation, and cancers.* Cell Commun Signal, 2011. **9**: p. 13.

270. Eapen, V.V. and J.E. Haber, *DNA damage signaling triggers the cytoplasm-to-vacuole pathway of autophagy to regulate cell cycle progression.* Autophagy, 2013. **9**(3): p. 440-1.
271. Byrd, T.F. and M.A. Horwitz, *Chloroquine inhibits the intracellular multiplication of Legionella pneumophila by limiting the availability of iron. A potential new mechanism for the therapeutic effect of chloroquine against intracellular pathogens.* J Clin Invest, 1991. **88**(1): p. 351-7.
272. Newman, S.L., et al., *Chloroquine induces human macrophage killing of Histoplasma capsulatum by limiting the availability of intracellular iron and is therapeutic in a murine model of histoplasmosis.* J Clin Invest, 1994. **93**(4): p. 1422-9.
273. Yamada, K., et al., *A major role for phospholipase A2 in antigen-induced arachidonic acid release in rat mast cells.* Biochem J, 1987. **247**(1): p. 95-9.
274. Erb-Downward, J.R., et al., *The role of laccase in prostaglandin production by Cryptococcus neoformans.* Mol Microbiol, 2008. **68**(6): p. 1428-37.
275. Valdez, P.A., et al., *Prostaglandin E2 suppresses antifungal immunity by inhibiting interferon regulatory factor 4 function and interleukin-17 expression in T cells.* Immunity, 2012. **36**(4): p. 668-79.
276. Chinappi, M., et al., *On the mechanism of chloroquine resistance in Plasmodium falciparum.* PLoS One, 2010. **5**(11): p. e14064.
277. Veses, V. and N.A. Gow, *Vacuolar dynamics during the morphogenetic transition in Candida albicans.* FEMS Yeast Res, 2008. **8**(8): p. 1339-48.
278. Hayek, S.R., S.A. Lee, and K.J. Parra, *Advances in targeting the vacuolar proton-translocating ATPase (V-ATPase) for anti-fungal therapy.* Front Pharmacol, 2014. **5**: p. 4.

Appendix A

Below is genomic DNA isolated from the cheek cells of Erik David Nielson. This DNA was extracted from a 0.5 % saline solution swished thoroughly in the mouth to harvest cheek cells. Subsequent cell lysis was mediated by 500 μL of 10% SDS, followed by an ethanol precipitation. In case of emergency open packet, rehydrate DNA, and clone.